Technische Universität München
Physik-Department
Institut für Theoretische Physik T30
Univ.-Prof. Dr. Michael Ratz

TECHNISCHE UNIVERSITÄT MÜNCHEN

Baryogenesis, Neutrino Masses, and Dynamical Dark Energy

Marc-Thomas Eisele

Vollständiger Abdruck der von der Fakultät für Physik der Technischen Universität München zur Erlangung des akademischen Grades eines

Doktors der Naturwissenschaften (Dr. rer. nat.)

genehmigten Dissertation.

Vorsitzender:		Univ.-Prof. Dr. Franz von Feilitzsch
Prüfer der Dissertation:	1.	Univ.-Prof. Dr. Michael Ratz
	2.	Univ.-Prof. Dr. Andrzej Jerzy Buras

Die Dissertation wurde am 11. September 2007 bei der Technischen Universität München eingereicht und durch die Fakultät für Physik am 9. Oktober 2007 angenommen.

Abstract:
This thesis considers several models that connect different areas of particle physics and cosmology. Our first discussion in this context concerns a baryogenesis scenario, in which the baryon asymmetry of our universe is created through the dynamics of a dark energy field, thereby illustrating that these two topics might be related. Subsequently, several neutrino mass models are analyzed, which make use of an extra-dimensional setting to overcome certain problems of their four-dimensional counterparts. The central discussion of this thesis concerns a leptogenesis model with many standard model singlets. Amongst other things, we show that the presence of these states can lower the standard bound for the necessary reheating temperature of the universe by at least one and a half orders of magnitude. To further motivate this approach, we also discuss an explicit, extra-dimensional leptogenesis scenario that naturally yields many of the ingredients required in this context.

Zusammenfassung:
Diese Dissertation behandelt mehrere Modelle, die verschiedene Gebiete innerhalb der Teilchenphysik und Kosmologie miteinander verbinden. Als erstes wird hierbei ein Baryogenese-Szenario diskutiert, in welchem die Baryon-Asymmetrie unseres Universums mittels der Dynamik eines Dunkle-Energie-Feldes erzeugt wird, und welches hierdurch einen möglichen Zusammenhang dieser Themengebiete veranschaulicht. Daran anschließend werden verschiedene Neutrinomassen-Modelle analysiert, die innerhalb eines extra-dimensionalen Rahmens mögliche Probleme der entsprechenden vier dimensionalen Modelle überwinden. Die zentrale Diskussion dieser Dissertation betrifft ein Leptogenese-Modell mit vielen Standard Modell Singlets. Unter anderem wird gezeigt, dass die Anwesenheit vieler Singlet Zustände die untere Schranke für die notwendige Reheating Temperatur des Universums in Bezug auf das Standard-Szenario um mindestens eineinhalb Größenordnungen herabsetzen kann. Um diesen Ansatz weiter zu motivieren, diskutieren wir zusätzlich ein konkretes, extra-dimensionales Leptogenese-Szenario, welches viele der, in diesem Zusammenhang, notwendigen Voraussetzungen in natürlicher Weise bereitzustellen vermag.

Meiner Familie

Wie jede Blüte welkt und jede Jugend
Dem Alter weicht, blüht jede Lebensstufe,
Blüht jede Weisheit auch und jede Tugend
Zu ihrer Zeit und darf nicht ewig dauern.
Hermann Hesse, Stufen

Contents

Introduction

Within the search for a more fundamental theory of nature, physics at the smallest and the largest accessible length scales have both been studied with ever-growing precision. In the corresponding fields of physics, i.e. particle physics and cosmology, this has led to the development of respective standard models, which successfully describe a large number of phenomena. Especially the standard model of particle physics (SM) can be considered as a truly great achievement. Being based on very few assumptions, it has undergone extensive experimental tests for more than three decades now and has been able to account for all observed phenomena at high-energy collider experiments, even predicting particles that were later on observed. The standard model of cosmology (the ΛCDM-model) is somewhat more empirical. Nevertheless, it has been found to nicely describe the large scale behavior of our universe in terms of very few parameters and has therefore also become established.

Yet, in spite of the huge success of these two standard models, we know today that their simple combination cannot give a complete description of nature. This is due to several reasons, one of them being the fact that the SM cannot account for the observed dark matter in our universe, which is a key ingredient of the ΛCDM-model. Another reason is the inability of the SM to explain neutrino oscillations, which have been observed by a number of different experiments today. In fact, both of these phenomena seem to indicate new physics at higher energies. In particular, dark matter can be explained by weakly interacting particles with masses beyond the reach of previous particle physics experiments, while neutrino oscillations can be explained by tiny neutrino masses, which in turn seem to be suppressed by even larger energy scales.

Moreover, even several observations that can be accommodated within the two standard models can be seen as hints for new physics at higher energies. One of these potential hints comes from the baryon asymmetry of our universe, which cannot be created dynamically within the SM. In the respective framework, it would therefore have to be included into early universe dynamics as an initial parameter. Yet, this rather unattractive feature can be avoided within extensions of the SM that operate at higher scales. Another hint of this kind comes from the observed vacuum energy density in our universe. While this phenomenon can be accounted for within the standard model of cosmology, its tininess seems

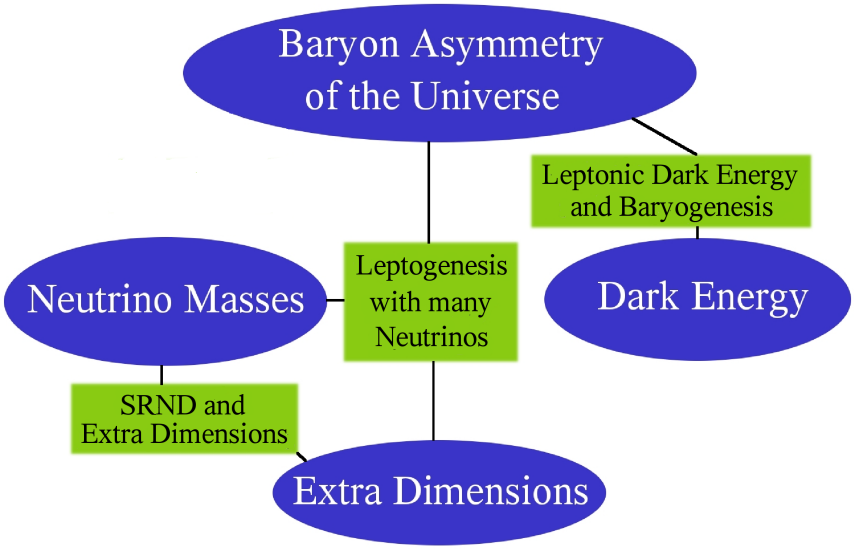

Figure 1: *This diagram illustrates the various connections of different areas of physics in the models considered in this thesis.*

to require a further motivation, which neither of the two standard models can provide.

Due to all these indications (and several others), physics beyond the electroweak scale is a very active area of research. Typically, it is further assumed that such new physics will help to simplify our view of physics at lower energies by unifying interactions and phenomena that previously seemed unrelated. If this assumption is true, we might also use this principle in reverse and attempt to receive hints about these new physics by trying to connect previously rather unrelated areas of research.

This combination of different topics of particle physics and cosmology is the main idea behind this thesis. In several models we present possible connections of miscellaneous areas of physics, namely the baryon asymmetry of our universe, dark energy, neutrino masses, and extra dimensions, as also illustrated in Fig. 1.

The present work will therefor be divided into an introductory part (chapters 1 to 4), in which several relevant topics of particle physics and cosmology are presented in some detail, and a central part (chapters 5 to 7), which mainly reviews the research of the author and his respective collaborators.

More precisely, we will give a brief introduction to several topics of cosmology in chapter 1, which will consist of two parts. In the first part, we will mainly discuss the basics of early universe dynamics and the established history of our universe, while we will focus on more advanced topics in the second part of this chapter. These more advanced topics include the cosmic microwave background, inflation, and quintessence fields. Subsequently, we give a brief overview over

the the standard model of particle physics, its Lagrangian and its motivations in chapter 2. This is followed by a more detailed discussion of neutrino masses in chapter 3 concerning their theoretical background, related experimental data and several approaches for model builders that address the smallness of neutrino masses as well as the structure of their masses and mixings. These approaches include the see-saw mechanism in four and five dimensions, single right-handed neutrino dominance, and family symmetries. In the final chapter of the introductory part (chapter 4), we review the baryon asymmetry of our universe and different scenarios that can create this asymmetry dynamically. In this context, we put a stronger focus on baryogenesis via leptogenesis, which will be especially relevant in the second part of the thesis.

The second part of the thesis starts with chapter 5 and an introduction to the idea of leptonic dark energy and baryogenesis, where we consider a baryogenesis mechanism that hides a $B - L$ asymmetry in a dark energy field, which compensates for an opposite asymmetry in the visible sector. In particular, we dicuss the particle content and the general dynamics of the model as well as further subtleties.

In chapter 6, we then consider a class of extra-dimensional neutrino mass models which combine single-right handed neutrino dominance and family symmetries to account for neutrino masses and mixings. Here, the extra-dimensional setting helps to avoid the cancellation of essential hierarchies that typically appear within the corresponding four-dimensional models. In addition to a more general discussion of the models, we also present explicit parameter values that yield the desired neutrino data in each case.

Chapter 7, finally, contains the central discussion of this thesis, in which we consider leptogenesis with many neutrinos. More precisely, we study the possible impact of many neutrino singlets on thermal leptogenesis scenarios via approximative, analytical formulae as well as numerical simulations. This analysis also includes a discussion of the possible impact of these states on bounds from the standard setting. To further motivate the idea of leptogenesis with many neutrinos, we also present a realization of a corresponding scenario within a concrete extra-dimensional model that can naturally yield singlet states with all the required features.

Subsequently, this is followed by the conclusions of this thesis, where we summarize the results of the different discussions and also address open questions of the presented models.

Moreover, in the appendix, we provide the interested reader with related background information, where the corresponding discussions address orbifolds, Boltzmann equations for leptogenesis, reaction rates of leptogenesis processes, and the Davidson-Ibarra bound in the presence of many singlets.

Conventions and Notation

In order to avoid the necessity of somewhat over-exact remarks during the presented calculations, we will fix some of the used notation, here.

In particular, if not indicated otherwise we will work in natural units throughout the whole paper, which implies $c = \hbar = k_B = 1$.

Moreover, In an inertial frame, the metric tensor g will be given by a diagonal matrix of the form $\mathrm{diag}(1, -1, -1, -1)$.

Considering spinors, we will work in the chiral basis where the γ-matrices take the form

$$\gamma_\mu = \begin{pmatrix} 0 & \sigma_\mu \\ \bar{\sigma}_\mu & 0 \end{pmatrix}, \quad \gamma_5 = i\gamma_4 = \begin{pmatrix} \mathbb{1}_{2\times 2} & 0 \\ 0 & -\mathbb{1}_{2\times 2} \end{pmatrix},$$

with $\sigma_\mu = (\mathbb{1}_{2\times 2}, -\sigma_i)$, $\bar{\sigma}_\mu = (\mathbb{1}_{2\times 2}, \sigma_i)$, and the Pauli matrices

$$\sigma_1 = \begin{pmatrix} 0 & 1 \\ 1 & 0 \end{pmatrix}, \quad \sigma_2 = \begin{pmatrix} 0 & -\mathrm{i} \\ \mathrm{i} & 0 \end{pmatrix}, \text{ and } \quad \sigma_3 = \begin{pmatrix} 1 & 0 \\ 0 & -1 \end{pmatrix}.$$

Further, we will frequently use the anti-symmetric matrix

$$\epsilon \equiv \mathrm{i}\sigma_2 = \begin{pmatrix} 0 & 1 \\ -1 & 0 \end{pmatrix},$$

and the right- and left-handed projection operators will, as usual, be given by

$$P_{R/L} \equiv \frac{\mathbb{1}_{4\times 4} \pm \gamma_5}{2}.$$

Occasionally, we will also make use of the 2-norm of a matrix M, which will be denoted by

$$||M|| \equiv \sqrt{\sum_{i,j} |M_{ij}|^2}.$$

Chapter 1

The Early Universe

The history of our universe and its interplay with particle physics is the primary subject of this thesis. The purpose of this chapter is therefore to provide the reader with some background material on this area, which can be helpful in the context of the more detailed discussions in the following chapters.

In particular, we will review the standard formal background for early universe dynamics in the following three sections and thereafter present the established picture of its more recent history in section 1.4.

For more comprehensive reviews on the early universe, we refer the reader to standard textbooks, e.g. Ref. [1].

The second half of this chapter will be dedicated to more advanced topics. In section 1.5 we will discuss the anisotropies of the cosmic microwave background and some of the information that can be inferred from them. This will be followed by a discussion of inflation in section 1.6, which is favored by large parts of the scientific community as the explanation for several conceptual problems of the early universe. The final section of this chapter will then be devoted to dark energy. In particular, to the conceptual problems of dark energy due to a cosmological constant and to quintessence as a possible solution to the cosmic coincidence problem.

1.1 Early Universe Thermodynamics

During large parts of its history, our universe can be considered as a thermal bath of different particle species in local thermal equilibrium (with some important deviations). This section is therefore concerned with the statistical properties of these particles, which will be crucial in the following sections, when we consider the corresponding dynamics of our universe more closely.

The relevant quantity from which one can deduce all the required statistical properties of a homogeneously distributed particle species is its phase space distribution $f_i(\vec{p})$. In particular, the respective particle density n_i, the energy

density ρ_i and its corresponding pressure p_i can be derived via

$$n_i = \frac{1}{(2\pi)^3}\int f_i(\vec{p})\,\mathrm{d}^3p\,, \tag{1.1}$$

$$\rho_i = \frac{1}{(2\pi)^3}\int E_i(\vec{p})f_i(\vec{p})\,\mathrm{d}^3p\,, \tag{1.2}$$

$$p_i = \frac{1}{(2\pi)^3}\int \frac{|\vec{p}|^2}{3E_i}f_i(\vec{p})\,\mathrm{d}^3p\,, \tag{1.3}$$

with $E_i \equiv (m_i^2 + |\vec{p}|^2)^{1/2}$, where m_i is the rest mass of the corresponding particle species.

To determine the respective phase space distributions, we note that particles that are not in local thermal equilibrium (LTE) in the early universe are typically still assumed to be in kinetic equilibrium. In both of these cases the phase space distribution is given by

$$f_i(\vec{p}) = \frac{g_i}{\exp\left[(E_i-\mu_i)/T_i + \tau_i\right]}\,, \tag{1.4}$$

where g_i is the number of internal degrees of freedom of the considered species, T_i is the corresponding temperature, μ_i is the corresponding chemical potential, and τ_i can take the values 1 (Fermi-Dirac statistics), -1 (Bose-Einstein statistics), and 0 (Maxwell-Boltzmann statistics).

In the relativistic limit ($T_i \gg m_i, \mu_i$) this leads to [1, 2]

$$n_i = \begin{cases} \frac{\zeta(3)}{\pi^2}\,g_i\,T_i^3 & \text{(Bose-Einstein)},\\ \frac{3}{4}\frac{\zeta(3)}{\pi^2}\,g_i\,T_i^3 & \text{(Fermi-Dirac)}, \end{cases} \tag{1.5}$$

$$\rho_i = \begin{cases} \frac{\pi^2}{30}\,g_i\,T_i^4 & \text{(Bose-Einstein)},\\ \frac{7}{8}\frac{\pi^2}{30}\,g_i\,T_i^4 & \text{(Fermi-Dirac)}, \end{cases} \tag{1.6}$$

$$p_i = \frac{\rho_i}{3}\,, \tag{1.7}$$

where $\zeta(3) \approx 1.202$ is the Riemann zeta function of 3.

In the non-relativistic limit, on the other hand, one finds for Bose-Einstein and Fermi-Dirac statistics alike [1]

$$n_i = g_i\left(\frac{m_iT_i}{2\pi}\right)^{3/2}\exp[-(m_i-\mu_i)/T_i]\,, \tag{1.8}$$

$$\rho = m_in_i\,, \tag{1.9}$$

$$p = n_iT_i \ll \rho_i\,. \tag{1.10}$$

Moreover, in the case of Maxwell-Boltzmann statistics the number density is for all temperature ranges given by [2]

$$n_i = g_i\frac{T_i^3e^{-\mu_i/T_i}}{2\pi^2}\left(\frac{m_i}{T_i}\right)^2K_2\left(\frac{m_i}{T_i}\right)\,, \tag{1.11}$$

where $K_2(x)$ represents the corresponding modified Bessel function of the second kind.

From Eq. (1.8) we can see that the abundance of non-relativistic species in thermal equilibrium is exponentially suppressed. For many cases it is therefore a good approximation to assume that only the relativistic degrees of freedom contribute to the energy density ρ and the pressure p of the universe, which are in this case given by

$$\rho = \frac{\pi^2}{30} g_* T^4 , \tag{1.12}$$

$$p = \rho/3 . \tag{1.13}$$

Here, T is the temperature of the photons, and g_* is the number of relativistic degrees of freedom defined by

$$g_* = \sum_{\text{bosons}} g_i \left(\frac{T_i}{T}\right)^4 + \frac{7}{8} \sum_{\text{fermions}} g_i \left(\frac{T_i}{T}\right)^4 , \tag{1.14}$$

where the sums only run over relativistic species with respective temperature T_i.

As long as the universe is in LTE, the entropy in a comoving volume will remain constant. Therefore, it is often convenient to specify the abundance of some quantity per comoving volume in terms of its density compared to the entropy density, where the latter is defined by the relation

$$s \equiv \frac{\rho + p}{T} . \tag{1.15}$$

From this definition we see that the entropy is typically dominated by relativistic particles as well. Similarly to Eq. (1.12) we can therefore write

$$s = \frac{2\pi^2}{45} g_{*S} T^3 , \tag{1.16}$$

in these cases, with

$$g_{*S} \equiv \sum_{\text{bosons}} g_i \left(\frac{T_i}{T}\right)^3 + \frac{7}{8} \sum_{\text{fermions}} g_i \left(\frac{T_i}{T}\right)^3 . \tag{1.17}$$

In this context, we also note that all relativistic species in our universe had the same temperature during the early periods of our universe, which implies $g_* = g_{*S}$ for these stages.

1.2 Early Universe Dynamics

Due to the short range of the strong and weak interaction of the standard model of particle physics and the electric neutrality of our universe on large scales, its behavior is basically determined by gravity, the weakest of all known interactions.

Gravity, in turn, has been found to be well described by the theory of general relativity. Therefore, the dynamics of the universe are determined by the Einstein equations, which can be written in the simple form

$$R_{\mu\nu} - \frac{1}{2}\mathcal{R}\, g_{\mu\nu} = 8\pi G\, T_{\mu\nu}\,. \tag{1.18}$$

Here, $g_{\mu\nu}$ is the metrical tensor of the system, $R_{\mu\nu}$ is the Ricci tensor, which depends on the metrical tensor and its derivatives, and $\mathcal{R} \equiv R_{\mu\nu}g^{\mu\nu}$ is the so-called Ricci scalar. The right-hand side of this equation can be considered as the source term of the system and contains Newton's constant G and the stress-energy tensor $T_{\mu\nu}$.

In spite of the simple form of Eq. (1.18), the corresponding solutions are typically complicated, which can, in parts, be ascribed to the complex dependence of $R_{\mu\nu}$ and $\mathcal{R}$ on the metric. This makes it generally hard to get an intuitive feeling for the solutions of the Einstein equations. However, in many cases the complexity of these equations can be greatly reduced by symmetries.

The cosmological principle, which claims that the universe is homogeneous and isotropic on large scales, renders such simplifying symmetries (cf. e.g. [3]). In fact, using spherical coordinates (r, ϑ, φ) the metric can be expressed via

$$\mathrm{d}s^2 \equiv g_{\mu\nu}x^\mu x^\nu = \mathrm{d}t^2 - a(t)^2\left[\frac{1}{1-k\,r^2}\,\mathrm{d}r^2 + r^2\,\mathrm{d}\vartheta^2 + r^2\sin^2(\vartheta)\,\mathrm{d}\varphi^2\right], \tag{1.19}$$

in this case. This metric is referred to as the Robertson-Walker metric. It contains the cosmic scale factor $a(t)$ and the free parameter k, where r is typically rescaled in such a way that k takes one of the values 1, 0, and -1.

It is therefore fortunate that the discovery of the cosmic microwave background and its high degree of isotropy by Penzias and Wilson in 1965 [4] indeed indicates a high degree of isotropy and homogeneity of our observable patch of the universe at the time of photon decoupling (cf. section 1.4) and justifies the assumption that our universe obeys the cosmological principle.

Moreover, the homogeneity and isotropy of our universe do not only help to simplify the metric within the relevant Einstein equations but also the stress-energy tensor, which can now be written as

$$T^\mu_\nu = \mathrm{diag}(\rho, -p, -p, -p)\,, \tag{1.20}$$

with energy density ρ and pressure p.

Additionally, general covariance, the symmetry principle of general relativity, yields a conservation law for the stress-energy tensor, which implies

$$\mathrm{d}(\rho a^3) = -p\,\mathrm{d}(a^3)\,, \tag{1.21}$$

in this case. We note that this relation states the (intuitively clear) fact that the energy loss in a comoving volume is equal to its change in physical physical size times the corresponding pressure.

Defining the equation of state parameter ω by

$$p \equiv \omega\rho\,, \tag{1.22}$$

we see from Eq. (1.7) that radiation yields a constant $\omega = 1/3$, while Eq. (1.10) tells us that $\omega = 0$ for matter. Additionally, Eq. (1.20) yields $\omega = -1$, if the energy momentum tensor is dominated a cosmological constant Λ ($T^{\mu\nu} = \Lambda g^{\mu\nu}$). Energy-sources that effectively yield such a cosmological constant are also referred to as vacuum energy.

If ω is time-independent (as for all three cases considered above), we can integrate Eq. (1.21) to

$$\rho \propto a^{-3(1+\omega)}\,, \tag{1.23}$$

which leads to different scaling laws for the various energy forms, namely

$$\begin{array}{lcll} \rho & \propto & a^{-4} & \text{(radiation)}, \\ \rho & \propto & a^{-3} & \text{(matter)}, \\ \rho & \propto & \text{const.} & \text{(vacuum energy)}. \end{array} \tag{1.24}$$

Moreover, Eqs. (1.19) and (1.20) also help to simplify the Einstein equations. E.g., the 0-0 component of Eq. (1.18) can now be written as

$$\frac{\dot{a}^2}{a^2} + \frac{k}{a^2} = \frac{8\pi G}{3}\rho\,, \tag{1.25}$$

which is called the Friedmann equation.

For later convenience, we also define the Hubble parameter

$$H = \frac{\dot{a}(t)}{a(t)}\,, \tag{1.26}$$

in this context.

Additionally, we note that, if ω is known, Eqs. (1.21) and (1.25) already suffice to completely describe the dynamics of the expansion and can be combined to the simple equation

$$\frac{\ddot{a}}{a} = -\frac{4\pi G}{3}(\rho + 3p)\,. \tag{1.27}$$

Now, we even see that it depends solely on the value of the equation-of-state parameter ω whether the universe decelerates ($\omega > -1/3$) or accelerates ($\omega < -1/3$).

Due to the fact that our universe is found to be approximately flat [5], which implies $k/a(t)^2 \approx 0$, we can even give simple analytic expressions for the behavior of the scale-factor in several important special cases. In particular, in a flat, expanding universe ($\dot{a} > 0$) with a fixed $\omega > -1$ Eqs. (1.23) and (1.25) lead to

$$\frac{a}{a_0} = \left[\frac{3}{2}(1+\omega)H_0(t-t_0) + 1\right]^{2/[3(1+\omega)]} \tag{1.28}$$

as well as

$$H = \left[\frac{3}{2}(1+\omega)(t-t_0) + H_0^{-1}\right]^{-1} . \tag{1.29}$$

Here, the index 0 denotes the respective values of a and H at $t = t_0$.

At late times ($t - t_0 \gg H_0^{-1}$) these expressions can be further simplified to

$$\begin{aligned} a &\propto (t-t_0)^{1/2}, \quad H = \frac{1}{2(t-t_0)} \quad \text{(rad. dom. universe)}, \\ a &\propto (t-t_0)^{2/3}, \quad H = \frac{2}{3(t-t_0)} \quad \text{(mat. dom. universe)}. \end{aligned} \tag{1.30}$$

For a universe dominated by vacuum energy, on the other hand, the same conditions lead to

$$\frac{a}{a_0} = \exp\left[H_0(t-t_0)\right] \quad \text{and} \quad H = H_0 = \text{const.}\,. \tag{1.31}$$

Further, in a flat universe ($k = 0$) the Friedmann equation tells us that the Hubble parameter and the energy density are related by

$$H^2 = \frac{8\pi G}{3}\rho_c\,, \tag{1.32}$$

where ρ_c is called the critical density.

From Eq. (1.12), we therefore see that a flat universe completely dominated by radiation

$$H \approx 1.66\, g_*^{1/2}\frac{T^2}{M_{\rm Pl}}\,, \tag{1.33}$$

where $M_{\rm Pl} = 1/G^{1/2}$ is the Planck mass.

As we live in an approximately flat universe, its various energy components are frequently specified in terms of fractions of the critical energy density, namely by

$$\Omega_i \equiv \frac{\rho_i}{\rho_c}, \tag{1.34}$$

where $\Omega_{\rm rad}$ corresponds to radiation, $\Omega_{\rm b}$ corresponds to baryons, $\Omega_{\rm m}$ corresponds to non-relativistic matter, $\Omega_{\rm dm}$ corresponds to dark matter, and Ω_Λ corresponds to vacuum energy.

1.3 Particle Kinematics

Now that we are more familiar with the expansion behavior of our universe, we will take a closer look at the effects of this expansion on the kinematics of the particles in our universe.

As the universe expands, the respective wavelengths λ of all particles increase by the same factor

$$\frac{\lambda(t_0)}{\lambda(t_1)} = \frac{a(t_0)}{a(t_1)} \equiv 1 + z\,, \tag{1.35}$$

where the last equation defines the so-called red-shift z, which is often used as a measure of time in the early universe. In fact, it is the observation that more distant galaxies undergo a higher red-shift that tells us that our universe is expanding.

As energy and momentum of massless particles are proportional to the inverse of their respective wave-lengths, the redshift implies that they scale with a^{-1}. Further, if these particles are decoupled, their density scales with a^{-3}. Combining these scaling laws, one can infer that a decoupled massless species whose distribution function is at some point of the form as in Eq. (1.4) will be described by the same distribution function at later times with a different temperature. In particular, the temperature will obey a scaling law of the form

$$T \propto a^{-1} \quad \text{for a decoupled, massless species.} \tag{1.36}$$

Non-relativistic, decoupled particles ($T \ll m$) also undergo the same red-shift and dilution. Yet, since their (kinetic) energy depends on p^2, they they will be described by the phase space distribution in Eq. (1.4) at later times, with

$$T \propto a^{-2} \quad \text{for a decoupled, non-relativistic species,} \tag{1.37}$$

if they obeyed Maxwell-Boltzmann statistics before they decoupled. Additionally, their distribution function also acquires a time-dependent chemical potential to ensure particle number conservation.

1.4 A Short History of our Universe

Let us now give a brief review over the history of our universe as far as it will be needed in the context of this thesis.

For this purpose, we will go backwards in time by means of Eqs. (1.21) and (1.25). In principle, going back in time in such a way can always be questioned, since the universe could also have started at some given instant with appropriate initial conditions. Today, we would obviously not be able to distinguish between such a universe and one that started much earlier. However, the fact that theory can nicely explain many features of our universe, seems to show the validity of our treatment, at least up to quite early times.

Before we get more detailed about the various epochs in the history of our universe, let us briefly consider its age. We therefore note that going backwards in time in an expanding universe also means going to smaller scale factors $a(t)$ and thereby to higher temperatures, as we can see from Eq. (1.24). This increasing

temperature implies that more and more particle species will become relativistic and our universe will sooner or later be dominated by radiation (going backwards in time). Hence, we can employ Eqs. (1.28) and (1.29), which show that a vanishes and H becomes divergent, as we approach $t \to t_0 - (2H_0)^{-1}$. Of course, this argument only holds if the universe has been dominated solely by radiation during these early epochs. In this case the point $t = t_0 - (2H_0)^{-1}$ is referred to as "big bang". Moreover, if the universe started with the big bang and was from then on governed by radiation its age is given by the simple relation [1]

$$t = (2H)^{-1} \approx \left(\frac{\mathrm{MeV}}{T}\right)^2 \mathrm{sec}\,, \tag{1.38}$$

as long as the dominant energy component in the universe does not change, due to Eq. (1.33). In fact, even if the universe started from a later point, or if it was matter dominated after some time as in the realistic case, Eq. (1.38) can typically still serve as a rough estimate. Plugging in the temperature of the cosmic microwave background, which we will discuss later on, one therefore finds an approximate age of our universe around 100 billion years. The actual value is somewhat lower, due to the fact that our universe was not radiation dominated during the most recent times. In particular, Ref. [5] finds a value of approximately 14 billion years in a more precise analysis.

At this point, one should however also note, that in case of an early phase in which our universe was dominated by vacuum energy (as in inflationary scenarios), the age of our universe could in principle be much older. Yet, in this case Eq. (1.38) still gives an estimate for the time since reheating (cf. Sec. 1.6), which is the more relevant quantity in many contexts.

We further note that the history of our universe crucially depends on the fact that certain processes are in in equilibrium, while it is of equal importance that certain other processes are not. Eq. (1.33) can also be helpful in this context, since processes with a typical reaction time Γ^{-1} that is larger than the age of the universe cannot be in thermal equilibrium. Therefore $\Gamma^{-1} > (2H)^{-1}$ usually characterizes an out-of-equilibrium process, whereas $\Gamma^{-1} < (2H)^{-1}$ typically indicates a process in equilibrium. In many cases this naive approximation works remarkably well. However, if this treatment of non-equilibrium phenomena is not precise enough, one typically makes use of Boltzmann equations to describe the dynamics of the corresponding system (cf. appendix B).

Let us now consider some of the different epochs in the history of our universe in more detail. The earliest time that is (indirectly) accessible by observation, is the epoch of big bang nucleosynthesis (BBN), when protons and nucleons started to form nuclei. This period took place between 0.01 seconds and 100 seconds after the big bang, which corresponds to a temperature range from 10 MeV to 0.1 MeV. The corresponding theory nicely predicts the abundances of the light elements D, ^{3}He, ^{4}He, and ^{7}Li solely depending on the baryon-to-photon ratio

η_B as the single input parameter and is therefore well established. For a more comprehensive review on this topic, we the reader is referred to the corresponding literature, e.g. Ref. [6].

Shortly, after this time the temperature of the universe fell below the mass of electrons and positrons and their abundances became exponentially suppressed. Therefore the entropy stored in these particles had to be transferred to the thermal bath. Moreover, since the neutrinos had decoupled from the thermal bath around a temperature of 1 MeV, this entropy increase of the photon sector did not affect the neutrinos and therefore the temperature of photons has afterwards been higher than the temperature of the neutrinos.

As the temperature was in the eV range the free electrons and protons started to form Hydrogen atoms and quickly all free charges vanished. This time is referred to as recombination and is accompanied by the decoupling of the photons, which could now freely propagate due to the lack of free charge. This lead to the cosmic microwave background (CMB), which we can still observe today. Due to the red-shift the photons had to endure since then, the temperature of the CMB is today approximately 2.73 K (cf. e.g. Ref. [7]).

Independently, the energy density stored in matter became comparable to the radiative energy density around the time of recombination. Due to the different scaling laws (cf. Eq. (1.24)) the universe was thereafter matter dominated and structure formation started, which finally resulted in the galaxies, stars, and planets, which we can observe today.

In its very late history ($z \leq 0.5$), our universe seems to have started an age of accelerated expansion, as implied by several independent astrophysical data sets. This fact requires a new form of energy, which is often referred to as dark energy. It will be discussed in some more detail in section 1.7. For this section, we restrict ourselves to the statement that, today, we live in a universe which is well described by the so-called ΛCDM model, i.e. a flat universe that is very homogeneous and isotropic on large scales and whose energy density is composed of baryonic matter, dark matter, and vacuum energy due to a (effective) cosmological constant. Recent best-fit values for the respective energy densities are $\Omega_\mathrm{b} = 0.04$, $\Omega_\mathrm{dm} = 0.20$, and $\Omega_\Lambda = 0.76$ [5].

So far, we have only reviewed the history of our universe since BBN. Since, it is unlikely that the universe started with this epoch, the previous times are of course also interesting. However, going to earlier and earlier times bares a serious problem: due the rising temperatures we discussed earlier, we will sooner or later encounter epochs, in which the relevant energies on our way backwards in time will be beyond the energy scales accessible in experiment, today. Therefore, we do not have any experimentally established knowledge about the physics governing these times.

On the other hand, this also has the benefit that the early universe might give us some hints about physics far beyond the reach of our experiments. Examples for periods that are likely to have taken place at such early times are inflation

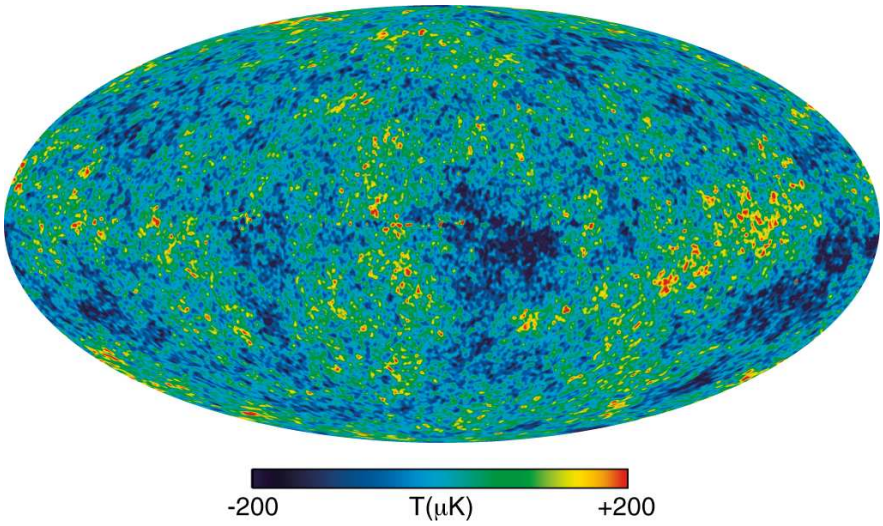

Figure 1.1: *The "Internal Linear Combination" (ILC) map of CMB anisotropies from 3-year WMAP data [8].*

and baryogenesis, which we will discuss in section 1.6 and chapter 4, respectively. Nevertheless, one needs to keep our limited knowledge about these energies in mind and be cautious with one's assumptions about the universe at these early stages.

1.5 The Cosmic Microwave Background

In section 1.2 it was stated that the homogeneity of the CMB can be taken as an indication for the homogeneity and isotropy of our universe (see also section 1.4). However, one cannot only gain valuable information from the isotropy of the CMB, but also from its anisotropies shown in Fig. 1.1. In particular, these fluctuations are important data sources for the determination of the baryon density and the dark energy of our universe. This section therefore briefly discusses the CMB anisotropies and the inferred data that we will use at later points.

Let us first consider some of the physical reasons for CMB anisotropies. The earliest causes for these fluctuations are the so-called primary fluctuations, which include the following three imprints of the region where the respective photons were last scattered (see e.g. Refs. [9–11]):

(a) photons emitted from regions of higher density will (on average) have shorter wave-lengths, due to the higher temperatures in these regions,

(b) photons that were last scattered in a potential well experienced an additional gravitational red-shift,

(c) photons last scattered by matter with a non-zero peculiar velocity (i.e. the velocity with respect to the cosmic rest frame) will receive a Doppler shift.

For angles larger than one degree, the biggest contribution to the anisotropies comes from a combination of points (a) and (b) in this list and is referred to as the Sachs-Wolfe effect [12]. Such large angles can be used to probe modes that are bigger than the Hubble scale at the time of decoupling.

However, in the context of this thesis we are more interested in the anisotropies corresponding to smaller angles. In this context, it is a good approximation to assume that, just before the time of decoupling, our universe was made up of non-relativistic dark matter and a baryon-photon plasma. This plasma can be treated as a perfect fluid, and it can therefore perform acoustic oscillations. Due to point (c) in the above list, these oscillations, then, leave their imprint on the anisotropies of the CMB, which can be observed on smaller angles.

Several cosmological parameters will therefore have an impact on the corresponding fluctuations (cf. e.g. Ref. [10]), as the acoustic oscillations depend on the respective sound horizon, which, in turn, depends mainly on Ω_{dm} and Ω_{b}. Additionally, the angle under which we can observe the fluctuations today depends on the behavior of the scale factor since decoupling, and in the ΛCDM-model therefore on Ω_Λ and Ω_{m}.

Hence, fitting these parameters (and several others) to the three year WMAP data, Ref. [5] finds the best-fit values $\Omega_{\mathrm{b}} = 0.04$, $\Omega_{\mathrm{dm}} = 0.20$, and $\Omega_\Lambda = 0.76$ under the assumption of a flat universe.

We see therefore that CMB data indicates that our universe is dominated by dark energy today. Additionally, we can also infer the size of the baryon asymmetry parameter n_B from this data set, if we assume that there is effectively no antimatter in the universe (cf. chapter 4).

1.6 Inflation

Even though the big bang model described so far, nicely explains the behavior of our universe, there are still several conceptual problems that concern the initial conditions of the ΛCDM-model.

These problems include (cf. e.g. Ref. [13]),

- **the flatness problem:**
  The Friedmann equation (1.25) can be rewritten in the form $\Omega - 1 = k/(aH)^2$. Using Eq. (1.30) we see that the term $1/(aH)^2$ becomes larger and larger in a radiation or matter dominated universe. This implies that the universe becomes less and less flat if $k \neq 0$, which, in turn, indicates a fine-tuning problem for our scenario, since only very small deviations from a flat universe at initial times would allow us to observe a universe which is still rather flat, today.

- **the horizon problem:**
  As we already mentioned in section 1.2, the cosmic microwave background is very isotropic. However, the causally connected region at the time of last scattering only takes up an angle of approximately one degree in the sky. Therefore, the isotropy over the full sky cannot be explained within a radiation and matter dominated universe.

- **unwanted relics:**
  If the universe was initially very hot, the production rate of magnetic monopoles during the spontaneous breaking of grand unified theories and the production rate of gravitinos (cf. chapter 4) in super-gravity theories would have become large and corresponding effects should typically have been observed.

We see that the initial conditions of the ΛCDM model have to face challenges of rather different nature. It is therefore amazing that all these different conceptual problems (and several more) can be solved by a phase of accelerated expansion in the early universe [14–17]. Such a period is called an inflationary phase, or simply inflation. In particular, such a phase would imply $\ddot{a} > 0$, which would decrease the term $1/(aH)^2$ during this period, thereby solving the flatness problem. Also, the horizon problem would be solved, since the blow-up of the scale factor a would expand a formerly causally connected patch of our universe over the (almost) complete horizon and the homogeneity of the CMB would therefore no longer be a mystery. Finally, unwanted relics would also be diluted away during such a period, due to the fact that their density is proportional to a^{-3} or even a^{-4}, if they are relativistic and in thermal equilibrium.

As we already stated in the context of Eq. (1.27), an accelerated expansion requires an equation-of-state parameter $\omega < -1/3$. In the simplest case, this is realized by a scalar field ϕ, the so-called inflaton, with potential $V(\phi)$ in the following way.

We first note that he energy density of the inflaton is given by

$$\rho_\phi = \frac{1}{2}\dot{\phi}^2 + V(\phi)\,, \tag{1.39}$$

whereas its pressure p_ϕ is given by

$$p_\phi = \frac{1}{2}\dot{\phi}^2 - V(\phi)\,. \tag{1.40}$$

We therefore see, that the condition $\frac{1}{2}\dot{\phi}^2 \ll V(\phi)$, which implies a slowly rolling scalar field, naturally leads to $\omega = -1$ and thereby to an inflationary phase of our universe, if ϕ is the dominating energy source of the universe.

Since the equation of motion for the inflaton is given by the Euler-Lagrange equation

$$\ddot{\phi} + 3H\dot{\phi} + \frac{\mathrm{d}V}{\mathrm{d}\phi} = 0\,, \tag{1.41}$$

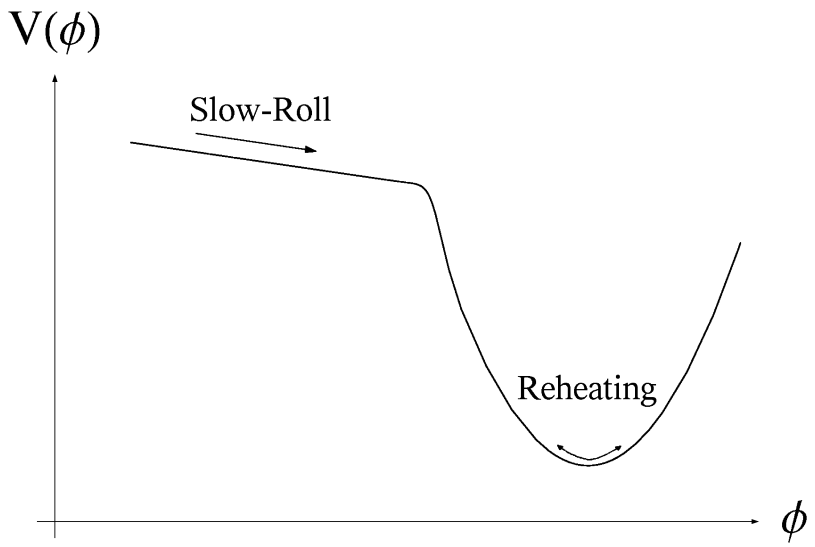

Figure 1.2: *This figure shows the qualitative potential of an inflaton field. During early times the field slowly roles down the flat part of the potential, which leads to an effective cosmological constant and thereby to a period of accelerated expansion. Later on the inflaton performs damped oscillations in the potential well and coherently produces particles.*

a slow-roll of ϕ can easily be achieved by a flat enough potential of the inflaton.

However, as the universe must not remain in an inflationary phase for all times, the potential must become steeper later on. Further, since the universe is effectively empty after an inflationary phase, it is typically assumed that, afterwards, the inflaton undergoes damped oscillations in a potential well, thereby coherently producing particles (cf. Ref. [18]). A qualitative picture of a typical inflaton potential can also be found in Fig. 1.2, which helps to illustrate the different phases of inflation. This period of coherent particle production in inflationary scenarios is referred to as reheating, and the maximal temperature after inflation in a universe dominated by radiation is referred to as the reheating temperature. It is important to note that this is not necessarily the maximal temperature after inflation, since the universe might also be in a matter dominated phase at the beginning of the reheating phase due to the oscillations of the inflaton (this depends on the exact shape of the potential).

The reheating temperature is a very important parameter in the potential history of our universe, since it may not have been to too high to avoid the re-production of the unwanted heavy relics that have been washed out by the accelerated expansion. On the other hand, there are also lower bounds on this parameter from BBN and, potentially, from baryogenesis scenarios (cf. chapter 4). Moreover, if the decay rate of the inflaton is given by Γ_ϕ, the reheating temperature can be easily estimated by the relation $\Gamma_\phi = H$ and Eq. (1.33), which yields $T_r \approx (10\Gamma_\phi M_{\rm Pl})^{1/2}$ (cf. e.g. Ref. [19]).

For completeness, let us also mention that we mainly followed the historic motivation for an inflationary period of our universe in this section. Today, the most important aspect of inflationary scenarios is often considered to be the generation of initial inhomogeneities from quantum fluctuations of the inflaton field. These lead to density fluctuations and form the seeds of structure formation at later times. The statistical properties of these fluctuations can be tested via the CMB and large scale structure and have been found to match the predictions of a slow-roll inflation to high accuracy [5].

1.7 Dark Energy

As one can see from the discussion in section 1.5, CMB measurements indicate that our universe is has recently started an era of accelerated expansion. Moreover, independent measurements from type-Ia supernovae also yield similar results, e.g. Ref. [20]. This expansion is usually ascribed to the fact that our universe is dominated by vacuum energy. However, the origin of this vacuum energy, which is also referred to as dark energy, is still a mystery. One of the most pressing questions in this context is, if this energy is due to a cosmological constant or to a dynamical Λ-term in the Einstein equations.

In this section will therefore briefly discuss some of the conceptual problems of dark energy due to a cosmological constant. This is followed by a brief introduction to quintessence fields as a possible alternative.

More comprehensive reviews on dark energy can be found in Refs. [10, 11, 21], on which some of the presented materials is also based.

1.7.1 Conceptual Problems of a Cosmological Constant

As discussed in the previous section, cosmological data implies a vacuum energy density of the order of the critical density ρ_c. Of course, one can now simply assign the corresponding parameter value to the cosmological constant in the Einstein equations and thereby describe the behavior of our universe, as it is done in the ΛCDM-model.

However, several conceptual problems remain in this case:

- Since Λ is a constant from general relativity and its mass dimension is four, one would naively expect $\rho_\Lambda \sim M_{\mathrm{Pl}}^4$ for a non-zero Λ, which would also be implied by naive considerations of the vacuum corrections of the standard model of particle physics. However, the measured value is more than one hundred orders of magnitude smaller. This is most likely the largest discrepancy between the expected non-zero value of a physical parameter and its observed size. While supersymmetric theories expect somewhat smaller values for ρ_Λ due to the cancellations of diagrams, the discrepancy still remains huge in this case.

- From the various phase transitions of the universe (e.g. electro-weak symmetry breaking, chiral symmetry breaking) one would expect contributions to the cosmological constant of the order $M_{\rm br}^4$, where $M_{\rm br}$ is the respective breaking scale. Somewhat miraculously, these contributions are also canceled by Λ to a very high precision.

- It is also far from obvious, why the scale of dark matter and the scale of dark energy are of the same order of magnitude today, since their scaling laws are completely different, if the vacuum energy is due to a cosmological constant (cf. Eq. (1.24)). This problem is also referred to as the cosmic coincidence problem.

- In addition to the previous point, it is also striking that dark energy has only very recently become the dominant energy form in our universe. This issue is referred to as the "why now?" problem, and it has also not been solved so far.

1.7.2 Quintessence

Quintessence offers a very simple solution to the cosmic coincidence problem described in the last section. Namely, if the vacuum energy density scales in the same way as the dominating background energy density, both of them can naturally be of the same order of magnitude for large periods in the history of our universe. In the case of quintessence, the time-dependence of the vacuum energy is due to the dynamics of a homogeneous, scalar field ϕ, and in the following we will try to understand the corresponding dynamics a little better.

If the potential of ϕ is $V(\phi)$, the Euler-Lagrange equations of motion yield

$$\ddot{\phi} + 3H\dot{\phi} + \frac{\mathrm{d}V}{\mathrm{d}\phi} = 0\,, \tag{1.42}$$

similarly to the inflaton.

Further, the corresponding energy density and pressure are also given by

$$\rho_\phi = \frac{1}{2}\dot{\phi}^2 + V(\phi) \quad \text{and} \quad p_\phi = \frac{1}{2}\dot{\phi}^2 - V(\phi)\,, \tag{1.43}$$

respectively, whereas the dynamics of the universe are now determined by the relation

$$H^2 = \frac{8\pi G}{3}(\rho_{\rm bgr} + \rho_\phi)\,, \tag{1.44}$$

where $\rho_{\rm bgr}$ is the energy density due to the dominant background component.

In general the behavior of the quintessence field and the universe is now fixed by $V(\phi)$ and its initial conditions. For a certain class of potentials, however, the late-time dynamics of the system are relatively independent of the initial conditions of ϕ. This is a typical feature of quintessence fields.

A typical example for such a potential is given by the exponential form [22–26]

$$V(\phi) = V_0 \exp\left(-\lambda \frac{\phi}{m_{\mathrm{Pl}}}\right) , \tag{1.45}$$

with the reduced Planck mass $m_{\mathrm{Pl}} \equiv 1/\sqrt{8\pi G}$.

In a universe in which the equation of state of the background is given by $p_{\mathrm{bgr}} = \omega_{\mathrm{bgr}} \rho_{\mathrm{bgr}}$ this potential yields two so-called attractor solutions, where $\Omega_\phi \equiv \rho_\phi / \rho_c$ approaches a fixed value at late times for a large range of initial conditions.

In particular,

- for $\lambda^2 > 3(\omega_{\mathrm{bgr}} + 1)$ the energy density of the quintessence field mimics the behavior of the background with $\omega_\phi = \omega_{\mathrm{bgr}}$ and $\Omega_\phi = 3(\omega_{\mathrm{bgr}} + 1)/\lambda^2$,
- whereas for $\lambda^2 < 3(\omega_{\mathrm{bgr}} + 1)$ the scalar field gets to dominate the universe, i.e. $\Omega_\phi = 1$, with $\omega_\phi = -1 + \lambda^2/3$.

However, both of these parameter ranges face serious conceptual problems. In the first case, the energy density due to the quintessence field becomes naturally comparable to the background energy density. However, since it also has the same equation of state, it cannot serve as a dark energy candidate. This is not a problem for the second parameter range, in which case the quintessence field can be a suitable dark energy candidate. However, since the quintessence field should not dominate the universe too early, the initial conditions would need to be fine-tuned in such a way that there would hardly be any benefits with respect to a cosmological constant.

Luckily, the benefits of both scenarios can be combined, if one uses a potential of the form

$$V(\phi) = V_0 \left(e^{-\alpha \frac{\phi}{m_{\mathrm{Pl}}}} + e^{-\beta \frac{\phi}{m_{\mathrm{Pl}}}}\right) , \tag{1.46}$$

where α is in the first parameter range and β is in the second one.

This way the described problems of each single parameter range can be avoided, as the quintessence field now behaves like radiation and matter during early times, but like a cosmological constant (or similar to it) at late times, as required by observation.

However, one should, however mention that, in this case, V_0 would need to be adjusted in such a way, that the energy density due to the quintessence field is of the observed order of magnitude at late times. Since ρ_ϕ does not change much, once the quintessence field starts to dominate the universe, V_0 might need to be fine-tuned. Therefore, one might say that this potential only yields a possible explanation for the cosmic coincidence problem but not for the "why now?" problem.

Another option for a quintessence potential that yields a sub-dominant behavior at early times and a dominant behavior at late times is given by an inverse

power law [23, 27], i.e.

$$V(\phi) = \frac{M^{4+\alpha}}{\phi^{\alpha}} \,. \tag{1.47}$$

This kind of potential has the advantage that the energy density of the corresponding field only scales approximately as the dominant background component. In fact, the field can eventually gets to dominate the universe just by itself, in this case. However, the late time behavior of such a universe is dominated by an equation of state parameter $\omega > -0.8$ [27] which conflicts with the recent bound from combined astronomical data of $\omega \leq -0.86$ at the 3σ level [28].

Independently of the exact shape of the quintessence potential, there are also strong constraints on the couplings of the quintessence field to SM particles. This is due to the fact that our universe is governed by an effective cosmological constant at late times, which implies $H^2 \approx G\,V(\phi)$, if the vacuum energy is due to a quintessence field. Since $M_{\rm Pl}$ is typically the only dimensionful quantity in the quintessence potential, the mass of the quintessence field at late times is approximately given by $m_\phi^2 = \mathrm{d}^2V(\phi)/\mathrm{d}\phi^2 \approx H^2$. Therefore, quintessence would be a very light field today, which would mediate new long-range interactions between the SM particles, if the corresponding couplings were strong enough. Yet, since such interactions have not been observed these couplings must obviously be very small.

Chapter 2

The Standard Model of Particle Physics

The standard model of particle physics (SM) describes remarkably well all observed interactions of the known elementary particles, with the exception of neutrino masses. In this chapter we will briefly review this model as far as it will be needed in the course of this thesis.

For a more comprehensive introduction to the topic the reader is referred to the standard textbooks, e.g. Refs. [29,30]. Further background material on spinors in relativistic field theories will also be discussed in the context of neutrino masses in chapter 3.

2.1 Gauge Symmetries

The SM is based on the idea of symmetries. In particular, it assumes that the fields describing the fermionic particles are arranged in representations of symmetry groups and that the corresponding action of the system is invariant under the respective transformations. More exactly, the symmetry group of the SM is the group $SU(3)_c \times SU(2)_L \times U(1)_Y$ and its fermions transform under this group according to table 2.1.

It is further assumed that these symmetries are so-called gauge symmetries, which implies that the corresponding transformations can independently be performed at each point in space-time. Since simple derivative terms in the Lagrangian are not invariant under such transformations, one needs to introduce a covariant derivative, in this case, denoted by the operator

$$D_\mu \equiv \partial_\mu + \mathrm{i}\, g_s\, G_\mu^a\, \mathrm{F}_a + \mathrm{i}\, g\, W_\mu^a\, \mathrm{T}_a + \mathrm{i}\, g'\, B_\mu\, \frac{Y}{2}\,. \tag{2.1}$$

Here, F_a, T_a, and Y are the generators of the respective symmetries $SU(3)_c$, $SU(2)_L$, and $U(1)_Y$, that still depend on the particular representation on which

				$SU(3)_c$	$SU(2)_L$	$U(1)_Y$
ℓ_{Li}	$\begin{pmatrix}\nu_{eL}\\ e_L\end{pmatrix}$	$\begin{pmatrix}\nu_{\mu L}\\ \mu_L\end{pmatrix}$	$\begin{pmatrix}\nu_{\tau L}\\ \tau_L\end{pmatrix}$	1	2	-1
e_{Ri}	e_R	μ_R	τ_R	1	1	-2
q_{Li}	$\begin{pmatrix}u_L\\ d'_L\end{pmatrix}$	$\begin{pmatrix}c_L\\ s'_L\end{pmatrix}$	$\begin{pmatrix}t_L\\ b'_L\end{pmatrix}$	3	2	$\frac{1}{3}$
u_{Ri}	u_R	c_R	t_R	3	1	$\frac{4}{3}$
d_{Ri}	d_R	s_R	b_R	3	1	$-\frac{2}{3}$

Table 2.1: *The fermions of the SM and their respective behaviors under the symmetry transformations of the corresponding gauge groups.*

they are applied. Further, G^a, W^a, and B are the gauge fields, which ensure that the covariant derivative of a multiplet transforms like the multiplet itself under the respective symmetry transformations, and g_s, g, and g' are the coupling constants of the respective gauge groups.

The gauge invariant kinetic term of any fermionic multiplet ψ_L of left-handed Weyl spinors can then be written as

$$\mathcal{L}_{\text{kin,f}} = \psi_L^\dagger \, \mathrm{i}\sigma^\mu \, D_\mu \, \psi_L \,, \tag{2.2}$$

while the kinetic term of any multiplet ψ_R of right-handed Weyl spinors reads

$$\mathcal{L}_{\text{kin,f}} = \psi_R^\dagger \, \mathrm{i}\, \bar{\sigma}^\mu \, D_\mu \, \psi_R \,, \tag{2.3}$$

with $\sigma^\mu \equiv (1, \vec{\sigma})$, $\bar{\sigma}^\mu \equiv (1, -\vec{\sigma})$, and σ_i being the Pauli matrices.

In order to also have kinetic terms for the gauge fields we introduce the corresponding field-strength tensors. In particular, for the fields G^a, this tensor is given by

$$G^a_{\mu\nu} \equiv \partial_\mu G^a_\nu - \partial_\nu G^a_\mu - g f_{abc} G^b_\mu G^c_\nu \,, \tag{2.4}$$

where f_a^{bc} are the structure constants of $SU(3)_c$ defined by

$$\left[\mathrm{F}^a, \mathrm{F}^b\right] = \mathrm{i} f_{abc} \mathrm{F}^c \,. \tag{2.5}$$

The kinetic terms for the corresponding gauge fields can then be written as

$$\mathcal{L}_{\text{kin,b}} = -\frac{1}{4} G^a_{\mu\nu} G^{\mu\nu a}. \tag{2.6}$$

The field-strength tensors $W^a_{\mu\nu}$ and $B_{\mu\nu}$ and the kinetic terms for W^μ and B^μ can be obtained in the same manner and are therefore not presented explicitely.

2.2 The Higgs Mechanism

Since all of the fermions in the SM are massive (with the exception of neutrinos), its Lagrangian obviously needs to contain mass terms for these fields (cf. section 3.1.1). However, due to the fact that the SM gauge symmetries do not allow for explicit mass terms for these particles, the SM contains an additional scalar field ϕ, the so-called Higgs field, which transforms as $(1, 2, 1)$ under the SM symmetry group $SU(3)_c \times SU(2)_L \times U(1)_Y$. In the following we will briefly sketch, how this introduction leads to masses for the fermions.

We first note that the transformation behavior of the Higgs fields allows for corresponding kinetic and potential terms in the Lagrangian density, which can be written as

$$\mathcal{L}_{\text{Higgs}} = (D_\mu \phi^\dagger)(D^\mu \phi) - V(\phi)\,, \tag{2.7}$$

with the Higgs potential

$$V(\phi) = -\mu^2 \phi^\dagger \phi + \lambda (\phi^\dagger \phi)^2\,. \tag{2.8}$$

In the SM, it is, now, assumed that $\mu^2, \lambda > 0$, which leads to the fact the potential has a global minimum at $|\langle\phi\rangle|^2 = \mu/\sqrt{2\lambda}$. As the gauge freedom allows us to put $\langle\phi\rangle = (0, \phi_0)^T$ everywhere, with $\phi_0 \geq 0$, one can see that the the vacuum expectation value (VEV) of the Higgs field breaks the gauge symmetry of the SM down to $SU(3)_c \times U(1)_{em}$, where $U(1)_{em}$ is a sub-group of $SU(2)_L \times SU(1)_Y$. This effect is also referred to as spontaneous symmetry breaking.

In addition to the kinetic and potential terms, the transformation behavior of the Higgs field also allows for Yukawa coupling terms with the SM fermions, which are invariant under the SM gauge symmetries. These terms read

$$\mathcal{L}_{\text{Yuk}} = g^\ell_{ij}\, e^\dagger_{Ri}\, \phi^\dagger\, \ell_{Lj} + g^d_{ij}\, d^\dagger_{Ri}\, \phi^\dagger\, q_{Lj} + g^u_{ij}\, u^\dagger_{Ri}\, \phi^{c\dagger}\, q_{Lj} + \text{h.c.}\,, \tag{2.9}$$

where the Yukawa couplings g^ℓ_{ij}, g^d_{ij},and g^u_{ij} are essentially free parameters of the theory. Moreover, we made use of $\phi^c \equiv -\mathrm{i}\sigma_2 \phi^*$, which is the charge conjugate field of ϕ and transforms in the same way as ϕ under $SU(3)_c \times SU(2)_L$ but has opposite hypercharge (i.e. the charge under the $U(1)_Y$). Now, plugging $\langle\phi\rangle = (0, \phi_0)^T$ into Eq. (2.9), one can see that the Higgs VEV gives masses to the fermions. Even further, plugging it into Eq. (2.7), one can see that the gauge bosons of the spontaneously broken symmetries also acquire masses. In this context, it is interesting to note that the fermion masses are free parameters of the theory due to the newly introduced Yukawa couplings. The masses of the gauge bosons, on the other hand, only depend on the size of the VEV of the Higgs field and on the gauge coupling constants and can therefore not be freely adjusted.

With the addition of the Higgs field, the SM is therefore complete. As we already mentioned, many of the predictions of the SM have so far been observed. Yet, one of its most important components, namely the Higgs field, has not been found yet, and the search for it is therefore still going on. For information on the

already measured parameter values of the SM, namely the couplings constants, the fermion masses, etc., we refer the reader to Ref. [31].

Chapter 3

Neutrino Masses

Neutrinos are the only massless fermions in the standard model. Within the last ten years, however, it has become clear that at least some of them need to be massive in order to explain observational data. This is especially exciting, since neutrinos do not possess any charge, and therefore the nature of their masses might be fundamentally different from that of the other SM particles. Moreover, neutrino masses might also be relevant for baryogenesis, as we will see in section 4.5.

Therefore, we will review some of the theoretical and phenomenological background of neutrino masses in this chapter. In particular, we will briefly review the different possible mass terms for neutrinos as well as neutrino mixing in the first section of this chapter, before presenting the corresponding experimental data in section 3.2. The second part of this chapter will be concerned with the model building aspects of neutrino masses. More precisely, we will introduce family symmetries as a possible explanation for mass hierarchies in section 3.3, while we we will afterwards discuss the see-saw mechanism in four and five dimensions as well as the concept of single right-handed neutrino dominance in section 3.4.

For a comprehensive review on neutrino masses, on which parts of the presented material is based, the reader is referred to Ref. [32].

3.1 Formal Background

3.1.1 Dirac and Majorana Mass Terms

As we already stated in the introduction, neutrinos might have masses that are fundamentally different from the ones of all other known particles. In this subsection, we will therefore briefly review the different kinds of fermionic mass terms in relativistic field-theories.

Let us start with the remark that any relativistic field theory is by definition Lorentz invariant. Furthermore, since the proper orthochronous Lorentz group

is equivalent to the group $SL(2,\mathbb{C})/\mathbb{Z}_2$, the action of any relativistic field theory has to be invariant under the corresponding symmetry transformation.[1]

In this context, we note that there are two two-dimensional representations of $SL(2,\mathbb{C})/\mathbb{Z}_2$, namely

$$\xi \;\rightarrow\; \exp\left(\mathrm{i}\frac{\vec{\sigma}}{2}\cdot\vec{\theta}+\frac{\vec{\sigma}}{2}\cdot\vec{\varphi}\right)\xi\,, \tag{3.1}$$

$$\bar{\eta} \;\rightarrow\; \exp\left(\mathrm{i}\frac{\vec{\sigma}}{2}\cdot\vec{\theta}-\frac{\vec{\sigma}}{2}\cdot\vec{\varphi}\right)\bar{\eta}\,, \tag{3.2}$$

which will be referred to as left- and right-handed Weyl-spinors, respectively. Here, the σ_i are the well-known Pauli matrices, θ is the angle of a corresponding rotation and φ is the rapidity of a corresponding boost.

For completeness, we also remark that $SL(2,\mathbb{C})/\mathbb{Z}_2$ is essentially a product of two $SU(2)$ subgroups, with respect to which the above representations can also be written as $(\frac{1}{2},0)$ and $(0,\frac{1}{2})$. Moreover, $\bar{\xi}\equiv-\epsilon\,\xi^*$ transforms as $(0,\frac{1}{2})$ and $\eta\equiv\epsilon\,\bar{\eta}^*$ as $(\frac{1}{2},0)$, with $\epsilon\equiv\mathrm{i}\sigma_2$.

In order to have a relativistic field theory, we can now combine these spinors to Lorentz invariant terms in the corresponding Lagrangian density. An example therefor are the kinetic terms

$$\xi^\dagger \mathrm{i}\sigma^\mu\partial_\mu\xi \quad\text{and}\quad \bar{\eta}^\dagger\mathrm{i}\bar{\sigma}^\mu\partial_\mu\bar{\eta}\,, \tag{3.3}$$

with $\sigma^\mu\equiv(1,\vec{\sigma})$ and $\bar{\sigma}^\mu\equiv(1,-\vec{\sigma})$.

However, such terms alone can only describe massless fermions. To describe massive particles, we need to add terms to the Lagrangian which are by definition quadratic or bi-linear in the corresponding fields. An example for such a term is given by the so-called Majorana mass term

$$\frac{1}{2}m_M\,\bar{\xi}^\dagger\xi+\text{h.c.}=\frac{1}{2}m_M\,\xi^T\,\epsilon\,\xi+\text{h.c.}\,, \tag{3.4}$$

which can be considered quadratic in ξ or bi-linear in its components.

We can see from Eqs. (3.1) and (3.2) this term is indeed Lorentz-invariant, as we required. However, if some $U(1)$ charge is associated with the field ξ, a Majorana mass term would break the corresponding symmetry, as we easily see from the right-hand side of Eq. (3.4). In such a case, a Majorana mass term would therefore be forbidden.

Hence, a single left-handed field ξ alone cannot describe charged, massive particles. Instead, one needs a second, right-handed field $\bar{\eta}$ for this purpose, with the same charge under the corresponding symmetry group as ξ. In this case, one can write down a so-called Dirac mass term via

$$m_D\,\bar{\eta}^\dagger\xi+\text{h.c.}=m_D\,\eta^T\,\epsilon\,\xi+\text{h.c.}\,. \tag{3.5}$$

[1] $SL(2,\mathbb{C})/\mathbb{Z}_2$ is the group of complex 2×2 matrices with unit determinant, where matrices that differ by a factor of -1 are identified.

In the presence of such a mixing term ξ and $\bar{\eta}$ are no longer eigenstates of the Hamiltonian. However, the mixing disappears, if one combines them into one representation of the Lorentz group. Namely, the so-called Dirac spinor

$$\psi \equiv \begin{pmatrix} \xi \\ \bar{\eta} \end{pmatrix} . \tag{3.6}$$

In this case, the Lagrangian of the corresponding particle can be written in the well-known form

$$\mathcal{L} = \overline{\psi}\, \gamma^{\mu} \partial_{\mu} \psi + m_D\, \overline{\psi} \psi \,, \tag{3.7}$$

with $\overline{\psi} \equiv \psi^{\dagger} \gamma_0$.

Now, we can also see the possible difference of neutrinos with respect to the other SM particles. Namely, since neutrinos are singlets under the unbroken part of the SM gauge group $SU(3)_c \times U(1)_{em}$, their masses might actually be of the Majorana kind, whereas all other mass terms in the SM Lagrangian are Dirac mass terms. In this case, we would only need two degrees of freedom to describe the neutrino fields in spite of their masses. Moreover, the neutrino could be considered as its own anti-particle in this case.

3.1.2 Mixing Matrices

In models with several generations of particles, mixing effects can naturally occur. As such mixings might contain hints about the underlying theory, they are an important topic for model builders, and we will, therefore, review this topic in in the following. In fact, our dicsussion will be quite detailed, as the explicit formulae at the end of this subsection will be needed to understand the concept of single right-handed neutrinos dominance in section 3.4.2.

Let us first consider mxing in case of Dirac fields. Suppose we have several left- and right-handed fields ξ_i and $\bar{\eta}_i$ which all have the same quantum numbers. In this case, we can write down Dirac mass terms for all different combinations of $\bar{\eta}_i$ and ξ_j, namely

$$m_{D,ij}\, \bar{\eta}_i^{\dagger}\, \xi_j + \text{h.c.}\,. \tag{3.8}$$

In general $m_{D,ij}$ is an arbitrary matrix, which can therefore be diagonalized by two unitary matrices U_R and U_L, via

$$U_R^{\dagger} m_D U_L = \text{diag}(m_1, m_2, \dots) \,, \tag{3.9}$$

with $m_i \geq 0$.

If the rest of the Lagrangian is completely symmetric under unitary transformations of the ξ_i and $\bar{\eta}_j$, one can perform a change of basis and the off-diagonal mass-terms can be rotated away. In this case, the matrices U_L and V_R are not physical.

However, in many cases, further interactions are not symmetric under such unitary transformations. In this case, the mixing matrices U_R and U_L are indeed physical and reappear in these interaction terms, if one switches to the physical basis, where all mass matrices are diagonal.

It can also happen (e.g. in the quark sector of the SM), that one may perform a change of basis in the right-handed sector, while one only has the freedom of multiplying different fields with different phases in the left-handed sector. In this case, it is convenient to go to a basis in which Eq. (3.8) becomes

$$\bar{\eta}^\dagger \, V^\dagger \, \mathrm{diag}(m_1, m_2, \dots) V \, \xi + \mathrm{h.c.}\,, \tag{3.10}$$

since this can then be written as

$$\overline{\psi} \, V^\dagger \, \mathrm{diag}(m_1, m_2, \dots) V \, \psi\,, \tag{3.11}$$

if one describes the system by means of Dirac spinors.

In the case of three generations of left- and right-handed particles V can, in fact, be parametrized by three mixing angles θ_{12}, θ_{13}, and θ_{23} and one phase δ via

$$V^\dagger = \begin{pmatrix} c_{12}c_{13} & s_{12}c_{13} & s_{13}e^{-\mathrm{i}\delta} \\ -s_{12}c_{23} - c_{12}s_{23}s_{13}e^{\mathrm{i}\delta} & c_{12}c_{23} - s_{12}s_{23}s_{13}e^{\mathrm{i}\delta} & s_{23}c_{13} \\ s_{12}s_{23} - c_{12}c_{23}s_{13}e^{\mathrm{i}\delta} & -c_{12}c_{23} - s_{12}c_{23}s_{13}e^{\mathrm{i}\delta} & c_{23}c_{13} \end{pmatrix}, \tag{3.12}$$

where $s_{ij} \equiv \sin\theta_{ij}$ and $c_{ij} \equiv \cos\theta_{ij}$.

The possible existence of such a mixing matrix was first discussed in the quark sector [33, 34] and the quark mixing matrix $V^\dagger$ is also referred to as the CKM-matrix.

Let us now consider the case of several left-handed fields ξ_i without any conserved quantum numbers. In this case, we can write down Majorana mass terms for all possible bilinear combinations of ξ_i, namely

$$\frac{1}{2} \, \bar{\xi}_i^{\,T} \, m_{M,ij} \, \epsilon \, \xi_j + \mathrm{h.c.}\,. \tag{3.13}$$

Due to the symmetry $\xi_i^T \epsilon \, \xi_j = \xi_j^T \epsilon \, \xi_i$ only the symmetric part of the arbitrary matrix $m_{M,ij}$ is relevant and therefore it can be considered as a (complex) symmetric matrix. In this case, we can rewrite Eq. (3.13) as

$$\frac{1}{2} \, \xi^T \, U^T \, \mathrm{diag}(m_1, m_2, \dots) \, \epsilon \, U \, \xi + \mathrm{h.c.}\,, \tag{3.14}$$

where U is a unitary matrix. As before it depends on the other parts of the Lagrangian if this matrix is physical or if it can be rotated away.

If neutrino masses are of the Majorana type, one needs two more phases to parameterize the matrix U compared to the parametrization of V (for three neutrinos). Namely, U can be written as

$$U^\dagger = V^\dagger \, \mathrm{diag}(e^{\mathrm{i}\phi_1/2}, e^{\mathrm{i}\phi_2/2}, 1)\,, \tag{3.15}$$

in this case, where ϕ_1 and ϕ_2 are the so-called Majorana phases.

In this context, we also note that, independent of Dirac- or Majorana-type masses, the mixing matrix in the neutrino sector is also referred to as PMNS-matrix [35] (see also Ref. [36]).

With respect to following sections, it will also be helpful to establish a connection between the mixing angles and the eigenvalues of a mass matrix., which we will do in the following. This analysis will be along the corresponding discussion in Ref. [37].

Let us ignore possible CP-violating effects for the moment and assume that the neutrino mass matrix is real. In the context of mixing angles it is further not relevant if the mass matrix is of Dirac- or Majorana-type and we will therefore only refer to the neutrino mass matrix as m_ν. Moreover, m_ν can then be diagonalized by the real, orthogonal mixing matrix V, defined by

$$m_\nu^d = V m_\nu V^T \,, \tag{3.16}$$

with $m_\nu^d \equiv \mathrm{diag}(m_1, m_2, m_3)$ and $m_1 \geq m_2 \geq m_3$.

Disentangling Eq. (3.12), one can, therefore, also write

$$V^T = R_{23} R_{13} R_{12} \,, \tag{3.17}$$

with the three rotations

$$R_{23} \equiv \begin{pmatrix} 1 & 0 & 0 \\ 0 & c_{23} & s_{23} \\ 0 & -s_{23} & c_{23} \end{pmatrix}, \; R_{13} \equiv \begin{pmatrix} c_{13} & 0 & s_{13} \\ 0 & 1 & 0 \\ -s_{13} & 0 & c_{13} \end{pmatrix}, \; R_{12} \equiv \begin{pmatrix} c_{12} & s_{12} & 0 \\ -s_{12} & c_{12} & 0 \\ 0 & 0 & 1 \end{pmatrix}. \tag{3.18}$$

On the other hand, V can also be expressed via the three eigenvectors of m_ν, namely

$$V^T = (\vec{v}_1, \vec{v}_2, \vec{v}_3) \,, \tag{3.19}$$

where each $\vec{v}_i$ is the normalized eigenvector corresponding to the respective eigenvalue m_i.

This yields the relation

$$R_{12}^T R_{13}^T R_{23}^T (\vec{v}_1, \vec{v}_2, \vec{v}_3) = \mathrm{diag}(1, 1, 1) \tag{3.20}$$

and therefore

$$R_{13}^T R_{23}^T \vec{v}_3 = \begin{pmatrix} 0 \\ 0 \\ 1 \end{pmatrix} \quad \text{and} \quad R_{12}^T R_{13}^T R_{23}^T \vec{v}_2 = \begin{pmatrix} 0 \\ 1 \\ 0 \end{pmatrix}, \tag{3.21}$$

from which we can consecutively determine the θ_{ij}, as we will see in the following.

First, we note that R_{23} has to fulfill the relation

$$R_{23}^T \vec{v}_3 = \begin{pmatrix} v_{3,x} \\ 0 \\ \pm\sqrt{v_{3,y}^2 + v_{3,z}^2} \end{pmatrix}, \tag{3.22}$$

where the sign in front of the expression is the same as the one of $v_{3,z}$.

This fixes θ_{23} through

$$\tan(\theta_{23}) = \frac{v_{3,y}}{v_{3,z}}. \tag{3.23}$$

Then, we can fix R_{13} via

$$R_{13}^T \begin{pmatrix} v_{3,x} \\ 0 \\ \pm\sqrt{v_{3,y}^2 + v_{3,z}^2} \end{pmatrix} = \begin{pmatrix} 0 \\ 0 \\ \pm\sqrt{v_{3,x}^2 + v_{3,y}^2 + v_{3,z}^2} \end{pmatrix}, \tag{3.24}$$

which, in turn, leads to

$$\tan(\theta_{13}) = \pm\frac{v_{3,x}}{\sqrt{v_{3,y}^2 + v_{3,z}^2}}. \tag{3.25}$$

In this equation, the sign in front of the expression is again the same as the one of $v_{3,z}$.[2]

Finally, from the relation

$$R_{13}^T R_{23}^T \vec{v}_2 = \begin{pmatrix} c_{13}v_{2,x} - s_{13}(c_{23}v_{2,z} + s_{23}v_{2,y}) \\ c_{23}v_{2,y} - s_{23}v_{2,z} \\ c_{13}(c_{23}v_{2,z} + s_{23}v_{2,y}) + s_{13}v_{2,x} \end{pmatrix}, \tag{3.26}$$

and the second condition in Eq. (3.21) the angle θ_{12} can also be determined through

$$\tan(\theta_{12}) = \frac{\cos(\theta_{13})v_{2,x} - \sin(\theta_{13})[\sin(\theta_{23})v_{2,y} + \cos(\theta_{23})v_{2,z}]}{\cos(\theta_{23})v_{2,y} - \sin(\theta_{23})v_{2,z}}. \tag{3.27}$$

While this is a rather complex expression, we see that it simplifies to the relation

$$\tan(\theta_{12}) \approx \sqrt{2}\frac{v_{2,x}}{v_{2,y} - \tan(\theta_{23})v_{2,z}}, \tag{3.28}$$

if we approximate $c_{13} \approx 1$, $s_{13} \approx 0$ and $c_{23} \approx s_{23} \approx 1/\sqrt{2}$, which agrees well with the experimental data presented in the next section.

[2]Of course, a negative sign of θ_{13} could, in principle, always be absorbed by a CP-phase δ in a more general consideration.

3.2 Neutrino Data

Let us now discuss some of the experimentally determined parameters in the neutrino sector.

As we already mentioned at the beginning of this chapter, neutrinos are massless in the standard model. Up to a certain accuracy this is indeed a good approximation. In fact, the analysis of the spectra in tritium β-decay experiments yields very low upper bounds for the mass of the electron anti-neutrino [38, 39]. In particular, at 95% confidence level Ref. [39] finds

$$m_{\nu_e} \leq 2.3 \text{ eV}. \tag{3.29}$$

From cosmology there comes an even more stringent bound, which limits the sum of all light neutrino masses. In particular, through the analysis of CMB data and further astronomical data sets, Ref. [5], e.g., reports an upper bound of

$$\sum m_\nu \leq 0.66 \text{ eV}, \tag{3.30}$$

also at 95% confidence level. Yet, since this bound is due to CMB data, it is obviously also dependent on our cosmological model.

In spite of these low bounds for neutrino masses, there have been observations that indicate that neutrinos are indeed massive, as we will briefly discuss in the following. As wesaw in section 3.1.2, the neutrino flavor basis does not have to coincide with the eigenvectors of a possible neutrino mass matrix. In this case a pure flavor state will be made up of different mass eigenstates, and these mass eigenstates will interfere differently at different times as a result of the Schrödinger equation. Therefore, a state of some definite flavor might actually evolve to a state of different flavor due to this mixing. In fact, in a two neutrino model with mixing angle θ_0 the transition probability from one pure flavor state to the other one is given by

$$P(\nu_e \to \nu_\mu, t) = \sin^2(2\theta_0) \sin^2\left(\frac{\Delta m^2}{4E} t\right) , \tag{3.31}$$

for relativistic neutrinos with energy E and $\Delta m^2 \equiv m_2^2 - m_1^2$.

As we stated earlier, such transitions have indeed been observed in many experiments, by now, and we, therefore, know that at least two of the neutrinos do have masses. Yet, we also see from Eq. (3.31) that the transition probability in this formula disappears in case of two degenerate neutrinos. This is due to the fact that one can always find coinciding flavor and mass eigenvectors in this case. Therefore, neutrino oscillations can only help to determine mass squared differences and mixing angles but not their absolute mass scale.

Nevertheless, detecting solar, atmospheric, and reactor neutrinos, oscillation experiments have been powerful tools for pinning down neutrino parameters in

the recent past. In particular, in December of 2004, Ref. [40] found through a global fit of neutrino oscillation data the bounds [40]

$$\begin{array}{lcl} \Delta m^2_{21} & = & (7.1 - 8.9) \cdot 10^{-5}\ \mathrm{eV}^2\,, \\ |\Delta m^2_{31}| & = & (1.4 - 3.3) \cdot 10^{-3}\ \mathrm{eV}^2\,, \\ \sin^2\theta_{12} & = & 0.23 - 0.38\,, \\ \sin^2\theta_{23} & = & 0.34 - 0.68\,, \\ \sin^2\theta_{13} & < & 0.051 \end{array} \tag{3.32}$$

on the 3σ level.

While this confirms our earlier statement that at least two of the three neutrinos have tiny masses, it is also noteworthy that the mixing in several of the neutrino sectors is rather large and quite different from the corresponding values in the quark sector.

The data set in Eq. (3.32) was the data that was used during our analysis of the neutrino mass models in chapter 6, and we will therefore mainly refer to this data set in the later parts of this thesis. For completeness, however, we note that in June of 2006, the online version of Ref. [40] was updated and found

$$\begin{array}{lcl} \Delta m^2_{21} & = & (7.1 - 8.9) \cdot 10^{-5}\ \mathrm{eV}^2\,, \\ |\Delta m^2_{31}| & = & (2.0 - 3.2) \cdot 10^{-3}\ \mathrm{eV}^2\,, \\ \sin^2\theta_{12} & = & 0.24 - 0.40\,, \\ \sin^2\theta_{23} & = & 0.34 - 0.68\,, \\ \sin^2\theta_{13} & < & 0.040\,, \end{array} \tag{3.33}$$

which slightly improves the above data set thanks to new experimental data.

3.3 Family Symmetries

For all known types of particles, one has found mass hierarchies among the members of different generations. While these hierarchies can be accommodated by hierarchical Yukawa couplings, their conceptual understanding is still missing. A possible explanation for such hierarchies are family symmetries, which we will briefly review in this section.

Family symmetries were first introduced to explain mass hierarchies in the quark sector [41]. The typical feature of these additional symmetries is that particles of different generations and chiralities transform differently under them. Therefore, they will typically not allow for explicit mass terms of the SM fermions. However, similar to the Higgs mechanism in the standard model (cf. section 2.2), the spontaneous breaking of these symmetries might lead to effective mass terms for these particles. As we will illustrate in the following toy-model, the different transformation properties of particles can then induce a hierarchy among their masses.

Our toy-model contains a left-chiral field ψ_L and a right-chiral field ψ_R, with SM quantum numbers that would allow for an effective mass term of the form

$$g\langle\phi\rangle\psi_R^\dagger\psi_L + \text{h.c.}\,, \tag{3.34}$$

in combination with the SM Higgs field ϕ and some Yukawa coupling constant g. However, we further introduce an additional family symmetry $U(1)_F$, under which ψ_L and ψ_R have the respective family charges q_L and q_R. Obviously, an explicit mass term as in Eq. (3.34) is now forbidden by the family symmetry, if $q_L - q_R \neq 0$. Yet, we also add a scalar field ϕ_F with charge $q_F = 1$ under the new symmetry to the particle content. If this field develops a VEV $\langle\phi_F\rangle$, an effective mass term of the form

$$g\langle\phi\rangle\left(\frac{\langle\phi_F\rangle^*}{M_{\text{NP}}}\right)^{q_L-q_R}\psi_R^\dagger\psi_L + \text{h.c.} \tag{3.35}$$

might arise, where M_{NP} is a scale of new physics.

We see from Eq. (3.35) that differently charged generations of fermions naturally receive mass terms that correspond to different powers of $\langle\phi_F\rangle^*/M_{\text{NP}}$ and are therefore typically of different size. Obviously, similar arguments also work for Majorana mass terms. This mechanism for the creation of hierarchical couplings is also referred to as the the Frogatt-Nielsen mechanism [41].

Let us also note that, in general, family symmetries can be global or local. However, both types yield side-effects that need to be controlled. In particular, in case of a global symmetry the couplings of the newly arising Goldstone boson (familon) due to the broken family symmetry must be small enough (see e.g. Refs. [42–47]), while in the case of a spontaneously broken, local family symmetry possibly emerging anomalies need to be canceled (e.g. by additional heavy particles).

3.4 The See-Saw Mechanism

As we saw in section 3.2, we know by now that at least two of the SM neutrinos have tiny non-zero masses. The smallness of these masses can be elegantly explained within the standard see-saw mechanism [48–50], which we will therefore briefly review in section 3.4.1. This mechanism makes use of the fact that a possible Majorana mass term for right-handed neutrinos is not bounded by the electro-weak scale, which, in turn, can be used to suppress the scale of an effective Majorana mass matrix for the light neutrinos. If combined with the concept of single right-handed neutrino dominance, the see-saw mechanism can even account for light neutrino mass hierarchies and for their observed mixings, as we show in section 3.4.2.

However, since right-handed neutrinos are SM gauge singlets, they might have further interesting features. One of them is the possibility that they might be

able to propagate in more dimensions than the standard model particles. In this case a Kaluza-Klein tower of particles can affect the see-saw mechanism and the standard formulae gets significantly altered, as we will discuss section 3.4.3.

3.4.1 The See-Saw Mechanism in 4D

In the SM, the quantum numbers of the neutrinos (cf. section 2) neither allow for explicit neutrino mass terms nor for renormalizable Yukawa coupling terms between them and the Higgs field. Therefore, the observation of neutrino masses requires an extension of the SM in one or the other way.

A suitable simple extension, in this context, is the addition of three right-handed fermions N_{Ri} with quantum numbers that allow for Yukawa coupling terms between these fermions, the SM neutrinos and the Higgs field. This way neutrinos can aquire masses via spontaneous symmetry breaking, as described in section 2.2. Similarly, to Eq. (2.9), the corresponding terms in the Lagrangian would then be

$$g^{\nu}_{ij}\, N^{\dagger}_{Rj}\, \phi^{c\dagger}\, \ell_{Li} + \text{h.c.}\,. \tag{3.36}$$

Due to the transformation behavior of the left-handed leptons and the Higgs doublet, the requirement that these terms are invariant under the SM symmetries implies that the N_{Ri} are complete singlets under the SM gauge group. Therefore, the complete Lagrangian can also contain a Majorana mass term of the form

$$\frac{1}{2}\,(M^{N}_{ij})^{\dagger}\, N^{T}_{Ri}\,\epsilon\, N_{Rj} + \text{h.c.} \tag{3.37}$$

for these particles.

Rewriting the neutrino sector in a purely left-handed basis ($\nu_{Li}, N^{c}_{Rj} \equiv -\epsilon N^{*}_{Rj}$) we then find one large Majorana mass matrix for these particles, namely[3]

$$\frac{1}{2}(\nu^{T}_{Li}\,\epsilon, N^{cT}_{Rj}\,\epsilon)\begin{pmatrix} 0 & -(m^{T}_{D})_{in} \\ -m^{D}_{jm} & M^{N}_{jn} \end{pmatrix}\begin{pmatrix} \nu_{Lm} \\ N^{c}_{Rn} \end{pmatrix} + \text{h.c.}\,, \tag{3.38}$$

with $m^{D}_{ij} \equiv g^{\nu}_{ij}\,\phi_0$.

Since the size of M^N is not restricted by the electro-weak scale, it can be much larger than m^D. If this is indeed the case, we can diagonalize the above Majorana mass matrix perturbatively and find [48–50] (cf. also Ref. [51] for notation)

$$\frac{1}{2}(\nu'^{T}_{Li}, N'^{cT}_{Rj})\begin{pmatrix} -(m^{T}_{D}M^{-1}_{N}m_{D})_{im} & 0 \\ 0 & M^{N}_{jn} \end{pmatrix}\begin{pmatrix} \nu'_{Lm} \\ N'^{c}_{Rn} \end{pmatrix} + \mathcal{O}(\epsilon^{2}_{D}) + \text{h.c.}\,, \tag{3.39}$$

with $\epsilon_D \equiv ||m_D M_R^{-1}||$ and

$$\begin{pmatrix} \nu'_{Li} \\ N'^{c}_{Rj} \end{pmatrix} \equiv \begin{pmatrix} \mathbb{1}_{im} & (m_D M^{-1}_{N})_{in} \\ (M^{-1}_{N}m^{T}_{D})_{jm} & \mathbb{1}_{jn} \end{pmatrix}\begin{pmatrix} \nu_{Lm} \\ N^{c}_{Rn} \end{pmatrix} + \mathcal{O}(\epsilon^{2}_{D})\,. \tag{3.40}$$

[3] We will use D and N as indeces or superscripts according to convenience in each case.

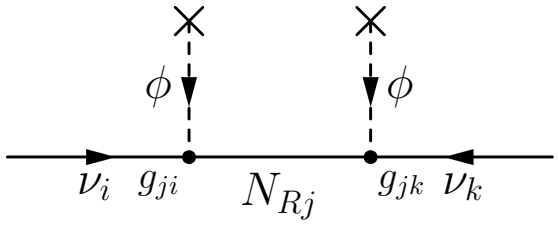

Figure 3.1: *This Feynman graph illustrates the well-known see-saw mechanism, where we work in a basis in which the heavy Majorana mass matrix is diagonal. One can see that the large masses in the propagator of the right-handed neutrinos naturally lead to a suppression of the corresponding light neutrino masses.*

Thus, the effective light neutrino mass matrix is then given by

$$m_\nu = m_D^T M_N^{-1} m_D \,, \tag{3.41}$$

and is therefore typically strongly suppressed with respect to the electro-weak scale. Due to this suppression, it is therefore easy for the see-saw mechanism to explain light neutrino masses.

For later convenience, we further note that the see-saw mechanism can also be illustrated via Feynman diagrams, as shown in Fig. 3.1.

3.4.2 Single Right-Handed Neutrino Dominance

While the see-saw mechanism alone can be a nice explanation for the smallness of the light neutrino masses, it neither explains their (possible) hierarchy nor the sizes of the mixing angles, which differ drastically from the quark sector (cf. section 3.2).

In the framework of the see-saw, single right-handed neutrino dominance [52, 53], on the other hand, can nicely lead to a hierarchy between the heaviest of the light neutrinos and the other two. Additionally, it can account for a large mixing in the 23-sector. If extended to sequential right-handed neutrino dominance [37], it can even account for a complete mass hierarchy in the light neutrino sector as well as a large 12-mixing (under the assumption that the mixing in the 13-sector is small). We will therefore briefly review this topic, here. For convenience, the extension to sequential right-handed neutrino dominance will in the following be tacitly included, when we refer to single-right handed neutrino dominance or SRND.

The main idea behind SRND is rather elementary and therefore quite attractive, since it is simply assumed that the contributions to the effective light neutrino mass matrix by the various right-handed neutrinos are of different sizes. To illustrate the implications of this assumption, let us for the moment work in the basis where the Majorana mass matrix of the right-handed neutrinos is diagonal $M_N = \mathrm{diag}(M_1, M_2, M_3)$ and parameterize the Dirac mass matrix of the

neutrinos by

$$m_D = \begin{pmatrix} a & a' & a'' \\ b & b' & b'' \\ c & c' & c'' \end{pmatrix} \equiv (\vec{u}, \vec{u}', \vec{u}'') \,. \tag{3.42}$$

If we now assume that there is a hierarchy in the right-handed neutrino masses, which is not compensated by the respective Yukawa couplings, we can see from Eq. (3.41) that the light neutrino mass matrix is approximately of rank one. Namely, we find

$$m_\nu \approx M_1^{-1} \begin{pmatrix} a \\ b \\ c \end{pmatrix} \otimes (a, b, c) \,. \tag{3.43}$$

Since a matrix of order one only has one non-zero eigenvalue, this naturally implies a mass hierarchy between the heaviest of the light neutrinos and the other two. Moreover, as the suppressed contribution of the second-lightest heavy neutrino will give mass to the second-lightest light neutrino (and so on), we will typically find the mass ratios of the light neutrinos $m_3 : m_2 : m_1$ to be around $M_1^{-1} : M_2^{-1} : M_3^{-1}$, in this case. Therefore, SRND can naturally induce a hierachy for the light neutrino masses.

We also note that $(a, b, c)^T$ approximately equals the eigenvector of m_ν that corresponds to m_3 (cf Eq. (3.43)). From Eq. (3.23), we, therefore, see that the condition $b \sim c$ ensures a large 23-mixing as required by observation. Additionally, if the first generation Yukawa coupling to the lightest of the heavy neutrinos is suppressed with respect to the other ones (i.e. $a \ll b, c$), Eq. (3.25) tells us that we will also find a tiny mixing in the 13-sector as observed in experiments.

Finally, since the eigenvectors of a symmetric matrix are orthogonal, we can use $\vec{u}' - \langle \vec{u}', \vec{u} \rangle \vec{u} / |\vec{u}|^2$ as an approximation for the eigenvector that corresponds to m_2. Under the assumption of maximal mixing in the 23-sector and vanishing mixing in the 13-sector, Eq. (3.28) then yields $a' \sim b' - c'$ as a condition for a large 12-mixing, as also observed.

Thus, except for the fact that the above discussion seems to imply $a \ll b$ but $a' \sim b'$, which corresponds to different hierarchies of the Yukawa couplings of different generations, the concept of SRND can explains the observed neutrino data rather naturally.

3.4.3 The See-Saw Mechanism in 5D

Even though the see-saw mechanism in four dimensions is a very attractive explanation for small neutrino masses due to its simplicity, it is not necessarily the end of the story. A possible extension of this mechanism is its five dimensional realization, where right-handed neutrinos can propagate in an additional dimension. In this case, each mode of the Kaluza-Klein tower will contribute to the

mass of the light neutrinos. Based on the work of Refs. [54–57] we will give a brief introduction to this topic, here, similarly to our discussion in Ref. [58].

Our model is set in five-dimensions, where the SM particles live in a four-dimensional sub-space, also referred to as 3-brane. Further, the extra dimension is compactified on an orbifold $S^1/\mathbb{Z}_2$ with radius R. (cf. appendix A), where the coordinates on the brane will be denoted by x^μ, while the extra-dimensional coordinate will be denoted by y.

The behavior of the SM particles is determined by the usual four-dimensional Lagrangian density of the SM $\mathcal{L}_{\rm SM}$

$$S_{\rm SM} = \int d^4x\, dy\, \mathcal{L}_{SM}\, \delta(y) \tag{3.44}$$

and possible couplings to particles living in the bulk, which we will specify during the course of this section.

Now, we introduce three additional SM gauge singlets Ψ_i, that can propagate in the extra dimension, and define the corresponding charge conjugate fields Ψ_i^c through the relation

$$\Psi_i^c \equiv \begin{pmatrix} 0 & \epsilon \\ \epsilon & 0 \end{pmatrix} \Psi_i^* \,. \tag{3.45}$$

Under the parity transformation $P_5 : y \to -y$ the Ψ_i are assumed to transform as

$$P_5 \Psi_i = \gamma_5 \Psi_i \,. \tag{3.46}$$

Neglecting their couplings to the SM for the moment, their most general behavior can then be described by the bulk action

$$S_{\rm bulk} = \int d^4x\, dy\, \left[\overline{\Psi}_i i\gamma^\alpha \partial_\alpha \Psi_i - \frac{1}{2}(M^S_{ij} \overline{\Psi^c}_i \Psi_j + M^V_{ij} \overline{\Psi^c}_i \gamma_5 \Psi_j + \text{h.c.}) \right] , \tag{3.47}$$

with the scalar-like Majorana mass M^S and vector-like Majorana mass M^V.[4]

As we already mentioned, one can additionally allow for Yukawa coupling terms between Ψ and the SM. These are given by

$$S_{\rm brane} = \int d^4x\, dy\, \left[-\frac{g_{ij}}{\sqrt{M_5}} \overline{\Psi}_i P_L \phi^{c\dagger} \left((0,0), \ell_j^T \right)^T + \text{h.c.} \right] \delta(y) + S_{\rm SM} \ , \tag{3.48}$$

where M_5 is a new mass scale and the g_{ij} are the usual Yukawa coupling constants. Further, we denoted the SM fields as in chapter 2. Later on, one can see that M_5 will be the suppression scale that leads to small neutrino masses, and therefore we assume it to be rather heavy. Its actual size will also depend on the size of the various Yukawa coupling constants. If one wishes to make the

[4] As in similar cases before, we will write S and V as indeces or superscripts according to convenience in each case.

considered models more restrictive, one can additionally assume M_5 to be the five-dimensional Planck scale, in which case M_5 and the four-dimensional Planck scale M_4 are typically taken to be related through the radius R of the extra dimension by $M_5^3 R \approx M_4^2$ [59, 60].

Due to these Yukawa couplings, the Higgs VEV $\langle\phi\rangle = (0, \phi_0)^T$ then yields Dirac mass terms for the left-handed SM neutrinos ν_j and the two lower components of Ψ_i. Further, the above transformation rules (Eq. (3.46)) allow us to write

$$\Psi_i(x,y) = \frac{1}{\sqrt{\pi R}} \begin{pmatrix} \frac{1}{\sqrt{2}}\Psi_{R,i}^{(0)}(x) + \sum_{n=1}^{\infty} \cos(ny/R)\, \Psi_{R,i}^{(n)}(x) \\ \sum_{n=1}^{\infty} \sin(ny/R)\, \Psi_{L,i}^{(n)}(x) \end{pmatrix}, \tag{3.49}$$

where $\Psi_{R/L,i}^{(n)}(x)$ are right- and left-handed Weyl spinors, respectively.

If we now perform the integration over the fifth dimension in the action, the part responsible for neutrino masses becomes

$$\begin{aligned} S = \quad & \int d^4x \left[\sum_{n=0}^{\infty} \hat{\Psi}_{R,i}^{c(n)\dagger} i\sigma^\mu \partial_\mu \hat{\Psi}_{R,i}^{c(n)} + \sum_{n=1}^{\infty} \Psi_{L,i}^{(n)\dagger} i\sigma^\mu \partial_\mu \Psi_{L,i}^{(n)} \right. \\ & + \left(\sum_{n=1}^{\infty} \frac{n}{R} \hat{\Psi}_{R,i}^{c(n)T} \epsilon \Psi_{L,i}^{(n)} + \frac{g_{ij}\phi_0}{\sqrt{2\pi R M_5}} \hat{\Psi}_{R,i}^{c(0)T} \epsilon\, \nu_j + \sum_{n=1}^{\infty} \frac{g_{ij}\phi_0}{\sqrt{\pi R M_5}} \hat{\Psi}_{R,i}^{c(n)T} \epsilon\, \nu_j \right. \\ & - \sum_{n=0}^{\infty} \frac{1}{2} (M_{S,ij}^* + M_{V,ij}^*) \hat{\Psi}_{R,i}^{c(n)T} \epsilon \hat{\Psi}_{R,j}^{c(n)} \\ & \left. \left. - \sum_{n=1}^{\infty} \frac{1}{2} (-M_{S,ij} + M_{V,ij}) \Psi_{L,i}^{(n)T} \epsilon \Psi_{L,j}^{(n)} + \text{h.c.} \right) \right] + S_{\text{SM}} \ , \end{aligned} \tag{3.50}$$

where $\hat{\Psi}_{R,i}^{c(k)} \equiv -\epsilon(\Psi_{R,i}^{(k)})^*$ is the left-handed Weyl spinor corresponding to the right-handed $\Psi_{R,i}^{(k)}$.

In the completely left-handed basis $(\nu, \hat{\Psi}_{R,i}^{c(0)}, \dots, \Psi_{L,i}^{(n)}, \hat{\Psi}_{R,i}^{c(n)}, \dots)$ we can therefore combine all neutrino mass terms to one large Majorana mass matrix, namely

$$\begin{pmatrix} 0 & -m_D/\sqrt{2} & \cdots & 0 & -m_D & \cdots \\ -m_D^T/\sqrt{2} & M_S^* + M_V^* & \cdots & 0 & 0 & \cdots \\ \vdots & \vdots & \ddots & \vdots & \vdots & \ddots \\ 0 & 0 & \cdots & -M_S + M_V & -n/R & \cdots \\ -m_D^T & 0 & \cdots & -n/R & M_S^* + M_V^* & \cdots \\ \vdots & \vdots & \ddots & \vdots & \vdots & \ddots \end{pmatrix}, \tag{3.51}$$

with the Dirac mass $m_{D,ij} \equiv g_{ji}\phi_0/\sqrt{\pi R M_5}$.[5]

[5]For reasons of convenience, the indices in this definition have been switched.

The exact diagonalization of this matrix is a non-trivial task, but if m_D is small enough compared to M_S or M_V one can make a perturbative approach. To quantify this condition, we first define the Majorana sub-matrix

$$M_n^{\rm sub} \equiv \begin{pmatrix} -M_S + M_V & -n/R \\ -n/R & M_S^* + M_V^* \end{pmatrix} \tag{3.52}$$

for each pair $\Psi_{L,i}^{(n)}, \hat{\Psi}_{R,j}^{c(n)}$, which, in turn, enables us to define the perturbation parameters

$$\eta_0 \equiv -(M_0^{\rm sub})^{-1} \frac{m_D^T}{\sqrt{2}}, \quad \eta_n \equiv -(M_n^{\rm sub})^{-1} \begin{pmatrix} 0 \\ m_D^T \end{pmatrix}, \tag{3.53}$$

with $M_0^{\rm sub} \equiv (M_n^{\rm sub})_{22}$.

Since the see-saw is a sum over an infinite amount of states in this case, it is not enough to require $||\eta_i|| \ll 1$. Instead, we make the more stringent constraint

$$\eta^2 \equiv ||\eta_0||^2 + \sum_{n=1}^{\infty} ||\eta_n||^2 \ll 1\,. \tag{3.54}$$

If this condition is fulfilled, we can make a change of basis defined by

$$\hat{\Psi}_R^{c(0)'} \equiv \hat{\Psi}_R^{c(0)} + \eta_0 \nu\,, \tag{3.55}$$

$$\begin{pmatrix} \Psi_L^{(n)'} \\ \hat{\Psi}_R^{c(n)'} \end{pmatrix} \equiv \begin{pmatrix} \Psi_L^{(n)} \\ \hat{\Psi}_R^{c(n)} \end{pmatrix} + \eta_n \nu\,, \tag{3.56}$$

$$\nu' \equiv \nu - \eta_0^\dagger \hat{\Psi}_R^{c(0)} - \sum_{n=1}^{\infty} \eta_n^\dagger \begin{pmatrix} \Psi_L^{(n)} \\ \hat{\Psi}_R^{c(n)} \end{pmatrix}, \tag{3.57}$$

with implicit flavor indices.

Then, the mass part of the Lagrangian is, to leading order, given by

$$\mathcal{L}_{\rm mass} = -\frac{1}{2}\nu'^T m' \epsilon \nu' - \frac{1}{2}\hat{\Psi}_R^{c(0)'T} M_0^{\rm sub} \epsilon \hat{\Psi}_R^{c(0)'} - \frac{1}{2}\sum_{n=1}^{\infty} \begin{pmatrix} \Psi_L^{(n)'} \\ \hat{\Psi}_R^{c(n)'} \end{pmatrix}^T M_n^{\rm sub} \begin{pmatrix} \epsilon \Psi_L^{(n)'} \\ \epsilon \hat{\Psi}_R^{c(n)'} \end{pmatrix} + \text{h.c.}\,, \tag{3.58}$$

with the light neutrino mass matrix

$$m' \equiv -\frac{1}{2} m_D (M_0^{\rm sub})^{-1} m_D^T - \sum_{n=1}^{\infty} (0,\, m_D)\, (M_n^{\rm sub})^{-1} \begin{pmatrix} 0 \\ m_D^T \end{pmatrix}. \tag{3.59}$$

In the case $M_V = 0$, we can additionally make the transformation

$$U^T M_S U \equiv \text{diag}(M_1^S, M_2^S, M_3^S)\,, \tag{3.60}$$

with $M^S \geq 0$, which leads to the light neutrino mass matrix.

$$m' = -m_D U^* \frac{\pi R}{2} \begin{pmatrix} \coth(\pi M_1 R) & 0 & 0 \\ 0 & \coth(\pi M_2 R) & 0 \\ 0 & 0 & \coth(\pi M_3 R) \end{pmatrix} U^\dagger m_D^T \,. \tag{3.61}$$

Accordingly, for $M_S = 0$, one finds

$$m' = -m_D U^* \frac{\pi R}{2} \begin{pmatrix} \cot(\pi M_1 R) & 0 & 0 \\ 0 & \cot(\pi M_2 R) & 0 \\ 0 & 0 & \cot(\pi M_3 R) \end{pmatrix} U^\dagger m_D^T \,, \tag{3.62}$$

with $U^T M_V U \equiv \mathrm{diag}(M_1^V, M_2^V, M_3^V)$ and $M_i^V \geq 0$ in this case.

These are the five-dimensional extensions of the see-saw formula for the models we will consider in chapters 6 and 7. Aside from the (hyperbolic) cotangent functions, the biggest difference compared to the standard case is the fact that the suppression scale of the light neutrino masses is typically not given by the masses of the heavy singlets, in this case, but by the scale M_5, as we also mentioned earlier. This can be seen, if we note that $m_D \propto (RM_5)^{-1/2}$, which implies the cancellation of the compactification scale in Eqs. (3.61) and (3.62).

Chapter 4

Baryogenesis

The observation that our universe seems to be almost solely made up of baryons and no anti-baryons is also called the baryon asymmetry of our universe (BAU). Moreover, its (potential) transition from a baryon symmetric to a baryon asymmetric one is referred to as baryogenesis.

Since baryogenesis is one of the central topics of this thesis, we will consider it in this section more deeply. We will therefor first discuss the observational evidence for a baryon asymmetry in our part of the universe in section 4.1. This will be followed by some general remarks on baryogenesis in section 4.2 and a discussion of sphaleron processes in section 4.3. In the subsequent sections, we will then focus on several popular baryogenesis scenarios, namely GUT-baryogenesis, baryogenesis via leptogenesis, and Affleck-Dine baryogenesis. Our treatment of baryogenesis via leptogenesis will be more detailed than the treatment of the other scenarios, as we will use large parts of the corresponding analysis in our treatment in chapter 7.

More comprehensive reviews on baryogenesis can also be found in Refs. [61,62].

4.1 The Baryon Asymmetry of our Universe

Before focusing on baryogenesis itself, we will briefly review some of the observations that seem to indicate that our universe is indeed baryon-asymmetric. Therefor our treatment will be based on the corresponding discussions in Refs. [1, 63].

Let us first start with several observations of our immediate vicinity in the universe. For this purpose, we note that the fact that no anti-matter has been found on earth obviously implies that our planet is made up of matter. As we do not observe annihilation radiation from solar winds and the other planets, one can further infer that all other planets in our galaxy consist of matter. And, since solar cosmic rays seem to imply that our sun is also made up of matter, we can deduce that at least the visible part of our galaxy seems to consist almost purely of baryons.

Moreover, the fact that we do not observe a γ-ray flux from nearby galaxy clusters is evidence that these clusters are also maximally baryon-asymmetric. Of course, this could also mean that a cluster solely consists of anti-matter. However, the possibility of a baryon-symmetric universe consisting of regions of matter and regions of anti-matter seems to be excluded by the observed value of the baryon-density, which we will discuss a little later in this section. Here, we only note that a separation of matter and anti-matter that would lead to the observed baryon density would have had to take place around the time when the temperature of the universe was 38 MeV. Otherwise, the annihilation of matter and anti-matter would not allow for a large enough (anti-)baryon-density. Yet, at such early times a causally connected region contained only 10^{-7} solar masses, whereas a lower bound for the separation scale would be given by the discussed galaxy clusters which contain 10^{14} solar masses. This indicates that also the observed galaxy clusters consist almost purely of matter, and we conclude that the visible part of our universe appears to be maximally baryon-asymmetric.

Due to the thermal abundance of anti-matter in the early universe the asymmetry was not always maximal and one therefore usually quantifies the baryon asymmetry in terms of the net baryon-to-photon ratio η_B or baryon-to-entropy ratio n_B, given by

$$\eta_B \equiv \frac{n_b - n_{\bar{b}}}{n_\gamma} \quad \text{and} \quad n_B \equiv \frac{n_b - n_{\bar{b}}}{s}\,, \tag{4.1}$$

respectively, where $n_b(n_{\bar{b}})$ is the (anti-)baryon density. We also note that these quantities are related by $\eta_B = 7.04\, n_B$ after recombination.

If our universe does not contain anti-matter, it is sufficient to measure the baryon density in order to determine the exact value of the baryon asymmetry. We can therefore use the fact that the CMB anisotropies are dependent on the baryon asymmetry as we discussed in section 1.5. In fact, some of the most precise measurements of the BAU come from a combination of CMB data, large scale structure, and Lyman α forest. In particular, at 1σ-confidence level Ref. [64] finds

$$\eta_B = 6.1^{+0.3}_{-0.2} \cdot 10^{-10}\,, \tag{4.2}$$

while there are also also independent constraints on this number from big bang nucleosynthesis which yield comparable results (cf. e.g. [65]).

4.2 Basics of Baryogenesis

The fact that the universe which we observe today is baryon-asymmetric can have several reasons. The simplest possibility is, of course, that the universe has always been baryon-asymmetric. While this option does not seem very attractive from a symmetry point of view, it has to be considered a realistic option. Another possibility is, of course, that the universe started from a baryon-symmetric initial

state and subsequently underwent a phase during which an asymmetry between baryons and anti-baryons has been created. As we already mentioned, such a process is referred to as baryogenesis.

While a period of baryogenesis is already attractive due to symmetry arguments, it is also required by inflational models. This can be ascribed to the fact that inflation basically yields an empty universe at the end of its phase of accelerated expansion, where all existing particles have been strongly diluted. As an empty universe is necessarily baryon-symmetric, the requirement for a period of baryogenesis is evident in this case.

Due to these strong motivations for such a period, baryogenesis has been an active field of research for the last decades and is still extensively studied. In fact, already forty years ago Sakharov pointed out three general conditions for a baryogenesis scenarios, the so-called Sakharov conditions [66]:

- **Baryon number violation:** This is, of course, an obvious condition for any scenario in which a true baryon asymmetry is created, since the creation of baryons does not allow baryon number to be a conserved quantum number.

- **C- and CP-violation:** Here, C and CP stand for charge conjugation and charge conjugation combined with a parity transformation, respectively. In the case in which these quantities were conserved, particles and anti-particles would be generated at the same rates, even if baryon number was violated. Therefore, the same amounts of matter and anti-matter would be produced, which, obviously, contradicts the definition of a baryogenesis process.

- **Deviation from thermal equilibrium:** This condition can be explained by the fact that thermal equilibrium requires a maximization of entropy, which, in turn, implies the vanishing of all chemical potentials that correspond to non-conserved quantum numbers. Additionally, we note that in any relativistic quantum field theory particles and anti-particles have the same masses due to the CPT-theorem. Therefore, thermal equilibrium would imply the same abundances of particles and anti-particles, which again conflicts with the definition of a baryogenesis process.

It is important to note that, even though the SM already features baryon number violation (cf. section 4.3) and C- and CP-violation (through the Yukawa couplings), it cannot generate the observed baryon asymmetry of our universe by itself. Therefore, baryogenesis requires an extension of the SM and can be considered as a test for possible new physics.

Let us also briefly mention that there exist models that realize an evolution of our universe from a baryon symmetric initial state to the one we observe today, without respecting all of the Sakharov conditions. One possibility, in this context,

is the option that we actually live in a baryon-symmetric universe with hidden anti-baryons. An example for such a model is given in Ref. [67], and the model considered in chapter 5 is also related to this idea. Additionally, the condition of thermal non-equilibrium can be evaded in models where CPT-invariance is effectively broken. A corresponding example is given in Ref. [68], where this happens due to early universe effects that can also be interpreted as the source of additional chemical potential terms [61].

4.3 Sphalerons

As we already mentioned in the previous section baryon number (B) and lepton number (L) are violated within the SM. While the corresponding processes are strongly suppressed today and will most likely never be observed, the situation was dramatically different in the early universe, where so-called sphaleron processes [69, 70] might have played a key role. We will therefore briefly discuss this topic in this section, based on the reviews in Ref. [62, 71].

Even though B and L are conserved in the SM on the classical level, certain quantum effects do not obey the corresponding symmetries. Therefore, B and L are so-called anomalous symmetries.

In fact, these anomalies are a part of the aftermath of the famous Adler-Bell-Jackiw anomaly [72,73], which is a result of the breakdown of the chiral symmetry in chiral gauge theories. In particular, for a gauge group G with coupling constant g_G and corresponding field-strength tensor $G^a_{\mu\nu}$, the Adler-Bell-Jackiw anomaly leads to different divergences of the left- and right-chiral currents, namely

$$\begin{aligned} \partial_\mu \bar{\psi}_L \gamma^\mu \psi_L &= -c_L \frac{g^2}{32\pi^2} G^a_{\mu\nu} \tilde{G}^{a\mu\nu} \\ \partial_\mu \bar{\psi}_R \gamma^\mu \psi_R &= +c_L \frac{g^2}{32\pi^2} G^a_{\mu\nu} \tilde{G}^{a\mu\nu} \end{aligned} \tag{4.3}$$

where we used the chiral fields $\psi_{L/R} \equiv P_{L/R}\psi$ and the dual tensor $\tilde{G}^{a\mu\nu} \equiv \epsilon^{\mu\nu\alpha\beta} G^a_{\alpha\beta}/2$. Here, $\epsilon^{\mu\nu\alpha\beta}$ is the totally antisymmetric tensor with $\epsilon^{0123} = 1$. Further, the c_L and c_R depend on the representation of ψ_L and ψ_R.

Let us also define the baryon and lepton currents of the SM

$$J^B_\mu = \frac{1}{3} \sum_q \psi_q \gamma_\mu \psi_q \quad \text{and} \quad J^L_\mu = \frac{1}{3} \sum_\ell \psi_\ell \gamma_\mu \psi_\ell \,, \tag{4.4}$$

where the ψ_q are the quark fields, and the ψ_ℓ are the lepton fields.

Plugging all the baryons and leptons of the standard model into Eq. (4.3), the different transformation behavior of left- and right-chiral fields under $SU(2)_L \times U(1)$ then yields

$$\partial^\mu J^B_\mu = \partial^\mu J^L_\mu = \frac{3}{32\pi^2} \left(-g^2 W^a_{\mu\nu} \tilde{W}^{a\mu\nu} + g'^2 B_{\mu\nu} \tilde{B}^{\mu\nu} \right) . \tag{4.5}$$

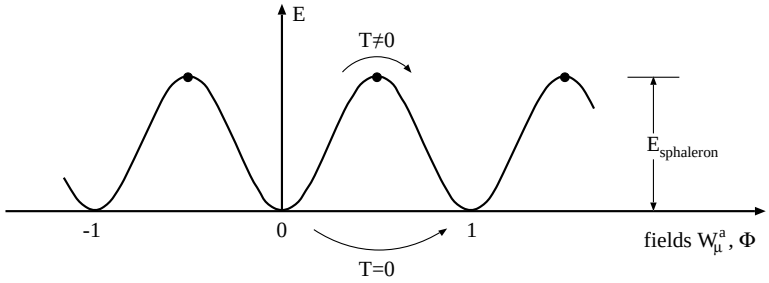

Figure 4.1: *This picture from Ref. [71] shows a qualitative slice through the vacuum structure of the SM, where different ground states correspond to different values of $B + L$. To get from one vacuum to another, the fields can either tunnel through the energy barrier or take the way over the barrier, if they are thermally excited.*

We see that baryon and lepton number are indeed violated in the SM. However, we also see that their difference $B - L$ is still conserved by the corresponding processes.

One can further show, that a change of $B + L$ in the context of Eq. (4.5) corresponds to a transition from one ground state of the SM to another. In fact, one can show that the SM possesses an infinite number of ground states with different values of $B + L$ (cf. Fig. 4.1). To get from one vacuum to another, the system can either tunnel through the energy barrier in between them or take the way over this barrier through thermal effects. The tunneling process is also referred to as an instanton process, whereas the latter one is called a sphaleron process.[1] Both of these processes are strongly suppressed today and will most likely never be observed. However, when the temperature of the universe was above the scale electro-weak scale, sphaleron processes might have been frequently observable [69, 70]. In fact, before the time of electro-weak symmetry breaking, the only relevant scale for these processes was given by the magnetic screening length $4\pi/(g^2T)$. On dimensional grounds one can therefore estimate the transition rate of such processes to be

$$\Gamma_{\mathrm{Sph}} = \kappa \left(\frac{4\pi}{g^2 T}\right)^4 . \tag{4.6}$$

The factor κ is a dimensionless constant, which has to be calculated within a more quantitative analysis. Ref. [74], e.g., finds $\kappa = (25.4 \pm 2.0) g^2/(4\pi)$. One can therefore see, that sphalerons were in equilibrium during large parts of the history of our universe.

In this context, we also note that the fact that sphalerons were in equilibrium at early times implies the erasure of any $B + L$ asymmetry in the left-handed sector during those periods. Additionally, it also implies the partial conversion

[1] Here, one should note that the corresponding transition point with the highest energy is also sometimes called sphaleron.

of a potential lepton asymmetry in this sector into a baryon asymmetry during these epochs. Indeed, these effects will be important in sections 4.4 and 4.5, respectively.

It is however also important to keep in mind that sphalerons only couple to the left-handed particles of the standard model, which implies that they are not necessarily able to erase $B + L$ asymmetries in the right-handed sector. This, in turn, depends on the size of the corresponding Yukawa couplings and the interested reader is referred to Refs. [75–77] for deeper discussions of this topic.

4.4 GUT Baryogenesis

Due to the fact that grand unified theories arrange baryons and leptons in the same multiplets, they naturally provide baryon number violating mechanisms. The possibility for baryogenesis in the context of such theories was, therefore, first addressed in Ref. [78] and in the context of heavy particle decays in Ref. [79] (see also [80]). In this section we will briefly discuss some of the features and problems of the corresponding scenarios. We will therefor remain on a qualitative level, since many of the technicalities of baryogenesis via the decay of heavy particles are similar to the corresponding details of leptogenesis, which will be discussed in section 4.5.

Further, reviews on GUT baryogenesis can be found in Refs. [61, 62, 81].

As we already mentioned, baryon number violation is natural in GUT models, since baryons and leptons appear in the same multiplets. Therefore, the decay of heavy bosons (e.g. Higgs bosons) with complex couplings to the SM fermions, can easily produce a baryon asymmetry. The abundance of such particles after inflation might therefore be the reason for the observed BAU. However, it is important to note that a $B - L$ conserving GUT can generally not produce the observed BAU, since it can only produce $B+L$ asymmetries, which will be erased by the sphaleron processes introduced in the previous section.

A more general problem of GUT-baryogenesis scenarios is the required abundance of the heavy bosons after inflation. Typically, the reheating temperatures in inflationary scenarios are lower than the GUT scale, which is around 10^{16}GeV, and therefore the corresponding production rate is suppressed after reheating. Additionally, typical inflaton masses are around 10^{14}GeV, which implies that they cannot simply decay into the heavy bosons that would yield GUT baryogenesis.

A possible solution to this problem might be given by the fact that the reheating temperature is not necessarily the maximal temperature after the inflationary period, but only the temperature at which the universe starts to be radiation dominated, as we also discussed in section 1.6. In fact, the temperature at the earliest stages of reheating might have been high enough to produce those particles. Of course, they would have been subsequently diluted, however, this dilution might have been weak enough for these particles to remain significantly abundant [82].

Yet, more stringent bounds on the reheating temperature come from supergravity theories. These theories feature a fermionic super-partner of the graviton, which is called the gravitino. The couplings of the gravitino are fixed by the theory and their production rate can therefore be calculated. Though suppressed by the Planck scale, these rates can indeed put strong constraints on the reheating temperature, since an overproduction of them can over-close the universe (if stable) or destroy the successful predictions of BBN (if unstable). Typical bounds for the reheating temperature T_r in these models are $T_r \lesssim 10^9 - 10^{10}$GeV [83,84], which make the combination of supergravity and GUT baryogenesis rather difficult.

However, a possible way out of this potential problem might be given by the so-called pre-heating phase, which can take place during the early times of re-heating [85, 86]. During this phase, the oscillations of the inflaton field can resonantly induce oscillations of another scalar condensate X, which may be heavier than the inflaton. These oscillations can already re realized on the classical level. In fact, the oscillations of the inflaton make the mass of X time-dependent in this case and there will be short periods when the mass of X (or some of its modes) is lighter than the inflaton. Ref. [87] illustrates that this effect can also be used to populate heavy states in the context of GUT baryogenesis.

Therefore, GUT baryogenesis might still have been the way in which the BAU we observe today has been produced.

4.5 Leptogenesis

Baryogenesis via leptogenesis is another very attractive baryogenesis scenario, since it can be realized naturally in see-saw models (cf. section 3.4) without any further additions to the particle content. In this case, the addition of heavy right-handed neutrinos to the SM would help to explain two previously unrelated phenomena, namely the smallness of neutrino-masses and the baryon-asymmetry of our universe.

Since standard thermal leptogenesis is an important topic in the context of this thesis, we will review here in more detail than the other models. Therefore, we will first introduce some basic material and notation in section 4.5.1. Afterwards, we will consider weak wash-out and strong wash-out scenarios in sections 4.5.2 and 4.5.3, respectively. This will be followed by a discussion of the parameter bounds from leptogenesis in section 4.5.4 and further complications of our treatment in section 4.5.5.

4.5.1 Fundamentals of Standard Thermal Leptogenesis

In this subsection, we will discuss the groundwork of standard thermal leptogenesis with three hierarchical heavy neutrinos as it has been developed in

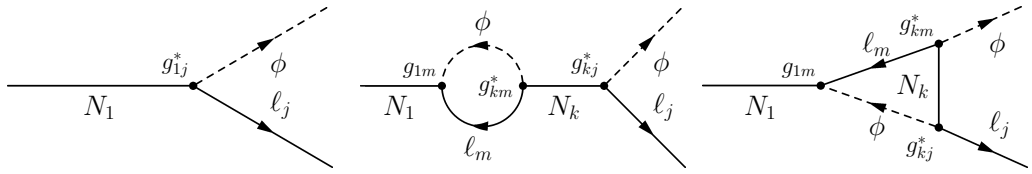

Figure 4.2: *This figure shows the relevant decay-diagrams for standard thermal leptogenesis, where the interference of the tree-level diagram with the wave-function- and the vertex-correction diagram can lead to CP violation and a net lepton-number production per decay. Due to the different projection operators, the wave-function-correction diagram with charge flow in the opposite direction can only contribute at higher orders of M_1/M_k.*

Refs. [88–96].

As leptogenesis is a feature of see-saw scenarios, we will work with the same Lagrangian as in section 3.4. However, for simplicity we will now work in the basis, where the right-handed neutrino mass matrix is diagonal. For the neutrinos, the mass and Yukawa part of the Lagrangian then read

$$\mathcal{L} = -\frac{1}{2} M_i N_{Ri}^{cT} \epsilon \, N_{Ri}^c - g_{ij} N_{Ri}^{cT} \phi^{c\dagger} \epsilon \, \ell_j + \text{h.c.}\,. \tag{4.7}$$

The addition to the SM Lagrangian does not only render masses for the light neutrinos, it also opens new possibilities for CP-violation, e.g. in the decay of the heavy singlets, where an interference of tree-level and loop diagrams, as illustrated in Fig. 4.2, can lead to different decay rates for the channels $N \to \ell\phi^*$ and $N \to \bar{\ell}\phi$.[2] In particular, in the case of hierarchical heavy neutrinos ($M_1 \ll M_2 \ll M_3$) one finds for the decay of N_1 [97]

$$\varepsilon_1 \equiv \frac{\Gamma(N_1 \to \ell_L + \phi) - \Gamma(N_1 \to \bar{\ell}_L + \phi^*)}{\Gamma(N_1 \to \ell_L + \phi) + \Gamma(N_1 \to \bar{\ell}_L + \phi^*)} \approx -\frac{3}{16} \sum_k \frac{\text{Im}\left[(gg^\dagger)_{1k}^2\right]}{(gg^\dagger)_{11}} \frac{M_1}{M_k}\,. \tag{4.8}$$

One can show that there exists an upper bound for this parameter [98, 99], the so-called the Davidson-Ibarra bound, which is given by[3]

$$|\varepsilon_1| \lesssim \frac{3M_1}{16\pi\phi_0^2}(m_3 - m_1) \;\approx\; \frac{3M_1\Delta m_{31}^2}{16\pi\phi_0^2(m_3 + m_1)}\,, \tag{4.9}$$

where $\Delta m_{31}^2 = m_3^2 - m_1^2$ is approximately the atmospheric mass-squared difference as given in section 3.2. We see that Eq. (4.9) is maximized by $m_1 = 0$, which leads to $\Delta m_{31}^2 = m_3^2$ and

$$|\varepsilon_1| \lesssim \frac{3}{16\pi}\frac{M_1 m_3}{\phi_0^2} \approx 10^{-7}\left(\frac{m_3}{0.05\text{eV}}\right)\left(\frac{M_1}{10^9\text{GeV}}\right) \tag{4.10}$$

[2] In the following we will drop the subscript R from N_R for simplicity.

[3] In the original paper, there is an additional factor of 2, due to the supersymmetric treatment.

where m_3 is fixed around 0.05 eV due to $m_1 = 0$ and the oscillation data from section 3.2.

As pointed out in Ref. [96] the possible CP-violation within $\Delta L = 1$ scatterings, such as $t^c q \to N\ell^c$, can also be relevant for leptogenesis. There, it is also shown that the CP-asymmetry produced in these scatterings exactly equals the asymmetry of the corresponding decay processes presented here in the case of hierarchical heavy singlets.

Let us now consider the dynamics of the scenario. At the beginning, we assume to be in a homogenous and isotropic universe (possibly after an inflationary period) dominated by the SM particles, which are all in thermal equilibrium with temperature T_r. The initial abundance of the right-handed neutrinos is typically assumed to be zero. Their abundance at later times is then determined by the differential Boltzmann equation [2, 89]

$$\frac{dN_{N_1}}{dz} = -\frac{1}{Hz}(\Gamma_D + \Gamma_{\Delta L=1})\left(N_{N_1} - N_{N_1}^{\text{eq}}\right), \tag{4.11}$$

where $z \equiv M_1/T$ is effectively a reparametrization of time in a background dominated universe. Further, N_{N_1} is the average abundance of the lightest right-handed neutrinos in a comoving volume containing one photon at early times, $N_{N_1}^{\text{eq}}$ is the corresponding value for the equilibrium distribution, Γ_D is their decay rate, and $\Gamma_{\Delta L=1}$ the rate for the $2 \leftrightarrow 2$ scattering processes, which violate lepton number by one (e.g. $N_1\ell \leftrightarrow tq$). The explicit values we used for the different reaction rates can be found in appendix C.

The other important equation in this context is the one for the $B - L$ asymmetry N_{B-L} [2, 89, 96] in the same comoving volume

$$\frac{dN_{B-L}}{dz} = -\frac{1}{Hz}\left[\varepsilon_1(\Gamma_D + \Gamma_{\Delta L=1})\left(N_{N_1} - N_{N_1}^{\text{eq}}\right) + \Gamma_W N_{B-L}\right], \tag{4.12}$$

where Γ_W is the reaction rate for wash-out processes consisting of inverse decays and $\Delta L = 1, 2$ scattering. Again, the explicit formulae for these rates that were used for the corresponding calculations can be found in appendix C.

As discussed in section 4.3, sphalerons will partially transform a lepton asymmetry into a baryon asymmetry until the baryons until the entropy of the corresponding system is maximized. In the present case, the baryon asymmetry per comoving volume will, therefore, be given by $N_B = 28/79 \cdot N_{B-L}$ [69, 70]. To find the final baryon asymmetry per photon (η_B) in a late universe, one needs to consider this sphaleron factor as well as the late time production of photons. Combining these two effects, we find (cf. Ref. [95])

$$\eta_B \approx 10^{-2} N_{B-L}(t \to \infty). \tag{4.13}$$

Equations (4.11) and (4.12) have been extensively studied numerically as well as analytically in Refs. [88–96]. In the analysis of the following sections, we will

rather aim at understanding the corresponding dynamics qualitatively, which will also help to conceive the effect of many decaying neutrinos in chapter 7. For reasons of simplicity we will therefor adopt the treatment of Ref. [95] and restrict our considerations at this point to decays, inverse decays and $\Delta L = 1$ scatterings involving the top quark. We will discuss further effects, which we will neglect in our treatment, in section 4.5.5.

Yet, before discussing the dynamics explicitely, we will introduce some convenient definitions. Let us first define the so-called decoupling parameter

$$K = \frac{\Gamma_D(z \to \infty)}{H(z=1)}\,. \tag{4.14}$$

This parameter gives a measure for the decoupling of the right-handed neutrinos at the time when their equilibrium abundances start being suppressed with respect to photons. One can therefore use this parameter to distinguish between the so-called weak wash-out and strong wash-out regime ($K \ll 1$ and $K \gg 1$, respectively).

In this context, it can also be helpful to denote K in terms of

$$K \equiv \frac{\tilde{m}_1}{m_*}\,, \tag{4.15}$$

where the parameter

$$\tilde{m}_1 \equiv \frac{(m_D m_D^\dagger)_{11}}{M_1} \tag{4.16}$$

is also called the effective neutrino mass and the quantity

$$m_* \equiv \frac{16\pi^{\frac{5}{2}}\sqrt{g_*}}{3\sqrt{5}}\frac{\phi_0^2}{M_{\rm Pl}} \approx 10^{-3}\text{eV} \tag{4.17}$$

is referred to as the equilibrium neutrino mass.

4.5.2 The Weak Wash-out Scenario

As we already mentioned, we distinguish between two quite distinct parameter regions of thermal leptogenesis, namely the weak and strong wash-out regimes. In this section we will discuss the first of these scenarios, while the latter will be discussed in the following section.

In weak wash-out scenarios ($K \ll 1$) none of the relevant processes that involve right-handed neutrinos is in equilibrium at early times. Therefore, the thermal production of neutrino singlets will be strongly suppressed and only a small number of them will be produced. Moreover, since all wash-out effects involve right-handed neutrinos, these are also strongly suppressed.

Yet, the wash-out effects are still crucial, as the decays and inverse decays of the heavy singlets (as well as the corresponding $\Delta L = 1$ scatterings) create

$B-L$ asymmetries of opposite sign but equal magnitude. If there were no wash-out processes, this would imply that the asymmetry which is created during the production of the heavy singlets would be exactly canceled by the asymmetry generated by the decay of these particles, later on. Therefore, it is important to note that the wash-out processes erase a small part of the first asymmetry, in spite of being suppressed. This small deficit then prevents the complete cancellation of the asymmetries and is responsible for the observed BAU at later times.

With this picture in mind, let us now be more quantitative and make some rough estimations for the reaction rates mainly based on dimensional analysis.

As long as $T \gtrsim M_1$, we can approximate the relevant reaction rates by [2]

$$\Gamma_D \approx \Gamma_{ID} \approx \frac{1}{8\pi}(gg^\dagger)_{11} M_1 \frac{M_1}{T} \tag{4.18}$$

$$\Gamma_{\Delta L=1} \approx \frac{|g_{\text{top}}|^2}{\pi^3}\,(gg^\dagger)_{11}\,T \overset{z\sim 1}{\approx} \frac{1}{2}\Gamma_D \tag{4.19}$$

where g_{top} is the Yukawa coupling constant of the top quark.

Due to their weak couplings, the right-handed neutrinos will not reach equilibrium abundance until this value is strongly suppressed. Therefore, we can assume $N_{N_1}^{\text{eq}} - N_{N_1} \approx N_{N_1}^{\text{eq}}$, while $z \lesssim 1$. Using Eq. (4.11) we can then approximate

$$N_{N_1}(z \approx 1) \approx \frac{(\Gamma_D + \Gamma_{\Delta L=1}) N_{N_1}^{\text{eq}}}{H(z=1)} \approx K\,, \tag{4.20}$$

with $N_{N_1}^{\text{eq}} = 3/4$ (at early times).

Without wash-out effects the $B-L$ asymmetry around this time would, therefore, be $N_{B-L}(z=1) \approx -\varepsilon_1 N_{N_1}(z \approx 1)$. However, due to our earlier considerations the wash-out effects cannot be neglected, and in order to find the fraction of the produced asymmetry that has been washed out, we approximate the wash-out rate to be

$$\Gamma_W \approx \frac{1}{2}\Gamma_{ID} + \frac{2}{3}\Gamma_{\Delta L=1} \approx \Gamma_D\,. \tag{4.21}$$

Here, the factor $1/2$ is due to the fact that half of the inverse decays will finally end up as the original states and the factor $2/3$ pays tribute to the fact that the s-channel processes are suppressed more strongly in the weak wash-out before $z \approx 1$ [89].

Using Eq. (4.12), we can now estimate the $B-L$ asymmetry ate $z=1$ by (cf. Ref. [95])

$$N_{B-L}(z=1) \approx \varepsilon_1 N_{N_1}(z \approx 1) \exp\left(-\frac{\Gamma_W}{H(z=1)}\right) \tag{4.22}$$

$$\approx \varepsilon_1 K \exp(-K) \tag{4.23}$$

$$\approx \varepsilon_1 K\,(1-K)\,. \tag{4.24}$$

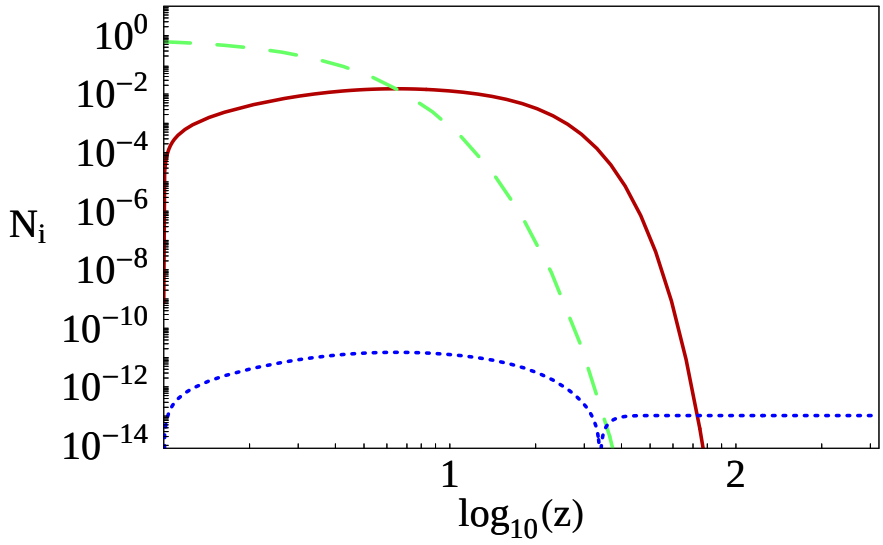

Figure 4.3: *This figure illustrates a typical example for a weak wash-out scenario. The green/dashed line shows the equilibrium density of the right-handed neutrinos N_1 per relativistic photon $N_{N_1}^{eq}$, while the red/solid line shows their actual density as calculated from the Boltzmann equations N_{N_1}. The blue/dotted line shows the absolute amount of the corresponding $B-L$ asymmetry $|N_{B-L}|$. Further, the graph was plotted with the parameters $K = 10^{-2}$, $M_1 = 10^7$ GeV, $T_r = M_1$, $\varepsilon_1 = 10^{-9}$, and a Higgs boson mass of $10^{-1}M_1$ (cf. App. C). One can see that the N_1 states become mainly populated until $z \approx 0.5$ and that the final $B-L$ asymmetry is much smaller than it is around $z \approx 1$ due to the discussed cancellations. For the final value of $|N_{B-L}|$ the numerics yield $1.0 \cdot 10^{-13}$, which agrees well with our approximative value from Eq. (4.25).*

After the temperature has dropped below M_1, inverse decays and $\Delta L = 1$ scatterings will be suppressed and the particles will decay around $H \approx \Gamma_D/2$, which corresponds to $z \approx K^{-1/2}$. As stated earlier, the decaying heavy singlets will then produce an asymmetry of the same amount but opposite sign as the inverse decays and scatterings did, when they populated these states. Therefore the first term in Eq. (4.24) will be exactly canceled, and the final $B-L$ asymmetry then amounts to

$$N_{B-L}(z=\infty) \approx -\varepsilon_1 K^2 \,. \tag{4.25}$$

An example for a numerically calculated solution of the corresponding Boltzmann equations can be found in Fig. 4.3, which supports our approximative treatment and helps to further illustrate the principles of weak wash-out leptogenesis.

4.5.3 The Strong Wash-out Scenario

Let us now consider the strong wash-out scenario, where $K \gg 1$ implies that the relevant processes that include the right-handed neutrinos are in equilibrium at early times, which has several competing effects.

In particular, the strong coupling ensures that the singlets will reach equilibrium abundances and will therefore be present in much larger numbers, at early times, than in the weak wash-out regime. Additionally, the larger wash-out rates lead to the fact that the $B-L$ asymmetry from the production of the singlets will be washed out before they decay again, thereby preventing the cancellation of asymmetries from the previous section.

On the other hand, the large K also leads to the fact that the wash-out processes are still active, when the majority of the singlets decays. Since this means, that the corresponding asymmetry is washed-out, the final asymmetry is only due to the small fraction of particles that decay after the freeze-out of the wash-out processes. Yet, this number is exponentially suppressed, and it is therefore not immediately clear if the strong wash-out regime can yield a larger asymmetry than the weak wash-out regime.

To find an estimate for the final asymmetry in this case, we will again make some approximations. We therefore note that the wash-out processes will get an additional exponential suppression factor after $z \approx 1$, since the right-handed neutrinos now have masses larger than the temperature and need to be produced on-shell in all the wash-out processes considered here.[4] With regard to Eq. (4.21) we therefore find (cf. Ref. [1])

$$\Gamma_W \approx \left(\frac{1}{2} \cdot \frac{1}{8\pi} (gg^\dagger)_{11} M_1 + \frac{|g_{\text{top}}|^2}{\pi^3} (gg^\dagger)_{11} T \right) z^{3/2} e^{-z} \,, \tag{4.26}$$

for $z \gtrsim 1$, which shows that we can neglect the term due to scatterings (the second term in the brackets) at late times.

In a naive approximation, we could assume that the wash-out processes will no longer be in thermal equilibrium and therefore not be able to erase a produced asymmetry when the condition $\Gamma_W \lesssim 2H$ is fulfilled. However, due to the rapid suppression of this term we can make a better approximation, as presented in the following.

As a result of the wash-out processes, the dynamical behavior of an initial asymmetry will be given by

$$\begin{aligned} N_{B-L}(t) &= N_{B-L}(t_0) \exp\left(- \int_{t_0}^{t} \Gamma_W(t) dt \right) \\ &= N_{B-L}(z_0) \exp\left(- \int_{z_0}^{z} \frac{\Gamma_W(z)}{H(z) z} dz \right) . \end{aligned} \tag{4.27}$$

Since Γ_W is suppressed very quickly, the exponential term can be neglected as soon as the integrand is smaller than one. Therefore, a better condition for the

[4] The off-shell contributions due to $\Delta L = 2$-scatterings will be discussed further in section 4.5.4.

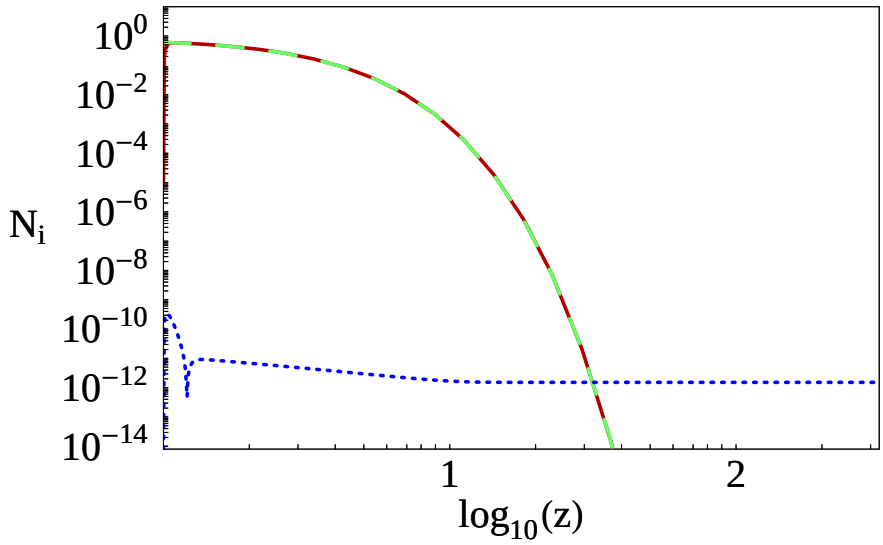

Figure 4.4: *Here, we see a typical example for leptogenesis in the strong wash-out scenario. The green/dashed line shows the equilibrium number of the right-handed neutrinos N_1 per relativistic photon $N_{N_1}^{eq}$ and almost perfectly matches the red/solid line, which illustrates their actual abundance N_{N_1} as calculated from the Boltzmann equations. The blue/dotted line shows the absolute amount of the corresponding $B-L$ asymmetry $|N_{B-L}|$. For this graph, we used $K = 10^2$ and all other parameter values as in the example in Fig. 4.3. For the final value of $|N_{B-L}|$ we find $1.5 \cdot 10^{-12}$, which matches our approximative value in Eq. (4.31) to a rough factor of 3.*

"time" z_* at which the wash-out processes become ineffective is

$$\frac{\Gamma_W}{z_*} \approx H \tag{4.28}$$

$$\Rightarrow z_*^{5/2} e^{-z_*} \approx K^{-1}\,. \tag{4.29}$$

By this time, the equilibrium number of right-handed neutrinos in our comoving volume has already decreased, and we find

$$N(z_*) \approx N^{\mathrm{eq}}(z_*) \approx z_*^{3/2} \exp(-z_*)/2 \approx (2 z_* K)^{-1} \approx \frac{0.05}{K}\,, \tag{4.30}$$

for the remaining particles.

Hence, our final result for the $B-L$ asymmetry is approximately given by the formula

$$N_{B-L}(z=\infty) \approx -\varepsilon_1 N(z_*) \approx -\varepsilon_1 \frac{0.05}{K}\,. \tag{4.31}$$

An example for a numerical solution of the corresponding Boltzmann equations is given in Fig. 4.4, which supports the rough estimations in this section.

4.5.4 Bounds From Leptogenesis

The assumption that the baryon asymmetry of our universe is due to standard thermal leptogenesis places bounds on several parameters from cosmology and particle physics, in particular, the reheating temperature after inflation and the quadratic mean of the light neutrino masses. As we will see in the following, both of these bounds are a result of the Davidson-Ibarra bound in Eq. (4.9).

Let us first consider the bound for the reheating temperature. Combining the Davidson-Ibarra bound with Eq. (4.13) and our estimates for the $B-L$ asymmetry from the Boltzmann equations (Eqs. (4.25) and (4.31)), we find

$$\eta_B \lesssim \begin{cases} 10^{-9} K^2 \left(\frac{m_3}{0.05\text{eV}}\right)\left(\frac{M_1}{10^9\text{GeV}}\right) & \text{for weak wash-out,} \\ 5\cdot 10^{-11} K^{-1} \left(\frac{m_3}{0.05\text{eV}}\right)\left(\frac{M_1}{10^9\text{GeV}}\right) & \text{for strong wash-out.} \end{cases} \tag{4.32}$$

We therefore see that the region around $K \approx 1$ will give the largest baryon asymmetry. However, since none of our approximations is valid in this parameter regime it is hard to give an exact value for the final asymmetry from these estimates. Within a more quantitative treatment Ref. [93] finds

$$M_1 \gtrsim 2\cdot 10^9\text{GeV} \tag{4.33}$$

as the lowest bound for the lightest of the singlet neutrino masses in case of zero initial abundance, which also implies

$$T_r \gtrsim M_1 \gtrsim 2\cdot 10^9\text{GeV} \tag{4.34}$$

for the reheating temperature.

Unfortunately, this bound creates a problem for supergravity, since the corresponding theories typically yield an upper bound on the reheating temperature around $T_r \lesssim 10^9 - 10^{10}$GeV [83, 84], as we already mentioned in the context of GUT baryogenesis. Therefore, supergravity and standard thermal leptogenesis seem only marginally compatible.[5]

However, the bound from Eq. (4.34) is only valid in the standard scenario of thermal leptogenesis, i.e. for three right-handed neutrinos with hierarchical masses and zero initial abundance. In the case of similar or degenerate masses of the right-handed neutrinos this bound does not hold [100, 101], since the Davidson-Ibarra bound loses its validity in these cases. Also the initial presence of right-handed neutrinos in non-thermal scenarios, e.g. via inflaton decay [102], can alter these bounds significantly (cf. e.g. Ref. [103]).

Let us now discuss the bound for the light neutrino masses derived by Refs. [70, 104–106], where we argue along the lines of the semi-quantitative approach of Ref. [107].

[5] Our treatment, here, has been in the non-supersymmetric framework. Yet, the supersymmetric treatment yields similar results (cf. e.g. Ref [94]).

Since we are interested in an upper bound, it is reasonable to assume (quasi-) degenerate neutrinos and a rather large $\overline{m} \equiv \sqrt{m_1^2 + m_2^2 + m_3^2}$. This implies [108]

$$m_1 \approx \tilde{m}_1 \approx m_3 \approx \overline{m}/\sqrt{3} \quad \text{and therefore} \quad K \approx \frac{\overline{m}}{\sqrt{3} m_*} \ll 1\,. \tag{4.35}$$

Thus, we only need to consider the strong wash-out regime. In these scenarios, the freeze-out of $\Delta L = 2$ scatterings around $z = 1$ and especially at later times is crucial to avoid the wash-out of the generated $B - L$ asymmetry and has so far been neglected. We now estimate the rate for these processes to be

$$\Gamma_{\Delta L=2} \approx \frac{\overline{m}^2 T^3}{\pi^3 \langle\phi\rangle^4}\,. \tag{4.36}$$

In this case, the corresponding freeze-out condition $\Gamma_{\Delta L=2}(z \approx 1) \ll H(z \approx 1)$ translates into an upper mass limit for M_1, namely

$$M_1 \lesssim \left(\frac{\text{eV}}{\overline{m}}\right)^2 5 \cdot 10^{10}\text{GeV}. \tag{4.37}$$

Additionally, Eq. (4.35) allows us to transform the Davidson-Ibarra bound from Eq. (4.9) to

$$\varepsilon_1 \lesssim \frac{3 M_1 \Delta m_{31}^2}{16\pi \langle\phi\rangle^2 \overline{m}}\,. \tag{4.38}$$

Combining the last two equations with Eqs. (4.2), (4.13), (4.31), and (4.35) we are then led to the rough upper mass limit

$$\frac{\overline{m}}{\sqrt{3}} \lesssim 0.1\text{eV} \tag{4.39}$$

for the light neutrinos.

In a more precise analysis Refs. [95, 109] find comparable bounds, which are only slightly higher.

4.5.5 Complications

Several effects have been neglected in the previous treatment, and we therefore comment on some of the more important ones in this section.

- **$\Delta L = 1$ scatterings with gauge bosons:**
  In the previous considerations, we have neglected $\Delta L = 1$ scatterings that include gauge bosons. Adopting the point of view from Ref. [95], we assume that these processes contribute at most in the way of the scatterings that involve the top quark. Since we are mainly concerned with orders of magnitude in our analysis, these effects should therefore not have an important impact on our results.[6]

[6] As also mentioned by Ref. [95], the neglect of the running of the top Yukawa coupling should, in fact, partially compensate for this.

- **Spectator Processes and Flavor effects:**
  The presented standard treatment for leptogenesis ignores the fact that sphalerons are already in equilibrium during the early times of leptogenesis as well as the possible change of several chemical potentials. These effects can contribute an order one suppression as shown in Ref. [110].

  Lately, much progress has been made concerning flavor effects in leptogenesis scenarios, e.g. in Refs. [92, 96, 100, 107, 111]. In particular, in our treatment, we ignored the fact that below temperatures around $T_r \lesssim 10^{12}$GeV the Yukawa couplings of the third-(and sometimes second-) generation leptons can be in thermal equilibrium at the times relevant for leptogenesis. This enables the system to distinguish between different lepton flavors and demands a more complex system of coupled Boltzmann equations. Typically, this can yield an additional factor of three for the final baryon asymmetry, while larger discrepancies can also appear. Nevertheless, Ref. [112] found that the overall lower bound for M_1 cannot be relaxed by flavor effects.

- **Quantum effects:**
  Quantum effects can also be more important for leptogenesis than indicated by our treatment.

  Examples in this context are the running of coupling constants [113], which can have order one effects on the final asymmetry, and thermal quantum effects as described in Ref. [94].

  Moreover, our semi-classical approach via Boltzmann equations is of limited validity compared to the full quantum dynamics described by Kadanoff-Baym equations (see e.g. Ref. [114]). So far, the Boltzmann equations for leptogenesis could be derived from the corresponding Kadanoff-Baym equations [115]. Yet, a full quantum mechanical treatment of leptogenesis in terms of Kadanoff-Baym equations still seems far away.

4.6 Affleck-Dine Baryogenesis

A completely different approach to explain the BAU has been introduced by Affleck and Dine in Ref. [116], where a $B - L$ asymmetry is produced by the dynamics of a scalar condensate instead of heavy particle decays. Since this scenario was one of the motivations for the model in chapter 5, we will briefly review it in this section.

The principle of Affleck-Dine (AD) baryogenesis is easily illustrated in a toy model of a scalar field ϕ with the potential [116]

$$V(\phi) = m^2|\phi|^2 + \lambda(\phi^4 + \phi^{*4})\,, \tag{4.40}$$

where possible further terms (e.g. to stabilize the potential) have been omitted for simplicity.

For small values of ϕ, namely $|\lambda\phi^2| \ll m^2$, this potential has an approximate $U(1)$ symmetry, which we identify with baryon number. Due to Noether's theorem, the baryon density n_b is then given by

$$n_b = \frac{\mathrm{i}}{2}(\dot{\phi}^*\phi - \phi^*\dot{\phi}) = |\phi|^2\dot{\theta}\,, \tag{4.41}$$

where θ is defined by $\phi \equiv |\phi|e^{i\theta}$.

We further note, that a field that starts with the initial values $\phi(t=0) = \phi_0$ and $\dot{\phi}(t=0) = 0$ will typically receive an acceleration in phase space due to the CP-violating λ term. Since the system starts with zero baryon density in this case, this acceleration already ensures the creation of a baryon asymmetry as we can see from Eq. (4.41).

Affleck and Dine applied this simple idea to flat directions [116], which frequently occur in models using supersymmetry (SUSY). Such flat directions are linear combinations of various elementary scalar fields that do not have a potential as long as SUSY is not broken. Therefore, a large VEV of such a flat direction does not contribute to the vacuum energy of the system in unbroken SUSY and might occur naturally after inflation. Yet, once SUSY breaking is turned on, potentials that include terms as in Eq. (4.40) might arise and a baryon asymmetry can be produced in the previously described manner. Later on, this scalar condensate will then decay due to further couplings and thereby transfer its asymmetry to the observed sector.

An important additional ingredient for this scenario has been considered in Ref. [117]. Based on the fact that the finite energy density of the early universe can also break SUSY (see e.g. Ref. [118]), it is shown that a previously flat direction can acquire a potential that has a global minimum at $\phi \neq 0$ at early times and a minimum at the origin at later times. Additionally, the CP violating terms of the potential can also depend on the Hubble rate and are therefore effectively time-dependent. This can naturally lead to a large VEV of the field after inflation and to a subsequent phase-kick of the scalar field as it tracks the potential minimum on its way towards the origin. As before, this phase kick generates a baryon (or lepton) asymmetry, and the subsequent decay of the scalar transfers this asymmetry to the SM.

Due to the non-thermal creation of the BAU in these baryogenesis scenarios, they typically yield much less stringent bounds for the reheating temperature than the scenarios that need to thermally produce heavy particle. Ref. [117], e.g., gives examples for models that work at a reheating temperature around 10^6 GeV, which is well below the gravitino bound mentioned in section 4.4. In addition to the fact that flat directions occur naturally in supersymmetric theories, this is one of the reasons why AD baryogenesis is also a popular baryogenesis scenario among model builders.

Chapter 5

Leptonic Dark Energy and Baryogenesis

As we have seen in the previous chapters, scalar fields might have played key roles in the history of our universe. Not only are they necessary in inflationary models, they might also be responsible for dark energy via quintessence and the baryon asymmetry of our universe through the Affleck-Dine mechanism. This raises the question, if it is possible that a single scalar field is responsible for several of these rather distinct phenomena.

Based on Ref. [119], we therefore present a model which establishes a connection between a dark energy field and the BAU in this chapter. The manner in which this is done here, was first suggested in Ref. [120] and features a scenario that hides a $B - L$ asymmetry in the dark energy sector, thereby compensating for an opposing asymmetry in the fermionic sector of our universe.

Since the major point of the presented work is to establish a potential connection between two distinct phenomena, and the model itself can be considered as a toy-model, we will restrict ourselves to a rather qualitative treatment here. For more quantitative results the reader is referred to Ref. [119].

In particular, we will discuss the newly introduced scalar sector of the model and its dynamics in section 5.1, whereas section 5.2 will be concerned with the couplings between these scalar fields and the standard model particles. In section 5.3, we briefly discuss some further points and conclude the analysis. For concluding remarks on this model in a more general context, we refer the reader to the conclusions at the end of this thesis.

5.1 The Model

As already mentioned in the introduction of this chapter, the key idea of the presented baryogenesis model is the generation of the BAU via a dark energy field. The scenario therefore starts at the beginning of reheating after an infla-

tionary period (cf. sec 1.6). Aside from a newly introduced dark energy field ϕ, it also includes a scalar field χ, that mediates between the dark energy and the visible sector, thereby avoiding possible constraints for time-varying masses and additional forces.

Ignoring fermionic couplings for the moment the Lagrangian of the new scalar sector is given by

$$\begin{aligned}\mathcal{L} &= \tfrac{1}{2}(\partial_\mu\phi)^*(\partial^\mu\phi) - V(|\phi|) + \tfrac{1}{2}(\partial_\mu\chi)^*(\partial^\mu\chi) \\ &\quad -\tfrac{1}{2}\mu_\chi^2|\chi|^2 - \tfrac{1}{2}\lambda_1|\phi|^2|\chi|^2 - \tfrac{1}{4}\lambda_2(\phi^2\chi^{*2} + \text{h.c.})\,, \end{aligned} \tag{5.1}$$

where we require $\lambda_1 \geq \lambda_2 \geq 0$ for stability reasons. We further assume that all interactions of ϕ are already included in its potential $V(\phi)$ and the couplings to χ, which implies that its behavior can be completely inferred from the corresponding Euler-Lagrange equations.

For the quintessence potential $V(\phi)$ we choose an exponential form, as discussed in section 1.7.2 but for a complex field now, which reads

$$V(|\phi|) = V_0(e^{-\xi_1|\phi|/m_{\rm Pl}} + ke^{-\xi_2|\phi|/m_{\rm Pl}}) \tag{5.2}$$

with the reduced Planck mass $m_{\rm Pl} \equiv 1/\sqrt{8\pi G}$ and typical quintessence parameter values ($\xi_1 = \mathcal{O}(10)$, $\xi_2 = \mathcal{O}(1), k \ll 1$) that yield the common tracker behavior.

We note that the Lagrangian in Eq. (5.1) has a $U(1)$ symmetry. Later on, we will choose the fermionic couplings of these fields in a way that identifies this symmetry with lepton number and assigns $L = -2$ to both fields. Thus, the corresponding symmetry of the complete model will be $B - L$ (cf. section 4.3).

In concordance with Eq. (4.41) the lepton number density stored in the quintessence condensate is now

$$n_\phi = \mathrm{i}(\dot\phi^*\phi - \phi^*\dot\phi) = -2|\phi|^2\dot\theta\,, \tag{5.3}$$

where $\phi \equiv |\phi|e^{i\theta}$, while the lepton number per comoving volume is

$$A_\phi = -2|\phi|^2\dot\theta\left(\frac{a(t)}{a(t_0)}\right)^3\,, \tag{5.4}$$

with the cosmic scale factor $a(t)$, as before, and analogous definitions for n_χ and A_χ with $\chi \equiv |\chi|e^{i\sigma}$.

Neglecting the fermionic couplings just a littler longer, the conservation of lepton number would imply

$$A_\phi + A_\chi = 0\,. \tag{5.5}$$

We therefore see that it is in principle possible to create opposing lepton asymmetries in the two scalar sectors. Of course, this formula alone does not imply that the dynamics of the system will ever lead to non-zero A_ϕ and A_χ. Yet, at this point we note that the last term in Eq. (5.1) can be written as $-\frac{1}{2}\lambda_2|\phi|^2|\chi|^2\cos(2\alpha)$

with $\alpha \equiv \theta - \sigma$ being the relative phase of the fields. Thus, if the scenario starts with an initial α_0 which does not equal a multiple of $\pi/2$, it will be accelerated towards its potential minimum. Since this implies non-zero phase velocities for both fields (cf. Eqs. (5.4) and (5.5)), such an initial CP-violation naturally leads to a lepton asymmetry for this model.

The exact dynamics of the system are given by the Euler-Lagrange equations that can be derived from Eq. (5.1). However, due to the fermionic couplings of χ and the fact that it will be oscillating in its potential, we include an additional damping factor in the corresponding equation (cf. Refs. [18, 86]). The equations of motion, therefore, take the form

$$\ddot{\phi} + 3H\dot{\phi} = -2\frac{\mathrm{d}V}{\mathrm{d}\phi^*} - \lambda_1|\chi|^2\phi - \lambda_2\phi^*\chi^2, \tag{5.6}$$

$$\ddot{\chi} + 3H\dot{\chi} + \Gamma\dot{\chi} = -(\mu^2 + \lambda_1|\phi|^2)\chi - \lambda_2\chi^*\phi^2\,, \tag{5.7}$$

with $\Gamma \equiv g^2 m_\chi/(8\pi)$. In this context g^2 is assumed to be the sum of the squares of the various coupling constants of the fermionic interactions of χ and $m_\chi \equiv (\mu_\chi^2 + \lambda_1|\phi|^2)^{1/2}$ is its effective mass.

As the decay of a χ particle to fermions transfers its lepton number to this sector, this damping factor also appears in the conservation law of the leptonic charge, and Eq. (5.5) takes the more general from

$$\frac{\mathrm{d}}{\mathrm{d}t}(A_\phi + A_\chi) + \Gamma A_\chi = 0\,. \tag{5.8}$$

On a qualitative level the dynamics of a typical baryogenesis scenario in this setting can then take the following form. We assume that both initial field values are of the order of the Hubble scale at the end of inflation H_{Inf}. Since the scalar mixing terms are in this case typically also of the order of the Hubble scale, order-of-magnitude considerations imply that the system will not be over-damped and that the phase space velocities will increase, thereby creating a lepton asymmetry in both scalar condensates. Since the typical quintessence behavior of ϕ will lead to a rapid increase of its VEV, the effective mass of χ will also start to grow, and with it its decay rate Γ. Thus, the corresponding condensate will subsequently decay due to the fermionic couplings around the time $\Gamma \approx H$. As we already discussed, these decays will then transfer the lepton asymmetry of the χ-field to the fermionic sector, where it will be partially transformed into a baryon asymmetry via $B - L$ conserving sphaleron processes (cf. section 4.3).

Later on, the VEV of ϕ will typically be in the Planck range and therefore also the mass of the χ field. This leads to an effective decoupling of the dark energy sector and the SM, and the asymmetries will not be able to cancel each other. According to Eq. (5.8), the final $B - L$ number per comoving volume in the fermionic sector will then be given by

$$A_{\mathrm{ferm}} \equiv -A_\phi|_{t\to\infty} = \int_0^\infty \mathrm{d}t\,\Gamma A_\chi\,. \tag{5.9}$$

In addition to the presented qualitative treatment, a quantitative approach based on numerical and analytical studies of Eqs. (5.6) and (5.7) has been performed in Ref. [119]. This approach supports the considerations of this section and finds it easy to generate a baryon asymmetry of the observed order of magnitude.

5.2 Fermionic Couplings

So far, we have not specified the ways in which one can couple the χ field to the fermionic sector. In fact, finding appropriate couplings is a more subtle task than one might naively expect, and we will need to make some additional assumptions in this context.

Since the mass of the χ field is more or less given by the VEV of ϕ, which is in the Planck range, the difficulties in finding appropriate couplings do not come from direct experimental bounds. Yet, the fact that χ is a gauge singlet does not leave much room for appropriate couplings, since direct couplings to SM particles with lepton number (e.g. left-handed neutrinos ν) of the form

$$g' \nu_L^T \epsilon \, \nu_L \, \chi + \text{h.c.}\,, \tag{5.10}$$

would break the SM gauge symmetry and therefore seem unattractive (even though they might in principle be able to do the job).

Therefore, it seems better to couple the χ-field to the right-handed neutrinos N_R, which are SM gauge singlets. This could be realized by a term of the form

$$g N_R^T \epsilon \, N_R \, \chi + \text{h.c.}\,. \tag{5.11}$$

However, since our model is $B - L$ conserving it does not allow for a see-saw scenario (cf. section 3.4) and the light neutrino masses therefore require tiny Yukawa couplings. This, in turn, would prevent a transfer of the asymmetry in the right-handed neutrino sector to the SM particles before the sphaleron processes freeze out (cf. Ref. [77]). Therefore, one needs to find some other way to transfer the asymmetry from the right-handed neutrino sector to the SM, in this case. One way that seems suitable for this task makes use of an additional scalar field S, that has the same quantum numbers as the SM Higgs, a quadratic potential, and mass m_S in the range $H_{\text{Inf}} \gg m_S \geq \mathcal{O}(\text{TeV})$. In this case, one can allow for a coupling term of the form

$$g' S^{c\dagger} \, N_R^\dagger \ell_L + \text{h.c.}\,, \tag{5.12}$$

and if S starts with a VEV around the size of H_{Inf}, this value will remain frozen in, until $H \sim m_S$. Therefore, the VEV could catalyze a left-right equilibration of the asymmetry at early times. Later on the field S would start to oscillate in its potential and decay into leptons. At this time, the energy density due to

the S-field is typically around $m_S^2 H_{\rm Inf}^2$, which is much smaller than the energy density of the universe at this time, which is around $m_S^2 M_{\rm Pl}^2$. Therefore, the entropy produced by the decay of the condensate can be neglected.

5.3 Concluding Remarks

With respect to our discussion from the previous sections and the more quantitative results from Ref. [119], one can therefore say that the presented model is indeed capable of producing the observed baryon asymmetry of our universe, and that the latter quantity might thus be related to the charge of a dark energy field.

For completeness, we note that the dynamics of the system have also been checked for instabilities in Ref. [119]. In particular in the context of Q-balls [121], this is a crucial test for any model that features a complex dark energy field, and it is therefore vital for the considered scenario that these instabilities were found to be under control within a linearized treatment.

Nevertheless, to render the model more realistic, future research needs to address some of its open points. In particular, the sizes of the different initial VEVs are crucial in this model and wait for a deeper motivation. Furthermore, on a conceptual level it would also be desirable if the new scalar sector could be embedded in a more natural framework.

Chapter 6

Single Right-Handed Neutrino Dominance in Five Dimensions

As we have seen in section 3.4.1, the standard see-saw mechanism can nicely explain the smallness of neutrino masses. If combined with the concept of single right-handed neutrino dominance (SRND) (cf. Sec. 3.4.2) it can even explain the mass hierarchy in the light neutrino sector and the corresponding mixing angles. Yet, SRND also postulates a mass hierarchy in the right-handed neutrino sector as well as certain hierarchies among the Yukawa couplings, which need to be further motivated. Therefore it has to be considered an intermediate step towards a more fundamental theory.

One can assume that a motivation for these hierarchies might be provided by an appropriate family symmetry (cf. section 3.3), as it has, e.g., been done in Ref. [37]. However, the combination of family symmetries and SRND can yield problems for certain classes of models, since the same charges that lead to a mass hierarchy in the right-handed sector can induce a hierarchy in the Yukawa couplings that cancels the first one. In particular, a large family charge of a right-handed neutrino typically induces a relatively light Majorana mass for this particle, which would seem to make it a good candidate for the particle that gives the leading contribution in SRND. However, the same large family charge can also induce relatively small Yukawa couplings of this particle which exactly cancel the first effect.

While this is not a problem of all models that try to combine family symmetry and SRND, it is interesting to see that affected models can be "revived" in five dimensions due to the non-linearity of the see-saw presented in section 3.4.3. Additionally, it is of course also interesting in its own right to consider the combination of family symmetry and SRND in such extra-dimensional models.

Based on Ref. [58], which itself is an ammendment to Ref. [122], the present chapter is, therefore, dedicated to this topic. It considers the combination of a $U(1)$ family symmetry and SRND in five dimensions for a class of family charge assignments and different natures of the five-dimensional Majorana mass term.

The structure of this chapter will be the following. First, we will briefly adapt the treatment from section 3.3 on family symmetries to our extra-dimensional setting in section 6.1. This will be followed by quantitative discussions of two classes of neutrinos mass models with different types of Majorana mass terms in sections 6.2 and 6.3. Each presented analysis includes both general considerations about these classes of models and explicit parameter values that yield observed neutrino data via SRND. Afterwards, we will draw some brief conclusions in section 6.4, while we, again, also refer to the conclusions in the final part of this thesis for remarks in a more general context.

For related discussions of further models the reader is referred to the, already mentioned, original references [58, 122].

6.1 Family Symmetry in 5D

As already mentioned, we will work within the setting presented in section 3.4.3. To be applicable for this chapter's analysis, the treatment from section 3.3 therefore needs to be adapted to the extra-dimensional environment. In particular, while we still assume to have an additional family symmetry $U(1)_F$, we now assume it to be spontaneously broken by the VEV of a scalar field ϕ_F in the bulk.

If ϕ_F has family charge $q^{\phi_F} = -1$, and the gauge singlets have the respective charges q_i^{Ψ}, the Frogatt-Nielsen mechanism might then induce effective Majorana mass terms for the singlets of the form

$$-\frac{1}{2}\left(\frac{\langle\phi_F^*\rangle}{M_5^{3/2}}\right)^{q_i^{\Psi^c}+q_j^{\Psi^c}} (M_{ij}^S \overline{\Psi^c}_i \Psi_j + M_{ij}^V \overline{\Psi^c}_i \gamma_5 \Psi_j) + \text{h.c.}\,, \tag{6.1}$$

with $q_i^{\Psi^c} = -q_i^{\Psi}$. Additionally, we made the simplifying assumption that all new effects are suppressed by powers of M_5 in this setting. We also note that the power of the suppression scale had to be adapted with respect to the treatment in four dimensions due to the different mass dimensions of bulk fields.

With respect to Eq. (3.48), we may also allow for Dirac mass terms of the form

$$-\frac{g_{ij}}{\sqrt{M_5}}\left(\frac{\langle\phi_F\rangle}{M_5^{3/2}}\right)^{q_i^{\Psi^c}+q_j^{\ell}} \overline{\Psi}_i P_L H^T \left((0,0),(\epsilon\ell_j)^T\right)^T \delta(y) + \text{h.c.}\,, \tag{6.2}$$

if the SM lepton doublets have the respective charges q_j^{ℓ} under the new family symmetry.

In this context, we also define

$$\frac{\langle\phi_F\rangle}{M_5^{3/2}} \equiv \varepsilon\,, \tag{6.3}$$

which will enable us to express the orders of magnitude of the various Majorana and Dirac mass terms as powers of the perturbation parameter ε.

6.2 SRND and Vector-Like Majorana Masses

The model we consider in this section is a simple example that nicely illustrates how potential difficulties in combining SRND and family symmetry can arise and be circumvented in five dimensions. To keep things simple, we will make several additional assumptions in the corresponding analysis. In the following section we will consider a model with a scalar Majorana mass term, but otherwise identical. There, we will not make these simplifying assumptions and the corresponding analysis can, in this sense, be considered more general.

In the present model, we assume the nature of the Majorana mass terms in Eq. (6.1) to be vector-like (i.e. $M_S = 0$) and assign the $U(1)_F$ charges

$$\begin{array}{lll} \Psi_1^c : r\,, & \Psi_2^c : s\,, & \Psi_3^c : 0\,, \\ \ell_1 : v\,, & \ell_2 : w\,, & \ell_3 : w\,, \end{array} \tag{6.4}$$

to the respective particles, while we additionally assume $r > s > 0$ and $v > w$.

Combining this with our discussion in section 6.1, we see that the Frogatt-Nielsen mechanism might generate a vector-like Majorana mass matrix M for the SM gauge singlets with entries of the order

$$M \approx M_\Psi \begin{pmatrix} \varepsilon^{2r} & \varepsilon^{r+s} & \varepsilon^r \\ \cdot & \varepsilon^{2s} & \varepsilon^s \\ \cdot & \cdot & 1 \end{pmatrix} . \tag{6.5}$$

Typically, the eigenvalues of this matrix are given by $M_1 \approx M_\Psi \varepsilon^{2r}$, $M_2 \approx M_\Psi \varepsilon^{2s}$, $M_3 \approx M_\Psi$, and it can be diagonalized by a unitary matrix U, which has entries of the order

$$U \approx \begin{pmatrix} 1 & \varepsilon^{r-s} & \varepsilon^r \\ \varepsilon^{r-s} & 1 & \varepsilon^s \\ \varepsilon^r & \varepsilon^s & 1 \end{pmatrix} . \tag{6.6}$$

For the corresponding Dirac mass matrix m_D, we can expect entries of the order (cf. Eq. (6.2))

$$m_D \approx \frac{\langle \phi \rangle}{\sqrt{\pi R M_5}} \begin{pmatrix} \varepsilon^{v+r} & \varepsilon^{v+s} & \varepsilon^v \\ \varepsilon^{w+r} & \varepsilon^{w+s} & \varepsilon^w \\ \varepsilon^{w+r} & \varepsilon^{w+s} & \varepsilon^w \end{pmatrix} , \tag{6.7}$$

where ϕ still denotes the standard model Higgs field as in the previous chapters and is not to be confused with the family symmetry breaking ϕ_F.

With respect to Eq. (3.62) it is also important to note that

$$m_D U^* \approx m_D \tag{6.8}$$

in terms of orders of magnitude.

For simplicity, let us assume that M_3 is approximately equal to an uneven multiple of $1/(2R)$ to a degree, where we can neglect its contribution to Eq. (3.62). In this case, Eq. (3.62) yields an effective Majorana mass matrix for the light neutrinos with entries of the order

$$m_{LL} \approx \frac{\langle\phi\rangle^2 \varepsilon^{2w}}{2M_5} \left[\cot(\pi M_1 R)\, \varepsilon^{2r} \begin{pmatrix} \varepsilon^{v-w} \\ 1 \\ 1 \end{pmatrix} \otimes (\varepsilon^{v-w}, 1, 1) + \cot(\pi M_2 R)\, \varepsilon^{2s} \begin{pmatrix} \varepsilon^{v-w} \\ 1 \\ 1 \end{pmatrix} \otimes (\varepsilon^{v-w}, 1, 1) \right]. \tag{6.9}$$

This equation nicely helps to illustrate the problems of the corresponding four-dimensional model, whose relevant features, in this context, can be reproduced by taking R^{-1} to infinity. In this case, we can make the substitution $\cot(\pi M_i R) \to (\pi M_i R)^{-1}$, from which one can see that the different pre-factors (ε^{2r} and ε^{2s}) in Eq. (6.9) will be exactly canceled by the hierarchy of the different eigenvalues of the Majorana mass matrix in Eq. (6.5). The same would also be true for the term that corresponds to M_3 in this case. In spite of the desired hierarchy in the heavy sector, the corresponding four-dimensional model does, therefore, not naturally yield SRND.

Yet, things are obviously different in five dimensions: if we are in a regime in which at least M_2 is comparable to R^{-1}, the two remaining contributions from the Majorana mass terms are typically not of the same order of magnitude, but are related by the relative factor

$$\alpha \equiv \varepsilon^{-2(r-s)} \frac{\cot(\pi M_2 R)}{\cot(\pi M_1 R)}\,, \tag{6.10}$$

which makes SRND easily realizable in this setting.

Even though we have so far only considered orders of magnitude, we can gain a lot of information from Eq. (6.9), as we will see in the following.

Since α can be considered as a measure for the deviation from rank one of the effective light neutrino mass matrix, it also gives an estimate for the ratio of the two heavier of the light neutrino masses, i.e. $m_2/m_3 \sim \alpha$ (if $\alpha < 1$).

Further, we can see that the eigenvector that corresponds to the heaviest of the eigenvalues will have entries of the relative ratios $\varepsilon^{v-w} : 1 : 1$, in terms of orders of magnitude, which is exactly what we need to create a large 23-mixing and a tiny 13-mixing (cf. section 3.4.2). Unfortunately, we can also see that it will require some tuning to create a large 12-mixing, since the second eigenvector will typically also have entries of the relative ratios $\varepsilon^{v-w} : 1 : 1$, while a large 12-mixing requires an approximate equality of the first entry and the difference of the two other ones, as we saw in section 3.4.2.

Yet, to explicitely derive the observed values for neutrino mixing angles and masses, we need to rewrite Eq. (6.9) in terms of explicit matrix entries. Let us therefore write

$$m_{LL} = \varepsilon^{2(w+r)} \frac{\langle\phi\rangle^2}{2M_5} \cot(\pi M_1 R) \times \left[\begin{pmatrix} a^2\delta^2 & ab\delta & ac\delta \\ ab\delta & b^2 & bc \\ ac\delta & bc & c^2 \end{pmatrix} + \alpha \begin{pmatrix} e^2\delta^2 & ef\delta & eg\delta \\ ef\delta & f^2 & fg \\ eg\delta & fg & g^2 \end{pmatrix} \right] . \quad (6.11)$$

According to our previous treatment we will assume that the parameters denoted by Latin letters ($a, b, c, e, f,$ and g) are of order one, while we will treat the parameters denoted by Greek letters ($\delta \equiv \varepsilon^{v-w}$and α) as small perturbation parameters.[1]

In Ref. [58], we also present the results of an approximate diagonalization of this matrix. These approximate formulae indeed confirm that the relative ratio of the two heavier eigenvalues is given by α. Unfortunately, they also confirm that the ratios of the entries of the second eigenvector are of the order $\varepsilon^{v-w} : 1 : 1$, which implies some tuning to find a large 12-mixing as we also discussed earlier. Nevertheless, these formulae can be used to find suitable parameter values in Eq. (6.11), as we also discuss there.

Here, we will restrict ourselves to the presentation of such a parameter set, that yields a mass hierarchy and mixings for the light neutrinos within the bounds of Eq. (3.32), namely

$$a = 0.5\,,\ b = 1\,,\ c = 1\,,\ e = 3.2\,,\ f = 1\,,\ g = -0.5\,,\ \delta = 0.2\,,\ \alpha = 0.3\,, \quad (6.12)$$

which leads to the neutrino parameters

$$\tan(\theta_{23}) \approx 1.17\,, \quad \tan(\theta_{13}) \approx 0.12\,, \quad \tan(\theta_{12}) \approx 0.57\,, \quad m_2/m_3 \approx 0.21\,, \quad (6.13)$$

One can see that these values indeed agree with the data from Eq. (3.32).

Additionally, as we treat M_5 as a free parameter, and we can always fix it in a way that leads to the required absolute mass scale for the light neutrinos.

6.3 SRND and Scalar-Like Majorana Masses

The model from the previous section can also be considered with a scalar-like mass term in Eq. (6.1) and $M_V = 0$, which seems more attractive from a Lorentz symmetry point of view. We will see that it is also easy to a a SRND in this case.

[1] The assumption that α is small also implies that M_2 is close to an uneven multiple of $1/(2R)$. However, if this was not the case, it would typically only lead to the fact that the contribution of M_2 would become the dominant one without changing much of the following results after a corresponding relabeling of the parameters.

Further, the simpler behavior of the hyperbolic cotangent function in Eq. (3.61) allows for an analysis that is, in some sense, more general without a greater extension of our previous analysis.

In fact, the treatment from the previous section remains valid up to Eq. (6.8). However, we now need to make use of Eq. (3.61), instead of Eq. (3.62), to determine the effective light neutrino mass matrix and therefore find

$$\begin{aligned} m_{LL} \approx \frac{v^2}{2M_5} \Bigg[& \coth(\pi M_1 R) \varepsilon^{2(w+r)} \begin{pmatrix} \varepsilon^{v-w} \\ 1 \\ 1 \end{pmatrix} \otimes (\varepsilon^{v-w}, 1, 1) \\ & + \coth(\pi M_2 R) \varepsilon^{2(w+s)} \begin{pmatrix} \varepsilon^{v-w} \\ 1 \\ 1 \end{pmatrix} \otimes (\varepsilon^{v-w}, 1, 1) \\ & + \coth(\pi M_3 R) \varepsilon^{2w} \begin{pmatrix} \varepsilon^{v-w} \\ 1 \\ 1 \end{pmatrix} \otimes (\varepsilon^{v-w}, 1, 1) \Bigg] . \end{aligned} \tag{6.14}$$

At this point we note that it seems only natural to assume that the scale of the right-handed neutrino masses and the compactification scale are in general of different orders of magnitude, and we will, therefore, assume $R^{-1} \ll M_i$ in this section. In this case all the hyperbolic cotangent functions turn to one, and we immediately find a hierarchy among the various contributions to the light neutrino mass matrix. In particular, the ratios between these contributions will be of the relative orders $1 : \varepsilon^{2s} : \varepsilon^{2r}$, thereby naturally leading to SRND.

For large enough r we can typically neglect the smallest of the three contributions in Eq. (6.14), which implies a treatment that is similar to the one from section 6.2. However, the important difference, here, is that the ratio of the remaining two contributions is now not a free parameter, but approximately given by ε^{2s}. Thus, if we assign the parameters a, b, c, e, f, g, α and δ in the manner of Eq. (6.11), α and δ are not completely independent anymore.

Yet, it is still not particularly hard to find suitable parameter values. All one needs to do is to fix ε, s, and $v - w$ in such a way that the parameters α and δ from Eq. (6.12) are approximately reproduced. An example for such a case is given by $\varepsilon = 0.58$, $s = 1$, $v - w = 3$, which yields $\alpha \approx 0.34$, $\delta \approx 0.20$ and

$$\tan(\theta_{23}) \approx 1.20\,, \quad \tan(\theta_{13}) \approx 0.12\,, \quad \tan(\theta_{12}) \approx 0.55\,, \quad m_2/m_3 \approx 0.23\,, \tag{6.15}$$

if we do not change the other parameters from Eq. (6.12). Again, these values nicely agree with the data in Eq. (3.32).

In Ref. [58] we additionally considered the (supposedly) less natural option $M_3 R \leq 1$, which typically leads to $M_1, M_2 \ll R^{-1}$. Here, we only note that the first two contributions to the light neutrino masses in Eq. (6.14) are typically suppressed with the same strength in this case, which leads to a more complicated

light neutrino mass matrix due to the increased number of relevant parameters. Nevertheless, this increase only enlarges the number of suitable parameter sets, and it is therefore still easy to realize SRND in this regime, as we also show in the above reference.

6.4 Concluding Remarks

From the analysis in the previous section we can see that the extra-dimensional setting of the models can indeed help to realize SRND scenarios rather naturally. In particular, the hierarchy among different contributions to the light neutrino mass matrix can be easily implemented in this framework. Moreover, the presented family charge assignments can also nicely motivate the smallness of θ_{13}.

Yet, our analysis also shows that the presented models generically require some tuning in order to find a large 12-mixing. It would therefore be desirable, if the corresponding parameter relations could be ascribed to some deeper principle. On more general grounds, the model would also benefit from a further motivation for the specific family charges and for the size of the suppression scale M_5, that is related to the absolute mass scale of the light neutrinos (see also Ref. [123] for recent progress in the latter context).

Hence, there are several conceptual challenges for this model, which will hopefully find a solution in the future. Nevertheless, even without these further motivations, the considered models show attractive features and help to illustrate the tremendous possible impact of extra-dimensions for phenomenology and model building.

Chapter 7

Leptogenesis With Many Neutrinos

As we have seen in section 4.5 leptogenesis is a very attractive explanation for the baryon asymmetry of our universe, that owes its popularity mainly to the fact that it can be realized within the standard see-saw scenario and does therefore not require any extensions of the SM, other than right-handed neutrinos.

Yet, we have also seen that leptogenesis in its simplest version is only marginally compatible with supergravity, due to its constraints on the reheating temperature. This fact has cost leptogenesis some of its popularity and makes it obviously desirable to find leptogenesis models in which the corresponding bounds get relaxed with respect to the standard case.

As we also mentioned in section 4.5, previous approaches in this direction typically included non-thermal production of right-handed neutrinos or the increase of the average CP-violation per decay of a right-handed neutrino through the interference with another right-handed neutrino of comparable mass.

Based on Ref. [124], this section presents a different approach to the problem by considering leptogenesis scenarios with many right-handed neutrino singlets, which is, in particular, motivated by the fact that many singlets can naturally appear in extra-dimensional and string models (cf. section 3.4.3 and Refs. [125,126], respectively). While non-thermal or resonance effects might also be incorporated in the respective scenarios, we will show that the presence of many right-handed neutrinos can already lower the standard bounds for thermal leptogenesis significantly, without these effects.

The structure of this chapter is the following: after presenting the basic equations of the setup in section 7.1, we will separately consider the possible impact of many right-handed neutrino states on strong and weak wash-out scenarios in sections 7.2 to 7.4. Thereafter, we will discuss the corresponding alteration of the bounds for standard thermal leptogenesis, which includes discussions on the Davidson-Ibarra bound, the lower bound for the reheating temperature, as well as the upper mass bound for light neutrinos, in section 7.5. In section 7.6, we will

then apply our analysis to an explicit extra-dimensional model, which naturally yields many singlets to further motivate our approach. We will close this chapter with several concluding remarks in section 7.7, again also referring the reader to the conclusions at the end of this this thesis for remarks in a more general context.

As in our treatment of standard thermal leptogenesis in section 4.5, there are some more subtle points, whose treatment is beyond the scope of the presented work. For further comments on these topics we refer the reader to the corresponding discussions in section 4.5.5 and Ref. [124].

7.1 Basic Equations

Due to the additional right-handed neutrino states the relevant equations for leptogenesis from section 4.5 need some adjustment to be applicable for our treatment. Therefore, we present the adapted equations in the following.

Not surprisingly, the Lagrangian of the neutrino sector still looks like the one in Eq. (4.7) in our new setting, namely

$$\mathcal{L} = -\frac{1}{2} M_i N_{Ri}^{cT} \epsilon N_{Ri}^{c} - g_{ij} N_{Ri}^{cT} \phi^{c\dagger} \epsilon \ell_j + \text{h.c.}\,. \tag{7.1}$$

Yet, the index i is now running from 1 to n_N (the number of right-handed neutrino states) instead of from 1 to 3, as it does in the standard case.

As long as our perturbative treatment remains valid, the change of the range of the index j in Fig. 3.1 is also the only thing that needs to be modified, when we consider the see-saw mechanism. Therefore, the effective light neutrino mass matrix is still given by

$$m_{\nu,ik} = g_{ij}^{T} M_j^{-1} g_{jk} \langle \phi \rangle^2 \,, \tag{7.2}$$

with the difference that g is now a $n_N \times 3$-dimensional matrix.

In this context, we also remark that, due to the increased number of corresponding diagrams, the Yukawa couplings can now be smaller than in the standard case, if the mass scale of the right-handed neutrinos is not changed (cf. Ref. [126] for a related argument). This in turn implies that the weak washout regime can become more natural in models with many singlets.

Generalizing Eq. (4.8), we further define

$$\varepsilon_i = \frac{\Gamma(N_i \to \ell_L + \phi) - \Gamma(N_i \to \bar{\ell}_L + \phi^*)}{\Gamma(N_i \to \ell_L + \phi) + \Gamma(N_i \to \bar{\ell}_L + \phi^*)} \tag{7.3}$$

as the average CP asymmetry per decay of the respective singlet.

Moreover, the Boltzmann equations from section 4.5.1 are now also easily generalized to

$$\frac{dN_{N_n}}{dz} = -\frac{1}{Hz} (\Gamma_{D,n} + \Gamma_{\Delta L=1,n}) \left(N_{N_n} - N_{N_n}^{\text{eq}}\right), \tag{7.4}$$

and

$$\frac{dN_{B-L}}{dz} = -\frac{1}{Hz}\sum_{n=1}^{n_{\text{eff}}}\left[\varepsilon_n(\Gamma_{D,n}+\Gamma_{\Delta L=1,n})\left(N_{N_n}-N_{N_n}^{\text{eq}}\right)+\Gamma_{W,n}N_{B-L}\right]. \quad (7.5)$$

Here, n_{eff} is the number of right-handed neutrino states that actively participate in the leptogenesis scenario, i.e. the number of states whose masses are around the scale of the reheating temperature or lower. The reaction rates $\Gamma_{D,n}$, $\Gamma_{\Delta L=1,n}$, and $\Gamma_{W,n}$ can be calculated as in the standard case, with the corresponding interchange of masses and coupling constants as discussed in appendix C.

7.2 The Strong Wash-Out Scenario

Let us first consider leptogenesis with many singlets in the strong wash-out regime, i.e. $K_i \gg 1$, where K_i denotes the straight-forward generalization of Eq. (4.14). In this case, it is sufficient to consider the lightest of these states and the ones with comparable masses, as the corresponding particles will wash-out any asymmetry produced by earlier decays.[1] We will therefore discuss the case of n_{eff} quasi-degenerate right-handed neutrinos, here.

Starting from our considerations in section 4.5.3, it is easy to see that the additional states will have two competing effects on the scenario. The first one is the increase of the number of decaying neutrinos, which would result in an increase of the the total amount of the produced $B-L$ asymmetry, if this was the only change. However, the total wash-out rate will also increase due to the sum in Eq. (7.5), which in turn implies that the time after which a produced asymmetry is not washed-out will be shifted to a later point. Obviously, this second effect would lead to a reduction of the final $B-L$ asymmetry and therefore might cancel the first one.

To find out which of these effects will be the dominating one, let us make some approximations in the manner of section 4.5.3. Now, the averaged wash-out rate will be (cf. Eq. (4.26))

$$\Gamma_W \approx \sum_{i=1}^{n_{\text{eff}}}\left(\frac{1}{2}\cdot\frac{1}{8\pi}(gg^\dagger)_{ii}M_i + \frac{|g_{\text{top}}|^2}{\pi^3}(gg^\dagger)_{ii}\,T\right) z_i^{3/2}e^{-z_i}, \quad (7.6)$$

with $z_i \equiv M_i/T$.

Hence, the freeze-out "time" of wash-out processes z_* is defined by the equation

$$z_*^{5/2}e^{-z_*} \approx \left(\sum_{i=1}^{n_{\text{eff}}} K_i\right)^{-1}, \quad (7.7)$$

[1] This argument is only valid in the one-flavor treatment see Ref. [127] for additional effects in the flavored case.

in this case.

As we are in the strong wash-out regime, the number density of each species of right-handed neutrinos at this time will still be simply given by the corresponding equilibrium value. Therefore, we find

$$N_i(z_*) = \frac{1}{2z_*}\frac{1}{\sum K_i} \approx \frac{0.05}{\sum K_i}\,, \tag{7.8}$$

for the corresponding value, which leads to the approximate final $B-L$ asymmetry per photon

$$N_{B-L}(z=\infty) \approx -\sum \varepsilon_i N_i(z_*) \approx -0.05\frac{\sum \varepsilon_i}{\sum K_i}\,. \tag{7.9}$$

Since we assumed that all the particles are in the strong wash-out regime, this expression is maximized by the conditions $K_i = \mathrm{Min}(\{K_j, 1 \leq j \leq n_{\mathrm{eff}}\})$ and $\varepsilon_i = \mathrm{Max}(\{\varepsilon_j, 1 \leq j \leq n_{\mathrm{eff}}\})$ for all i, which would make the different particle states identical within our treatment. However, as long as the CP asymmetry is not increased with respect to the standard case, Eq. (7.9) shows that the final asymmetry would (at best) not be reduced, since we would get a factor of n_{eff} in the numerator and the denominator of Eq. (7.9). In fact, a closer look at Eq. (7.8) shows that even in the extreme case considered above the asymmetry will be slightly reduced compared to the one-particle case due to the factor z_*^{-1}, which also tends to smaller values, now.

Thus, at least in the case $\varepsilon_i \leq \varepsilon_1$ the presence of many right-handed neutrinos will not be able to increase the final asymmetry in a strong wash-out scenario.

A numerical example that verifies these considerations is shown in figure 7.1, where we consider the scenario from section 4.5.3 with 10 identical neutrinos.

7.3 The Weak Wash-Out Scenario I

As we have seen in the previous section, the presence of many heavy neutrinos could not alter the bounds for thermal leptogenesis in the strong wash-out regime with respect to the corresponding standard case (excluding possible effects on the CP-asymmetry). This was due to the competing effects of the singlets on particle number and the wash-out rate. In the weak wash-out regime, however, the wash-out processes were the crucial ingredients that prevented the complete cancellation of the asymmetries from the production and the decays of the singlets (cf. section 4.5.2). This is quite exciting, since the effects of many right-handed neutrinos on particle density and wash-out rate would therefore not mainly cancel each other in this case, but would both amplify the final asymmetry.

To test this statement, let us be more quantitative and consider the case where all our decaying particles are in the weak wash-out regime, i.e. $K_i \ll 1$. For

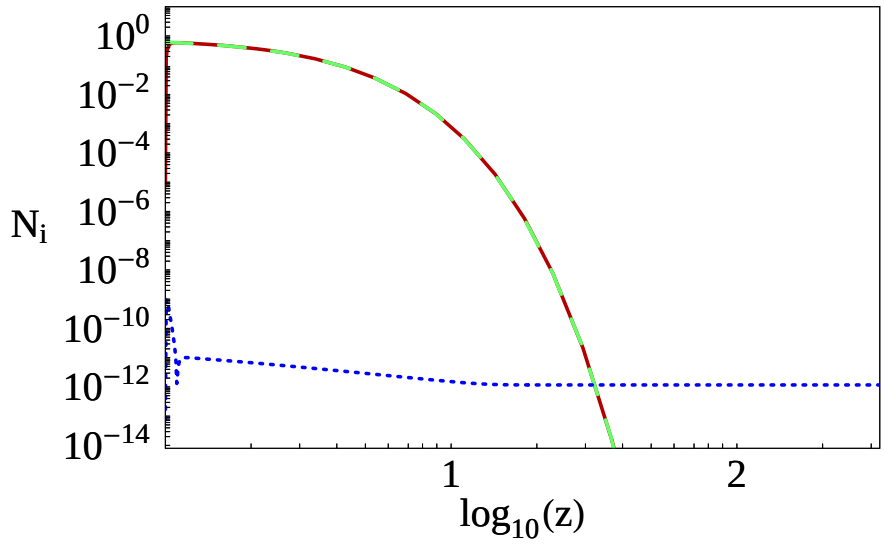

Figure 7.1: *This figure shows the numerical solutions for a scenario with 10 decaying singlets, which is in all other aspects identical to the setup in in figure 4.4. The green/dashed line shows the equilibrium abundance per comoving volume of one of the particle species $N_{N_i}^{eq}$, the red/solid line shows the its actual abundance as calculated from the Boltzmann equations N_{N_i}, and the blue/dotted line shows the absolute amount of the corresponding $B-L$ asymmetry in the same volume $|N_{B-L}|$. For the final value of the latter quantity we find $1.2 \cdot 10^{-12}$ and therefore a slightly smaller value than in the corresponding one-particle scenario, which agrees with our considerations in the text.*

simplicity, we will additionally assume that all decaying states are approximately of the same mass as we did in section 7.2.

If the reheating temperature is of the order of the singlet masses or higher, we can then use Eq. (4.20) to estimate the particle abundance of each singlet state via

$$N_{N_i}(z \approx 1) \approx \frac{(\Gamma_{D,i} + \Gamma_{\Delta L=1,i}) N_{N_i}^{\mathrm{eq}}}{H(z=1)} \approx K_i \,. \tag{7.10}$$

Moreover, since the wash-out rate is the sum over the rates of all possible inverse decays and $\Delta L = 1$-scatterings (with appropriate pre-factors), we can write

$$\Gamma_W \approx \sum_{i=1}^{n_{\mathrm{eff}}} \frac{1}{2}\Gamma_{ID,i} + \frac{2}{3}\Gamma_{\Delta L=1,i} \approx \sum_{i=1}^{n_{\mathrm{eff}}} \Gamma_{D,i} \,, \tag{7.11}$$

for $T \gtrsim M_i$.

Similarly to the same manner in which we reached Eq. (4.24), we can therefore estimate the $B-L$ asymmetry around $z=1$ by

$$N_{B-L}(z=1) \approx \sum_{i=1}^{n_{\mathrm{eff}}} \varepsilon_i N_{N_i}(z \approx 1) \exp\left(-\frac{\Gamma_W}{H(z=1)}\right) \tag{7.12}$$

$$\approx \left(\sum \varepsilon_i K_i\right) \exp\left(-\sum K_i\right) \,, \tag{7.13}$$

with the important difference that we are generally not allowed to linearize the exponential function around zero this time. This is due to the fact the sum over the K_i can be now bigger than one, even though each K_i is much smaller.

As the decays of the thermally produced particles yield an asymmetry of the size $-\sum \varepsilon_i N_{N_i}(z \approx 1)$ (cf. sec.4.5.2), the sum of the $B-L$ asymmetries from production and decay therefore reads

$$N_{B-L}(z \to \infty) \approx \left(\sum \varepsilon_i K_i\right) \left[\exp\left(-\sum K_i\right) - 1\right] . \tag{7.14}$$

While this yields

$$N_{B-L}(z \to \infty) \approx -\left(\sum \varepsilon_i K_i\right) \left(\sum K_i\right) , \tag{7.15}$$

if $\sum K_i \ll 1$, we can approximate

$$N_{B-L}(z \to \infty) \approx -\sum \varepsilon_i K_i \, , \tag{7.16}$$

if $\sum K_i > 1$.

In the context of the latter equation, we note that the phrase "weak wash-out" might be confusing, here, since the combined wash-out processes are in equilibrium around $z \approx 1$, in this case. However, as the combined processes will typically still be frozen out by the time the singlets decay, we will keep referring to this scenario as a weak wash-out scenario.

From Eqs. (7.15) and (7.16) it is now evident that many right-handed neutrinos can indeed easily increase the final $B-L$ asymmetry in the weak wash-out regime. In particular, in the case of similar masses and couplings, the asymmetry increases proportional to n_{eff}^2 for smaller n_{eff} and has a linear dependence on n_{eff} as soon as the condition $\sum K_i > 1$ is fulfilled. This is also illustrated by the numerical solutions shown in figure 7.2.

Yet, we already stress, that the treatment from this section is only valid, as long as the energy density of the right-handed neutrinos does not become comparable to the background energy density that governs the expansion of the universe. Once these energies become comparable, the analysis becomes more complex, and we will consider this case in section 7.4. In the present context, it is sufficient to remark that our present treatment remains sensible as long the number of actively participating singlet states n_{eff} obeys the rough upper bound

$$n_{\text{eff}} \lesssim \frac{90}{\sqrt{K}} \, , \tag{7.17}$$

as we show in Ref. [124].

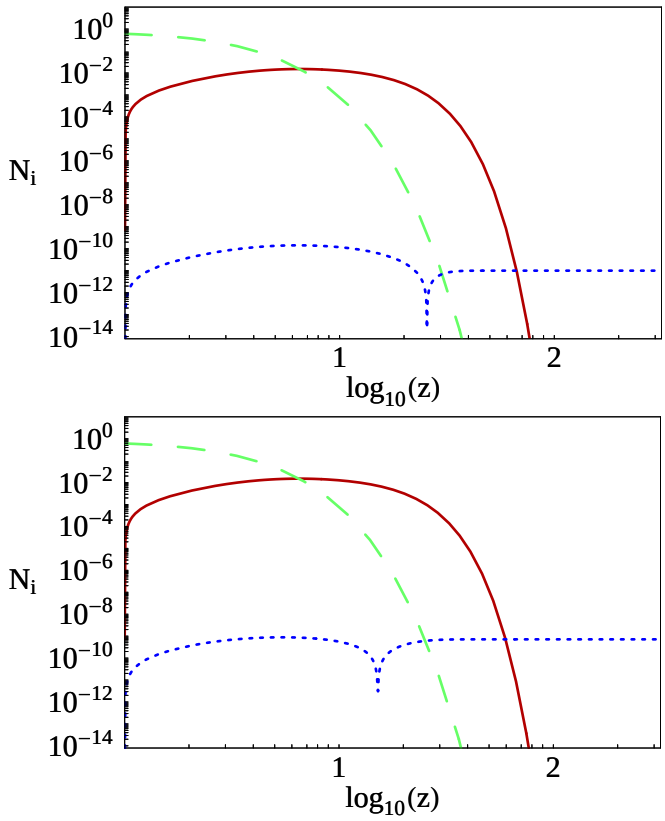

Figure 7.2: *These two graphs illustrate the numerical solutions of two weak wash-out scenarios with many singlets. Except for the increased number of singlet states (10 in the first graph, 100 in the second), we used the same parameter values as in the setup considered in figure 4.3. As in earlier figures, the red/solid line shows the abundance of particles of one singlet species in a comoving volume containing one photon N_{N_i}, whereas the green/dashed line illustrates the abundance of the corresponding equilibrium value $N_{N_i}^{eq}$. The blue/dotted line still represents the absolute amount of the corresponding $B-L$ asymmetry $|N_{B-L}|$. For the first scenario we found a final value of $|N_{B-L}(t \to \infty)| = 1.0 \cdot 10^{-11}$, which is by a factor of 10^2 larger than the corresponding one-particle scenario, as suggested by our approximative approach in Eq. (7.15). In the second scenario the wash-out processes are in equilibrium around $z = 1$ and the final asymmetry was found to be $|N_{B-L}(t \to \infty)| = 7.2 \cdot 10^{-10}$. This also matches roughly our corresponding estimation in Eq. (7.16).*

7.3.1 Weak and Strong Wash-Out

As we have seen, the increase of the wash-out rate at early times can have a large impact on leptogenesis in the weak wash-out regime. In the previous section, this was achieved via the addition of many weak wash-out states. However, in the case of less singlet states in the weak wash-our regime, this can also be achieved by the addition of a few states in the strong wash-out regime. These states can also wash-out the asymmetry produced during the creation of the weakly coupled particles and thereby prevent a cancellation of asymmetries, when these particles

decay again. In fact, one strong wash-out state can do the job of hundreds of weak wash-out states in this context.

To formulate this more quantitatively, let us also consider the case, where parts of our set of thermally excited right-handed neutrinos have $K_i \ll 1$ and others $K_i \gg 1$. We will refer to the corresponding numbers of particle species $n_{\text{eff,w}}$ and $n_{\text{eff,s}}$ and further assume that all of these particles are within the same mass range.

Combining our above considerations with our estimates from the previous sections, we can now approximate the final asymmetry by

$$N_{B-L}(z=\infty) \approx -0.05 \frac{\sum_{i=1}^{n_{\text{eff,s}}} \varepsilon_i}{\sum_{i=1}^{n_{\text{eff,s}}} K_i} - \sum_{i=1}^{n_{\text{eff,w}}} \varepsilon_i K_i \,, \tag{7.18}$$

where the sums in the two terms obviously run over different particle species. We note again that, due to the wash-out of the strongly coupled particles, the asymmetry produced by the decays of the weakly coupled singlets is not canceled, here.

In figure 7.3 we give a numerically calculated example for one strongly coupled and ten weakly coupled particles, which nicely agrees with this estimate.

7.4 The Weak Wash-Out Scenario II

In section 7.3, we have seen that one can indeed increase the final baryon asymmetry of leptogenesis scenarios by increasing the number of right-handed neutrinos. However, the approximative formulae in Eqs. (7.16) and (7.18) correspond to the Boltzmann equations (7.4) and (7.5) and are therefore only valid in a universe which is dominated by background radiation, and where the energy loss of this background due to the production of the singlet states can be neglected. As we already mentioned in section 7.3, this is ensured as long as $n_{\text{eff}} \lesssim 90/K^{1/2}$.

Yet, once we start to consider larger numbers of singlets, we have to include the dynamics of the universe into our system of differential equations (cf. section 1.2). Additionally, once the energy density stored in the singlets becomes comparable to the background energy density, we can no longer neglect the fact that a further production of singlets reduces the latter quantity. Otherwise, we would be able to produce an infinite number of massive singlets from a finite energy, which is obviously not possible.

As already mentioned, we can therefore no longer use Eqs. (7.4) and (7.5) to describe the dynamics of our model in this case. Nevertheless, we are still interested if the final $B-L$ asymmetry can get further increased in this regime, and for our numerics we will therefore make use of the more complex system of

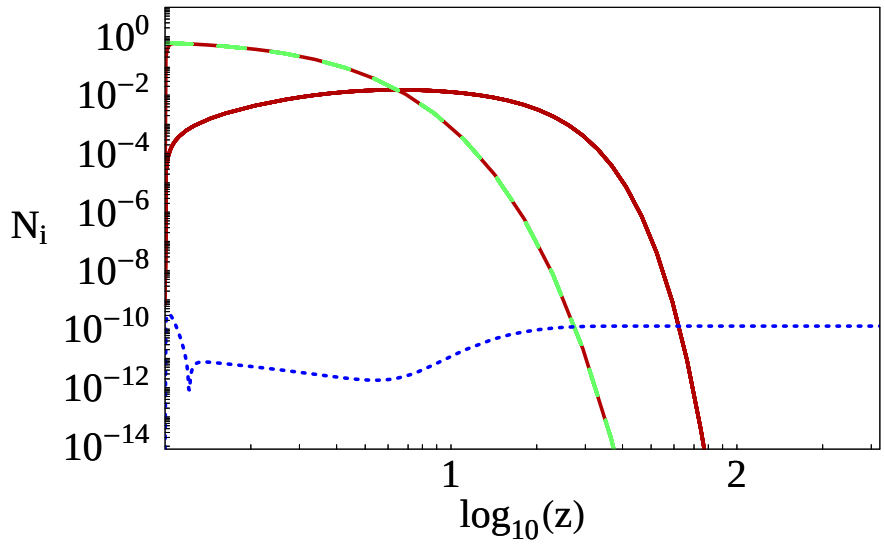

Figure 7.3: *This figure illustrates the numerical results of a leptogenesis scenario with one strongly coupled right-handed neutrino ($K = 10^2$) and ten weakly coupled ones ($K = 10^{-2}$). All the other parameter values were chosen as in the previously considered numerical examples. Once again, the green/dashed line shows the thermal equilibrium abundance of each of the species in a comoving volume containing one photon $N_{N_i}^{eq}$. The corresponding actual abundances N_{N_i} are illustrated by the red/solid lines, whereas the absolute amount of the $B-L$ asymmetry in the same volume $|N_{B-L}|$ is shown by the blue/dotted line and takes the final value $1.3 \cdot 10^{-10}$. We see, that the strongly coupled singlet closely follows the equilibrium value and washes out the $B-L$ asymmetry produced during the population of the weakly coupled states. At later times the latter particles decay and the main part of the final asymmetry is produced.*

differential equations

$$\frac{dN_{N_n}}{dt'} = -\frac{1}{H_0}(\Gamma_{D,n} + \Gamma_{\Delta L=1,n})\,(N_{N_n} - N_{N_n}^{\rm eq})\,, \tag{7.19}$$

$$\frac{dN_{B-L}}{dt'} = -\frac{1}{H_0}\sum_{n=1}^{n_{\rm eff}}\left[\varepsilon_n(\Gamma_{D,n} + \Gamma_{\Delta L=1,n})\,(N_{N_n} - N_{N_n}^{\rm eq}) + \Gamma_{W,n}N_{B-L}\right], \tag{7.20}$$

$$\frac{d(\rho_\gamma a^3)}{dt'} = -(\rho_\gamma a^3)\frac{H(t')}{H_0} - \sum\frac{d(N_{N_n})}{dt'}\langle E_n\rangle\,, \tag{7.21}$$

$$\frac{da}{dt'} = \frac{H(t')}{H_0}a(t')\,, \tag{7.22}$$

where $t' \equiv tH_0$ is the time measured in units of $H_0 \equiv 1.66 g_*^{1/2} M_1^2/M_{\rm Pl}$, and a now represents a comoving length scale, where the volume a^3 contains one photon at early times (of course, the number of photons in this volume can now change with time due to the production and decay of the singlets). Further, N_{N_n} is the abundance of particles of the species N_n in the same comoving volume, and N_{B-L} is the corresponding value for the $B-L$ asymmetry.

Additionally, we also make use of the relations

$$H(t') = \sqrt{\frac{8\pi}{3}}\frac{1}{M_{\rm Pl}}\sqrt{\frac{\pi^2}{30}g_* T^4 + \sum \frac{N_{N_n}}{R^3}\langle E_n\rangle}\,, \tag{7.23}$$

$$\langle E_n\rangle = 3\,T + M_n\frac{K_1(M_n/T)}{K_2(M_n/T)}\,, \tag{7.24}$$

$$T = \left(\frac{30}{\pi^2}g_*^{-1}\rho_\gamma\right)^{\frac{1}{4}}\,, \tag{7.25}$$

where $\langle E_n\rangle$ is the mean energy [2] of the species N_n, which is assumed to be in kinetic equilibrium and described and Maxwell-Boltzmann distribution.[2]

In addition to a numerical treatment of these quite complex equations, we can again make some approximations in the manner of the previous sections, that can help us to estimate the final lepton asymmetry of the corresponding scenarios. We therefor note that it makes limited sense to consider values of $n_{\rm eff}$ beyond the point where the energy density stored in the right-handed neutrinos becomes comparable to the energy density of the radiative background, if we are mainly interested in maximizing the final $B-L$ asymmetry. This is due to the fact that there will not be enough energy left to significantly increase the number density of the right-handed neutrinos if $n_{\rm eff}$ is increased further. In fact, for larger values of $n_{\rm eff}$ the radiation energy might even be transferred to the singlet sector so quickly that there will not be enough time for the wash-out processes to prevent the cancellation of the asymmetries which have been produced during creation and decay of the singlets. If this was the case, it would most likely lead to a decrease of the final asymmetry.

Hence, we restrict our considerations to scenarios, where the number of singlet states does not surpass the value discussed in the previous section. This condition can be quantified by the relation $\rho_N(T \approx M_1) \lesssim \rho_\gamma(T \approx M_1)$, which in turn implies

$$n_{\rm eff} K M_1^4 \lesssim \frac{\pi^2}{30}g_* M_1^4\,, \tag{7.26}$$

if all significantly abundant singlet states have masses around M_1.

If this condition is fulfilled, the corresponding number density of each singlet state per photon around $T \approx M_1$ is still given by Eq. (7.10). Moreover, with the help of Eqs. (1.5) and (7.10) we can also estimate the absolute particle number

[2]Since the singlets are only weakly coupled to the SM lepton doublets and have no further interactions, the assumption of kinetic equilibrium is only considered as an approximation in this context.

density of each state at the time of its decay to be

$$\begin{aligned} n_N(t=\Gamma^{-1}) &= n_N(z=1)\left(\frac{a(z=1)}{a(t=\Gamma^{-1})}\right)^3 , && (7.27)\\ &\approx n_{\text{eff}} K \left(2\,\frac{\xi(3)}{\pi^2} M_1^3\right)\left(\frac{3}{2}K^{-1}\right)^{-2} , && (7.28)\\ &\approx 0.1\cdot n_{\text{eff}} K^3 M_1^3 . && (7.29) \end{aligned}$$

We further note that, just before these particles decay, they will be the dominant component of the energy density. Therefore, we cannot neglect the photons produced by these decays, if we want to determine the final baryon-to-photon ratio. From the energy density of the singlets

$$\rho_N \approx M_1 n_N , \tag{7.30}$$

we therefore approximate the entropy density after their decay by [1]

$$s \approx \frac{4}{3} g_*^{1/4} \rho^{3/4} . \tag{7.31}$$

Together with Eq. (1.16) we can, then, approximate the number density of photons after the singlets decay by

$$n_\gamma(t=\Gamma^{-1}) \approx 2\,\frac{\xi(3)}{\pi^2}\frac{45}{2\pi^2 g_*} s \approx 0.4\cdot 10^{-2}\, n_{\text{eff}}^{\frac{3}{4}} K^{\frac{9}{4}} M_1^3 . \tag{7.32}$$

Hence, our estimate for the maximal final value of the $B-L$ asymmetry per photon (at early times) reads

$$\frac{n_{B-L}}{n_\gamma} \approx -\varepsilon_1 \frac{n_N(t=\Gamma^{-1})}{n_\gamma(t=\Gamma^{-1})} \approx -\varepsilon_1\, 25\, n_{\text{eff}}^{\frac{1}{4}} K^{\frac{3}{4}} . \tag{7.33}$$

We see that the linear dependence of the $B-L$ asymmetry on n_{eff} from the previous section does no longer hold, once the singlets become the dominant energy source in the universe. In additional, we remind the reader, that this dependence one $n_{\text{eff}}^{\frac{1}{4}}$ is also only valid as long as n_{eff} remains within the bounds of Eq. (7.26).

A numerical solution using Eqs. (7.19)-(7.25) for this scenario is also shown in Fig. 7.4, which roughly matches our approximation from Eq. (7.33).

7.5 Parameter Bounds

In this section, we want to briefly discuss the possible impact of many right-handed neutrinos on the bounds presented in section 4.5. We will therefore first

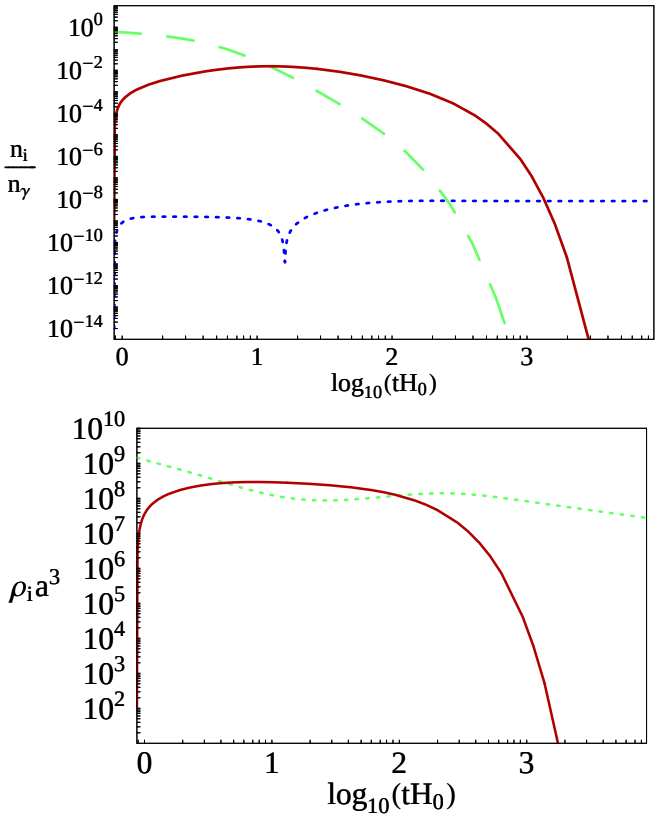

Figure 7.4: *These graphs illustrate the numerically calculated dynamics of the leptogenesis scenario in a singlet dominated universe from the text. For both graphs, the parameters* $K = 10^{-2}$ *and* $n_{eff} = 3000$ *were used, with all other parameters as in the previously considered cases. The upper graph shows the equilibrium abundance of the singlets (green/dashed) per photon* $n^{eq}_{N_i}/n_\gamma$*, their corresponding actual abundance (red/solid)* n_{N_i}/n_γ *and the absolute amount of the* $B-L$ *asymmetry (blue/dotted) per photon* $|n_{B-L}/n_\gamma|$*, which is found to be* $8.4 \cdot 10^{-9}$ *at the end of the calculation. This roughly agrees with our estimate in Eq. (7.33). The time* t *was chosen such that* $t = 0$ *corresponds to the singular point in the previously radiation dominated universe. The lower graph shows the radiation energy in a comoving volume that contains one photon at early times* $\rho_\gamma a^3$ *(green/dotted) and the corresponding energy stored in the singlets* $\rho_N a^3$ *(red/solid) in GeV. We therefore see on this graph that the singlets, indeed, get to dominate the universe before their decay.*

discuss their possible effect on the Davidson-Ibarra bound, which is a crucial parameter for the bounds in the corresponding standard cases and therefore obviously also important in the present discussion. Yet, already independently of a possible relaxation of the Davidson-Ibarra bound the upper bound for the necessary reheating temperature gets significantly relaxed in our setting, as we will discuss afterwards. Subsequently, we will also consider the possible impact of the singlets on the upper bound for the light neutrino masses in the approximative manner of section 4.5.4.

7.5.1 The Davidson-Ibarra Bound Revisited

The Davidson-Ibarra bound presented in Eq. (4.9) gives an upper bound for the net CP-asymmetry per decay of the lightest of three right-handed neutrinos with hierarchical masses. In the case of many decaying singlets it is therefore important to know, if such an upper bound also exists for the corresponding CP-asymmetries defined in Eq. (7.3).

However, in this context we note that in the scenarios we discussed in this chapter, we considered the case of many singlets with quasi-degenerate masses. Since the original Davidson-Ibarra bound is only valid for hierarchical masses, these quasi-degenerate particles could already render this bound invalid in the standard three-singlet scenario (cf. Refs. [100, 101]). Yet, the particles of comparable masses might also have similar Yukawa couplings. In this case, the CP-asymmetries which are due to the interference of the corresponding diagrams can become negligible, as it will be the case in the extra-dimensional scenario we present in section 7.6. In such scenarios, the relevant CP-asymmetries come from loop diagrams that include heavier singlets with different Yukawa couplings. In this case, it is not so obvious what happens to the Davidson-Ibarra bound and we will therefore discuss this in more detail, here.

We first note that, under the above assumptions, the average CP-violation per decay of one of the right-handed neutrinos ε_i is still given by the interference of the diagrams in Fig. 4.2, where only the indices need some adaption and the number of the diagrams is increased by the larger number of singlets that can propagate in the respective loops.[3] Therefore, we can simply use Eq. (4.8) to determine the various ε_i and thereby find

$$\varepsilon_i = -\frac{3}{16\pi}\sum_k \frac{\mathrm{Im}\left[(gg^\dagger)^2_{ik}\right]}{(gg^\dagger)_{ii}}\frac{M_i}{M_k} + \mathcal{O}\left(\frac{M_i^2}{M_k^2}\right) \tag{7.34}$$

$$= -\frac{3}{16\pi}\frac{M_i}{\langle\phi\rangle^2}\frac{1}{(gg^\dagger)_{ii}}\mathrm{Im}\left[(gm_\nu^\dagger g^T)_{ii}\right] + \mathcal{O}\left(\frac{M_i^2}{M_k^2}\right) \tag{7.35}$$

with k running from 1 to n_N, now.

As we only needed to increase the range of certain indices, our analysis has been almost identical to the three-singlet case, up to this point, and the corresponding formulas therefore still look very similar. However, in the case of more than three singlets it is, nevertheless, no further possible to derive the Davidson-Ibarra bound from Eq. (7.35) [128]. In fact, as we show in appendix D, Eq. (7.35) now leads to the weaker relation

$$|\varepsilon_1| \lesssim \frac{3}{16\pi}\frac{M_1 m_3}{\langle\phi\rangle^2} \approx 10^{-7}\left(\frac{m_3}{0.05\mathrm{eV}}\right)\left(\frac{M_1}{10^9\mathrm{GeV}}\right). \tag{7.36}$$

[3] In principle, the large number of possible diagrams in this case can invalidate the perturbative approach via Feynman diagrams. However, for Yukawa couplings that yield the light neutrino masses without delicate cancellations this is typically not the case.

At first glance, this equation seems to match Eq. (4.10). Yet, in the latter equation m_3 is fixed around 0.05 eV. In the presence of many singlets, instead, m_3 is in general a free parameter in Eq. (7.36), and therefore the standard Davidson-Ibarra bound can be considerably weakened.[4]

However, as we shall also see in section 7.6, the original Davidson-Ibarra bound in Eq. (4.9) is still valid in many cases. This is due to the fact that the number of free parameters for the Yukawa couplings can be reduced by symmetries. In particular, the condition of maximal CP asymmetries for all decaying particles from our previous considerations might further motivate such effects. Moreover, in spite of our discussion in section 7.5.3, it is also not perfectly clear what happens to the upper mass bound for the light neutrinos, in many-singlet scenarios. If this upper mass bound remains comparable to the standard bound, m_3 (and with it ε_i) will only be allowed to increase by an approximate factor of two or three.

Therefore, we will remain conservative at this point and not consider possible CP asymmetries beyond the original Davidson-Ibarra bound in the following subsections. Nevertheless, it should be kept in mind, that there might be possibilities to further relax the following bounds due to the arguments given in this subsection.

7.5.2 Lower Bounds for M_1 and T_r

Let us now discuss the the possible impact of leptogenesis with many singlets on the necessary reheating temperature, which is of special relevance due to the bounds from gravitino production, we mentioned in section 4.5.4.

As we saw in the previous sections, the presence of many right-handed neutrinos can only help to increase the final baryon asymmetry in the weak wash-out regime, if the Davidson-Ibarra bound is not relaxed. With respect to our discussion at the end of section 7.5.1, it will thus be sufficient to consider this parameter region, here.

Among these scenarios, we found the largest final asymmetry in the case where n_{eff} was maximized with respect to Eq. (7.26). If we therefore combine this equation with Eqs. (4.10),(4.13), and (7.33), we find the approximate upper bound

$$\eta_B \lesssim 5 \cdot 10^{-8} \sqrt{K} \left(\frac{m_3}{0.05\text{eV}}\right) \left(\frac{M_1}{10^9\text{GeV}}\right) , \tag{7.37}$$

for the final baryon asymmetry.

As K has to fulfill the additional condition $K \ll 1$ in this relation, we can use $K \approx 10^{-2}$ to find an approximate lower bound for the reheating temperature around of $T_r \approx M_1 \gtrsim 10^8$ GeV. We further note that an increase of K by an order

[4]The analysis in Ref. [96] that shows the the CP-asymmetries of decays and $\Delta L = 1$ scatterings are identical in the case of hierarchical heavy neutrinos is independent of the number of singlet states. Therefore, it is sufficient to consider the decay asymmetries at this point.

of magnitude or so, would slightly increase the result of this formula. However, the corresponding numerics show that we would not be allowed to neglect the wash-out processes around the corresponding decay-time anymore, in this case, and that the corresponding final asymmetry already tends to smaller values in the respective parameter range.

Numerically we were, nevertheless, able to push the lower bound for M_1 and T_r a little further. More precisely, we were able reproduce the observed BAU with the parameter values $K = 10^{-2}$, $n_{\text{eff}} = 10^4$ and

$$T_r = M_1 = 6.5 \cdot 10^7 \text{GeV}. \tag{7.38}$$

As we can see, this relaxes the corresponding lower bound in Eq. (4.33) for standard thermal leptogenesis by approximately one and a half orders of magnitude. Even more, we note that this result was achieved using the standard Davidson-Ibarra bound. Within the context of our discussion in section 7.5.1, an even further relaxation of this bound might therefore actually be possible.

7.5.3 Upper Bound for Light Neutrino Masses

Let us now consider the possible impact of many singlets on the upper mass bound for the light neutrinos in leptogenesis scenarios.

We therefore note that the corresponding analysis for the three-singlet case in section 4.5.4 needs significant adjustment in the present case. This is due to the fact that we cannot draw the conclusion that we are in the strong wash-out regime from the fact that we have three degenerate light neutrinos, now. In particular, three degenerate light neutrinos can easily be realized by a model with three singlets which are in the strong wash-out regime and many more singlets that are weakly coupled. In this case it might be possible that the latter ones determine the size of the final baryon asymmetry while the strongly coupled singlets determine the size of the light neutrino masses (cf. also section 7.3.1). In spite of the relatively large masses for the light neutrinos within the discussion of the corresponding upper bound, we will therefore assume to be in the weak wash-out regime.

As we saw in section 4.5.4, the upper mass bound for light neutrinos is due to $\Delta L = 2$ scatterings in the early universe. It is therefore important to note that the corresponding reaction rate does not get modified in the presence of many singlets, since the relevant Feynman diagrams are the same as the ones that yield neutrino masses and the sum of these diagrams is therefore fixed.

As we also discussed in section 4.5.4, these $\Delta L = 2$ scatterings need to be frozen out at the time of the decay of the singlets. In the following we will therefore require them to be frozen out around $T = M_1$, which is obviously quite conservative in the weak wash-out regime.

Nevertheless, if we now combine Eqs. (4.37), (4.38), (4.13), and (7.33), we find

$$\left(\frac{\overline{m}}{\mathrm{eV}}\right) \lesssim 6\, n_{\mathrm{eff}}^{\frac{1}{12}}\, K^{\frac{1}{4}}\,, \tag{7.39}$$

as a rough upper bound for the quadratic mean of the light neutrino masses.

Thus, even obeying the original Davidson-Ibarra bound, our approximations indicate that the bound on the absolute neutrino mass scale from leptogenesis with many singlets becomes less stringent than the corresponding bounds from other areas (cf. section 3.2).

This is very interesting in the context of our discussion in section 7.5.1. However, so far our results come from a rather qualitative approach, and therefore this result will need to be confirmed by a more thorough analysis.

7.6 An Extra-Dimensional Example

In this section we will present a realization of leptogenesis with many neutrinos within a concrete model. Therefore, we will employ the extra-dimensional setting that was introduced in section 3.4.3 and also used in the neutrino mass models in chapter 6. Hence, we will assume that the SM particles are constrained to a 3-brane, while three additional SM singlets can propagate in the bulk of a compactified extra dimension. As we will see, this setting can easily provide many quasi-degenerate neutrino singlets through Kaluza-Klein excitations of the bulk states, which makes it a promising setting for leptogenesis with many neutrinos.

We will therefore first discuss the relevant features of this model in the context of leptogenesis in some detail. Afterwards, we will use large parts of our previous analysis, to describe the dynamics of the corresponding leptogenesis scenario and to get an estimate for the lower bound for the reheating temperature in this setting.

Further leptogenesis scenarios that also consider leptogenesis in extra-dimensional settings can be found in Refs. [129–132]. Even though these scenarios also include many right-handed states, the respective working principles are quite different, which we discuss more thoroughly in Ref. [124].

7.6.1 The Setting

As already stated, we will work within the setting introduced in section 3.4.3. Additionally, we will assume a scalar-like Majorana mass terms for the singlets, which implies $M_V = 0$ in Eq. (3.47).

As before, we can formally integrate over the extra-dimension and are afterwards left with an effective four-dimensional theory that contains the SM particles and a Kaluza-Klein tower of singlet modes. In the basis in which the sub-matrix

in Eq. (3.52) is diagonal and positive, the infinite Majorana mass matrix of the neutrino sector in Eq. (3.51) can then reads[5]

$$\begin{pmatrix} 0 & -m_0^T & \cdots & -\mathrm{i}\, m_{n,-}^T & -m_{n,+}^T & \cdots \\ -m_0 & M & \cdots & 0 & 0 & \cdots \\ \vdots & \vdots & \ddots & \vdots & \vdots & \ddots \\ -\mathrm{i}\, m_{n,-} & 0 & \cdots & \sqrt{M^2 + n^2/R^2} & 0 & \cdots \\ -m_{n,+} & 0 & \cdots & 0 & \sqrt{M^2 + n^2/R^2} & \cdots \\ \vdots & \vdots & \ddots & \vdots & \vdots & \ddots \end{pmatrix} . \tag{7.40}$$

with

$$(m_0)_{ij} = \frac{m_{D,ji}}{\sqrt{2}} \quad \text{and} \quad (m_{n,\pm})_{ji} = \pm \frac{m_{D,ij}}{\sqrt{2}} \sqrt{1 \pm \frac{M_i}{\sqrt{M_i^2 + n^2/R^2}}} \tag{7.41}$$

and

$$\left(\sqrt{M^2 + n^2/R^2}\right)_{ij} = \delta_{ij} \sqrt{M_i^2 + n^2/R^2}\,. \tag{7.42}$$

We see that the Kaluza-Klein tower consists of pairs of fields with degenerate masses, in this case. We further note that many different pairs will, additionally, have quasi-degenerate masses, if the condition $M_i R \gg 1$ is fulfilled. Since this is a rather natural condition, the effective four dimensional theory can therefore naturally yield many quasi-degenerate singlet states, as we claimed earlier.

From the matrix in Eq. (7.40), we can also infer the Yukawa couplings of the different modes $\Psi_{\pm,i}^{(n)}$ to the SM leptons. These are given by the relations

$$(Y_0)_{ij} \equiv \left(\frac{m_0}{\langle\phi\rangle}\right)_{ij} = \frac{g_{ij}}{\sqrt{2\pi R M_5}}\,, \tag{7.43}$$

$$(Y_{+,n})_{ij} \equiv \left(\frac{m_{n,+}}{\langle\phi\rangle}\right)_{ij} = +\frac{g_{ij}}{\sqrt{2\pi R M_5}} \sqrt{1 + \frac{M_i}{\sqrt{M_i^2 + n^2/R^2}}}\,, \tag{7.44}$$

$$(Y_{-,n})_{ij} \equiv \left(\frac{\mathrm{i}\, m_{n,-}}{\langle\phi\rangle}\right)_{ij} = -\mathrm{i}\frac{g_{ij}}{\sqrt{2\pi R M_5}} \sqrt{1 - \frac{M_i}{\sqrt{M_i^2 + n^2/R^2}}}\,. \tag{7.45}$$

In this context, we remark that the coupling strengths of the $\Psi_{+,i}^{(n)}$ and $\Psi_{-,i}^{(n)}$ modes become similar for $n \gg M_i R$, whereas we find

$$(Y_{+,n})_{ij} \approx +\frac{g_{ij}}{\sqrt{\pi R M_5}} \left(1 - \frac{1}{8}\left[\frac{n}{M_i R}\right]^2\right)\,, \tag{7.46}$$

$$(Y_{-,n})_{ij} \approx -\frac{g_{ij}}{2\sqrt{\pi R M_5}} \frac{n}{M_i R}\,, \tag{7.47}$$

[5]The author would like to thank Naoyuki Haba for related, private notes on the five dimensional see-saw (with vector-like masses) [133], that inspired the presented treatment.

for $0 < n \ll M_i R$, which illustrates the (later on) important effect that the couplings of the lighter modes of $\Psi^{(n)}_{-,i}$ can be strongly suppressed with respect to their "partner" modes $\Psi^{(n)}_{+,i}$, if the condition $M_i \gg R^{-1}$ is fulfilled.

7.6.2 CP-Asymmetries

In the previous section, we have seen that our setting can naturally yield many quasi-degenerate neutrinos, which makes this model interesting for leptogenesis with many neutrinos. Therefore, we will now determine the average CP-asymmetry $\varepsilon_{\pm,i}$ per decaying singlet $\Psi_{\pm,i}$. With the Yukawa couplings from the previous section and our considerations from section 7.5.1, this is now fairly straight-forward.[6]

Let us in the following assume $M_3 \geq M_2 \gg M_1 \gg R^{-1}$. Applying Eq. (7.35), we then find

$$\varepsilon^{(n)}_{\pm,i} = -\frac{3}{16\pi}\frac{M_{i,n}}{\langle\phi\rangle^2}\frac{1}{[(Y_{\pm,n})(Y_{\pm,n})^\dagger]_{ii}}\mathrm{Im}\left[(Y_{\pm,n})m_\nu^\dagger(Y_{\pm,n})^T)\right]_{ii}, \tag{7.48}$$

with $M_{i,n} = \sqrt{M_i^2 + n^2/R^2}$, which leads to the CP asymmetries

$$\varepsilon^{(n)}_{+,i} = -\frac{3}{16\pi}\frac{M_{i,n}}{\langle\phi\rangle^2}\frac{1}{[gg^\dagger]_{ii}}\mathrm{Im}\left[(gm_\nu^\dagger g^T)\right]_{ii} \tag{7.49}$$

$$\varepsilon^{(n)}_{-,i} = \frac{3}{16\pi}\frac{M_{i,n}}{\langle\phi\rangle^2}\frac{1}{[gg^\dagger]_{ii}}\mathrm{Im}\left[(gm_\nu^\dagger g^T)\right]_{ii} = -\varepsilon^{(n)}_{+,i}, \tag{7.50}$$

after some further transformations.

Thus, each mode features two particle species of the same mass, that yield exactly opposite CP-asymmetries. Further, the CP asymmetries only depend on the five dimensional wave number n through the proportionality factor $M_{i,n}$, which shows that the dependence of the Yukawa couplings on n does not appear in the CP-asymmetries.

Let us also stress, that in the case $M_3 \geq M_2 \gg M_1 \gg R^{-1}$, in which we have many quasi-degenerate neutrinos, we do not get any resonance or higher-order effects that further increase the various $\varepsilon^{(n)}_{\pm,i}$. Therefore, our use of Eq. (7.35) was perfectly valid, here. The absence of these effects is in turn due to the fact that all the quasi-degenerate particles with masses around M_1 have the same Yukawa couplings (except for a purely real or imaginary overall factor).

Furthermore, as we also show in Ref. [124], the simple relations between the various Yukawa couplings in this model also ensure that the original Davidson-Ibarra bound from Eq. (4.9) is still valid, here, instead of the relaxed version in Eq. (7.36).

[6] Since there are cancellations between the various contributions to the see-saw in this model, the perturbative approach using Feynman diagrams might generally encounter problems in this setting. However, if the cut-off for our extra-dimensional theory is around the scale M_5, this problems seems to vanish.

7.6.3 Leptogenesis

We will now consider the actual leptogenesis process in this model, still assuming $M_3 \geq M_2 \gg M_1 \gg R^{-1} \gg 1$.

As we already noted in the context of Eq. (7.50), the various pairs $\Psi_{\pm,i}$ will yield $B-L$ asymmetries of the exact same size but opposite sign, when they decay. This implies that it might be hard to find a significant net asymmetry, if they are all strongly coupled. However, since Eqs. (7.44) and (7.45) show that the '+'- and '-'-modes couple to the SM leptons with different strengths, we will find different abundances of the corresponding particles in the weak wash-out regime. This can be considered as a lucky coincidence, since our previous treatment has shown that many singlet states can only increase the final BAU in the weak wash-out regime (if the Davidson-Ibarra bound holds).

Let us be more quantitative, now, and define the respective decoupling parameters of the different $\Psi_{\pm,i}$ by

$$K_{n,\pm} \equiv \frac{\Gamma_{D,n,\pm}(T \to 0)}{H(T=M_1)} = \frac{\left[(Y_{\pm,n})(Y_{\pm,n})^\dagger\right]_{11} M_{1,n}/(8\pi)}{1.66 g_* M_1^2/M_{\rm Pl}} = \left(1 \pm \frac{M_1}{M_{1,n}}\right) K_0\,, \tag{7.51}$$

for $n \geq 1$, with a corresponding definition for K_0.

Similarly, to our previous treatments, we now assume a reheating temperature around $T = M_1$. In this case, there are of the order of $M_1 R$ quasi-degenerate neutrinos with masses around M_1 which will reach significant particle abundances. Moreover, as long as $M_1 R$, and thereby $n_{\rm eff}$, does not exceed the bound from Eq. (7.26), the maximal abundances per photon of these particles will be given by their respective decoupling parameters $K_{n,\pm}$, as long as we are in the weak wash-out regime (cf. Eq. (7.10)).

Therefore, it is important to note that all the '+'-particles will have comparable decoupling parameters $K_{i,+} \approx K_0$, while all the relevant '-'-particles will have significantly smaller decoupling parameters $K_{i,-} < K_0$, as we can see from Eq. (7.51). Thus, within a rough treatment, we can neglect the abundance of the '-'-particles and simply assume that we have $M_1 R$ identical '+'-particles. In this case, we can use Eqs. (7.16) and (7.33) to find the estimates

$$N_{B-L} \approx 10^{-7} \left(\frac{m_3}{0.05{\rm eV}}\right) \left(\frac{M_1}{10^9{\rm GeV}}\right) (M_1 R)\, K_0\,, \tag{7.52}$$

or

$$\frac{n_{B-L}}{n_\gamma} \approx 2.5 \cdot 10^{-6} \left(\frac{m_3}{0.05{\rm eV}}\right) \left(\frac{M_1}{10^9{\rm GeV}}\right) (M_1 R)^{\frac{1}{4}}\, K_0^{\frac{3}{4}} \tag{7.53}$$

for the final $B-L$ asymmetry.

Which of these two formulae we need to apply depends on the number of singlets and therefore on the size of $M_1 R$ (cf. Eq. (7.17)). If $M_1 R K_0$ is smaller than one, we might even have to use Eq. (7.15), instead.

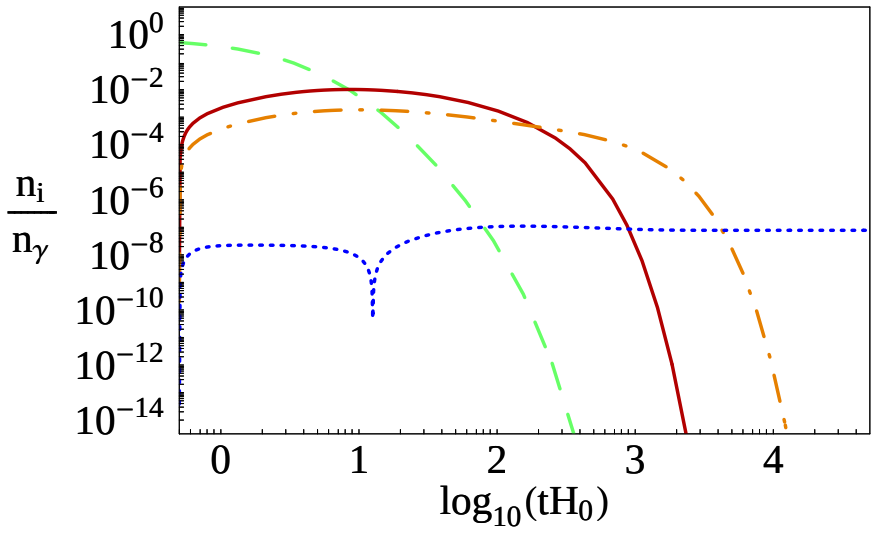

Figure 7.5: *This graph shows the numerical solution for M_1R pairs of particles with parameter values as described in the text. In particular, the green/dashed line represents the equilibrium abundance of each of the particle species per photon $n^{eq}_{N_i}/n_\gamma$. The red/solid line shows the corresponding value for a "+"-mode $n_{N_{i,+}}/n_\gamma$, while the density of the corresponding "-"-mode $n_{N_{i,-}}/n_\gamma$ is illustrated by the orange/dashed-dotted line. We see that the suppressed number of "-"-mode-particles is not able to erase the asymmetry produced by the decays of the "+"-modes. The absolute amount of the $B-L$ density n_{B-L}/n_γ is again represented by the blue/dotted line and reaches a final value of $7.8 \cdot 10^{-8}$.*

Further, to find the baryon asymmetry at very late times, we additionally need to include the dilution factor from Eq. (4.13) in Eqs.(7.52) and (7.53). Once this is done, one can see that parameters such as $M_1 = 2 \cdot 10^8$ GeV, $R^{-1} = 10^5$ GeV, and $K_0 = 10^{-2}$ in Eq. (7.53) seem to yield a baryon asymmetry of the right order of magnitude. Within our rough treatment, we therefore see that M_1 (and with it the reheating temperature) would already be one order of magnitude below the corresponding bound from standard thermal leptogenesis, in this case.

For a numerical treatment, we note that pairs of modes with higher wave-numbers (that still reach significant numbers) tend to contribute slightly less to the final baryon asymmetry (cf. Ref. [124]). For a conservative numerical estimate, we therefore simulated $2 \times M_1R$ states that are identical to the modes $\Psi_{\pm,n=M_1R}$ in Fig. 7.5. In the corresponding analysis, we were able to produce a final baryon asymmetry that was even slightly larger than the observed value with $R^{-1} = 10^5$ GeV, $K_0 = 10^{-2}$, and

$$T_r = M_1 = 2 \cdot 10^8 \text{GeV}, \tag{7.54}$$

assuming maximal CP asymmetry.

Therefore, both approximations indicate a relaxation of the bound for the reheating temperature by an order of magnitude within this explicit model. More-

over, since our corresponding assumptions seem rather conservative, this bound might even be relaxed further within a more precise numerical calculation.

Of course, lower values for the reheating temperature seem also possible if one considers smaller compactification scales ($R^{-1} < 10^5$ GeV), as this could further increase the number of actively participating singlet states n_{eff}. However, due to our arguments in Ref. [124], this option seems to conflict with bounds from the production of extra-dimensional gravitons.

7.7 Concluding Remarks

Let us briefly summarize the results of this chapter.

Considering leptogenesis scenarios with many singlets, we have found that the presence of these additional states can increase the final baryon asymmetry with respect to the standard case and that the corresponding lower bound for the reheating temperature can be significantly relaxed. In particular, within a numerical treatment we were able to relax this bound by one and a half orders of magnitude without the need for any resonance effects. Especially in the context of gravitino bounds, leptogenesis scenarios with many singlets are therefore an interesting option.

To implement this idea into a realistic setting, we additionally considered an extra-dimensional model, which naturally yields many right-handed neutrinos. Within a somewhat more approximative treatment of the corresponding leptogenesis scenario, our analysis still indicated a relaxation of the standard bound for the reheating temperature by at least one order of magnitude, in this more explicit model.

Furthermore, we also gave arguments that indicate the relaxation of the upper mass bound for the light neutrinos from standard leptogenesis, in the presence of additional singlets. This is especially interesting, since the Davidson-Ibarra bound does not generally hold in the considered context but was found to be proportional to the light neutrino mass scale. The combination of these two effects might therefore even further relax the previously discussed bound for the reheating temperature.

As a final remark, we also note that we have made a few simplifying assumptions within our analysis and the inclusion of further effects might therefore have additional interesting consequences. Especially, the inclusion of flavor effects might be an interesting topic in this context and leaves room for further investigation.

Conclusions

If nature is indeed governed by one simple underlying theory, we can expect to find more and more connections of different areas of physics on our way towards this unified description. In this thesis, we therefore discussed several models that comprise such possible connections. In particular, they relate different sub-sets of the topics baryogenesis, neutrino masses, dark energy and extra dimensions.

In view of these topics, the thesis started with reviews on selected background material from cosmology and particle physics. Subsequently, the first model was presented, which featured a connection between the baryon asymmetry of our universe and its observed accelerated expansion. This was achieved through the introduction of two new scalar fields, where one of them was the source of a dynamical dark energy term in the Friedmann equations, while the other acted as a mediator between this sector and the standard model particles. Within a $B - L$ conserving scenario, these two fields dynamically developed opposing asymmetries at early times, followed by the decay of the mediating field and the involved transfer of its asymmetry to the observable sector. In addition to a discussion of the Lagrangian of this scenario and the corresponding key dynamics, we also discussed different couplings between the mediating field and the observable sector.

As a second possible connection of distinct areas of physics we considered a class of models that features an interplay of extra-dimensions and family symmetries in order to explain the observed pattern of neutrino mass hierarchies and mixings. Here, the alteration of the see-saw formula, due to additional Kaluza-Klein modes of right-handed neutrinos, could help to overcome the cancellation of hierarchies that are needed within the concept of single right-handed neutrino dominance. We considered different natures of the extra-dimensional mass terms and presented explicit parameter values that yielded the desired neutrino data in each case.

The central work of this thesis was the discussion of leptogenesis with many neutrinos, which naturally establishes a connection between the baryon asymmetry of our universe and the masses of the light neutrinos, as all leptogenesis scenarios do. In the corresponding analysis, we were able to use much of the material from our introductory discussion of standard thermal leptogenesis to illustrate the possible effects of additional heavy singlet states in the weak and

strong wash-out regime. In particular, within a generalization of the presented standard treatment, we illustrated that the final baryon asymmetry of weak wash-out scenarios can be significantly enhanced without any increase of the respective CP asymmetries. Additionally, we confirmed this result numerically and found that the lower bound for the necessary reheating temperature in such scenarios could be relaxed by one and a half orders of magnitude within our treatment. Therefore, leptogenesis with many neutrinos might significantly relax the tension between leptogenesis and bounds from gravitino production in supergravity theories.

Moreover, as the standard Davidson-Ibarra bound for the net CP asymmetry per heavy particle decay does not generally hold in the presence of more than three right-handed neutrinos, we also derived a new corresponding bound for our setting, which was found to be proportional to the light neutrino mass scale. This is in particular interesting, as we additionally gave arguments that indicate the relaxation of the upper mass bound for the light neutrinos in scenarios with many singlets. Therefore, the combination of these effects might yield an even lower bound for the necessary reheating temperature in the respective scenarios, without any need for resonance effects.

To further motivate leptogenesis with many neutrinos, we then discussed a more explicit, extra-dimensional scenario, which operates in the same framework as the neutrino mass models that we considered earlier. In particular, we were able to show that the respective model can naturally yield many quasi-degenerate singlets and is, in this aspect, an almost ideal setting for the considered type of leptogenesis scenarios. Furthermore, we analyzed the corresponding dynamics within rather conservative estimations and again found a significant relaxation of the respective lower bound for the reheating temperature.

Thus, all the considered models offer attractive features and illustrate the enormous amount of possibilities for an interplay of different areas of particle physics and cosmology. Yet, there are, of course, also several open questions that remain within their context, and we will therefore briefly discuss a selection of them in the following.

In particular, in the model connecting dark energy and baryogenesis a further motivation for the introduction of the additional scalar sector would be desirable. However, this is already a problem in simpler quintessence models and should therefore probably be addressed in a more general context first. Another open point in this scenario are the initial VEVs of the different scalar fields, which have a strong impact on the size of the final baryon asymmetry and could also not be ascribed to a deeper principle so far.

In the context of the extra-dimensional neutrino mass model, it would be desirable to further motivate the various family charges of the different generations. Yet, this can again be seen as a problem of a larger class of models and should probably also be addressed in a more general framework. On a similar conceptual level, the necessary tuning of some of the Yukawa couplings in these scenarios

likewise waits for a deeper motivation.

In addition to such conceptual questions, leptogenesis with many neutrinos also features more concrete open issues. In particular, the indication for a relaxed upper bound for the light neutrino masses makes a more detailed analysis of this subject desirable. Moreover, the potential interplay of this effect and the relaxed Davidson-Ibarra bound is an interesting topic of its own, as it might relax the lower bound for the reheating temperature even further. Additionally, flavor effects have also not been considered so far and might have interesting consequences.

We therefore see that each of the considered models also offers questions for interesting future research, and it is the hope of the author that one or more of these will find an answer in the not too far future.

Acknowledgments

At this point, I would like to appreciate the company and help I have encountered by many people within the last three years.

In particular, I would like to thank

- Manfred Lindner for the opportunity to do research at his chair, for the possibility to go to interesting schools, workshops, and conferences all over Europe, as well as for the nice and loyal atmosphere he created in our group. I also appreciate his help in finding me a new advisor, when I had decided to finish my Ph.D. in Munich.

- Michael Ratz for taking me over as his Ph.D. student, when my old group left Munich. Even more, I thank him for the interest he has had in my research and the many valuable discussions in the context of the presented leptogenesis project. I am also grateful for his willingness to explain things to me at so many occasions and for the opportunity to present my research at an international conference. Finally, I appreciate it immensely that he still gave me the feeling of being taken seriously after I had decided to give my life a different direction after my Ph.D..

- Florian Bauer and Mathias Garny for being great co-workers and the excited but, at the same time, relaxed atmosphere they created during our joint project.

- Naoyuki Haba for the opportunity to work with him, for the things he explained to me during that time and the material he provided me with, as well as for initial discussions that eventually led to my main project in this thesis.

- Yosef Nir for valuable comments on my project on leptogenesis with many neutrinos, in particular, for his remark that the Davidson-Ibarra bound loses its validity in this context.

- Jan Hamann, Felix Schwab, Mark Rolinec, Mathias Garny, and Kai Schmidt-Hoberg for the proof-reading of this thesis as well as valuable comments.

- Herbert Müller and especially Stefan Recksiegel for perfect computer support.

- Karin Ramm for taking care of all those little things.

On a more personal level, I would also like to thank

- my office-mate Mark Rolinec for being the friend he has become within this time.

- Anton Poschenrieder for many valuable conversations during a time when we were in similar situations, and when I was not sure about my next best step.

- Elmar Wyszomirski, Felix Schwab, and Michael Spranger for a all the fun I have had with them and for being far more than just colleagues.

- Vassiliki Kanellopoulos, Selma Uhlig, Felix Schwab, Tobias Gail, and Andreas Weiler for their patience concerning my first steps.

- the many other people that helped creating a friendly atmosphere in the physics department. This includes Klemens Rottler, Andreas Weinberger, Claudia Hagedorn, Markus Müller, Alexander Blum, Tobias Gail, Jan Hamann, Mathias Garny, Michael Schmidt, Florian Bauer, Florian Plentinger, Andreas Hohenegger, Joern Kersten, Joachim Kopp, Alexander Merle, Harald Grießhammer, Joe Sato, Werner Rodejohann, Toshi Ota, Olliver Just, Michael Klaput, Sebastian Schatt, Christoph Promberger, Michael Wick, Monika Blanke, Björn Duling, Wolfgang Altmannshofer, David Straub, Michaela Albrecht, Katrin Gemmler, Diego Guadagnoli ...

If someone works on a project for more than three years it is obvious that the life outside of work has a tremendous impact on the results of this project. Therefore, I would have to thank many more people at this point. However, since I would not be able to express my thanks to these people properly, I will abstain from this public thank you almost entirely. To those people that are or have been important in my life and who read these lines, I can only say that I hope you are aware of how important you are to me and how grateful I am for meeting and knowing you.

The only people within this group I would like to thank at this point explicitely are Mama, Papa, Opa, Julia, and Guido for their support and for always giving me the security to know where I belong.

Appendix A

Orbifolds

Here, we will briefly review some of the characteristics of orbifolds, as they were used in the extra-dimensional models in chapters 3, 6, and 7.

A one-dimensional orbifold can be considered as a circle S^1, that has been compactified by a discrete symmetry condition. Namely, if the circle is parametrized by an angle $\phi\,\epsilon\,[-\pi,\pi]$, the points ϕ and $-\phi$ are identified. Mathematically one-dimensional orbifolds are denoted by $S^1/\mathbb{Z}_2$, as it is also illustrated in Fig. A.1

In field-theories such an orbifold is often parameterized by $y \equiv \pi R\phi$, where R is the radius of the corresponding circle. Further, an extra-dimensional action that respects this orbifold symmetry can be expressed as a field theory on a circle which is invariant under the parity transformation $P_5 : y \to -y$. Since the kinetic term of the five-dimensional action of a fermion $\Psi$is given by

$$S = \int d^4x\, dy\, \overline{\Psi}\gamma^\alpha \partial_\alpha \Psi\,, \tag{A.1}$$

we see that a fermionic field may not transform trivially under P_5, due to the term $\overline{\Psi}\gamma^5\partial_5\Psi$, which would acquire a minus sign with respect to the other derivative terms. This can be prevented by the transformation behavior

$$P_5\Psi_i = \gamma_5\Psi_i\,, \tag{A.2}$$

which we also used in section 3.4.3.

Since, each field of the theory also has to fulfill the circular periodicity condition,

$$\Psi(x^\mu, y + 2\pi R) = \Psi(x^\mu, y)\,, \tag{A.3}$$

we can decompose the field Ψ into Fourier modes. However, due to the different transformation laws of the upper and the lower components of Ψ in Eq. (A.2) they are made up of different Fourier modes, namely

$$\Psi(x,y) = \frac{1}{\sqrt{\pi R}} \begin{pmatrix} \frac{1}{\sqrt{2}}\Psi_R^{(0)}(x) + \sum\limits_{n=1}^{\infty} \cos(ny/R)\, \Psi_R^{(n)}(x) \\ \sum\limits_{n=1}^{\infty} \sin(ny/R)\, \Psi_L^{(n)}(x) \end{pmatrix}, \tag{A.4}$$

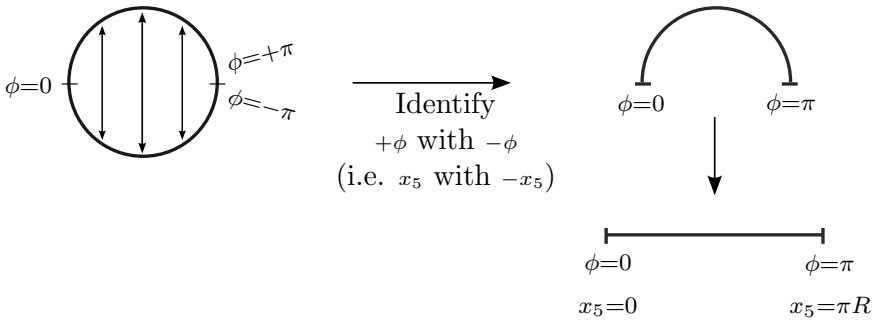

Figure A.1: *This figure from Ref. [134], nicely illustrates the "orbifolding" of a circle to an interval.*

with the respective left- and right-handed fields $\Psi^{(n)}_{L/R}$.

Thus, the lowest mode of a Dirac spinor in five dimensions can be a two-component Weyl spinor. In fact, orbifolding an extra dimension is a popular way to induce chirality in five-dimensional theories, which is especially important in theories with universal extra dimensions due to the chirality of the SM.

Appendix B

Boltzmann Equations

Boltzmann equations represent a semi-classical approach to describe non-equilibrium dynamics in many areas of physics, including several processes in the early universe. In this thesis, we used a simplified version of the Boltzmann equation in the context of leptogenesis in chapters 4 and 7. Based on Refs. [1, 2, 89], we will review this topic in some more detail here.

For a phase space distribution $f_\psi(p^\mu, x^\mu)$ of some particles species ψ, the corresponding Boltzmann equation reads

$$\hat{L}[f_\psi] = \hat{C}[f_\psi]\,, \tag{B.1}$$

with collision operator $\hat{C}$ and the Liouville operator

$$\hat{L} \equiv p^\alpha \frac{\partial}{\partial x^\alpha} - \Gamma^\alpha_{\beta\gamma} p^\beta p^\gamma \frac{\partial}{\partial p^\alpha}\,, \tag{B.2}$$

where $\Gamma^\alpha_{\beta\gamma}$ is the affine connection of the metric.

In the Friedmann-Robertson-Walker model space is assumed to be homogeneous and isotropic. In this case, we can use Eq. (1.1) to transform the Boltzmann equation to

$$\frac{\mathrm{d}n}{\mathrm{d}t} + 3Hn = \frac{g}{(2\pi)^3}\int \hat{C}[f_\psi]\frac{\mathrm{d}^3 p_\psi}{E_\psi}\,, \tag{B.3}$$

where a process of the type $\psi + a + \cdots \leftrightarrow i + j + \ldots$ yields the collision term

$$\begin{aligned}\frac{g}{(2\pi)^3}\int \hat{C}[f_\psi]\frac{\mathrm{d}^3 p_\psi}{E_\psi} \;=\; & -\int \mathrm{d}\Pi_\psi \mathrm{d}\Pi_a \ldots \mathrm{d}\Pi_i \mathrm{d}\Pi_j \ldots \\ & \times (2\pi)^4 \delta^4(p_\psi + p_a \cdots - p_i - p_j \ldots) \\ & \times \Big[|\mathcal{M}_{\psi+a+\cdots\to i+j+\ldots}|^2 f_a \ldots f_\psi (1 \pm f_i)(1 \pm f_j) \ldots \\ & - |\mathcal{M}_{i+j+\cdots\to\psi+a+\ldots}|^2 f_i f_j \ldots (1 \pm f_a) \ldots (1 \pm f_\psi) \Big]\,.\end{aligned} \tag{B.4}$$

Here, $\mathcal{M}$ is the Matrix element corresponding to the process and the $\pm$ depends on the fact if the respective particle species is bosonic or fermionic. We also used the phase-space differential

$$\mathrm{d}\Pi_k \equiv g_k \frac{1}{(2\pi)^3} \frac{\mathrm{d}^3 p_k}{E_k}\,, \tag{B.5}$$

with g_k being the respective number of internal degrees of freedom.

In the case of Maxwell-Boltzmann statistics we can drop all the $(1 \pm f)$ terms in Eq. (B.4), and, if we further assume that all the particle species are in kinetic equilibrium (not necessarily chemical equilibrium), their phase space distribution can be written

$$f(E) = \frac{n}{n^{\mathrm{eq}}} e^{-\frac{E}{T}}\,. \tag{B.6}$$

Under these assumptions the Boltzmann equation corresponding to the above process can be simplified to

$$\begin{aligned} \frac{\mathrm{d}n}{\mathrm{d}t} + 3Hn &= -\frac{n_\psi n_a \dots}{n_\psi^{\mathrm{eq}} n_a^{\mathrm{eq}} \dots} \gamma(\psi + a + \dots \to i + j + \dots) \\ &\quad + \frac{n_i n_j \dots}{n_i^{\mathrm{eq}} n_j^{\mathrm{eq}} \dots} \gamma(i + j + \dots \to \psi + a + \dots)\,, \end{aligned} \tag{B.7}$$

with

$$\begin{aligned} \gamma(\psi + a + \dots \to i + j + \dots) &\equiv \int \mathrm{d}\Pi_\psi \mathrm{d}\Pi_a \dots \mathrm{d}\Pi_i \mathrm{d}\Pi_j \dots \\ &\quad \times (2\pi)^4 \delta^4(p_\psi + p_a \dots - p_i - p_j \dots) f_\psi^{\mathrm{eq}} f_a^{\mathrm{eq}} |\mathcal{M}_{\psi + a + \dots \to i + j + \dots}|^2\,. \end{aligned} \tag{B.8}$$

In the case of CP-conserving decays and inverse decays $\psi \leftrightarrow i + j \dots$, this relation can, then, be further simplified to

$$\gamma(\psi \leftrightarrow i + j \dots) = n_\psi^{\mathrm{eq}} \Gamma_D = n_\psi^{\mathrm{eq}} \frac{K_1(m_\psi/T)}{K_2(m_\psi/T)} \Gamma_0\,. \tag{B.9}$$

Here, m_ψ is the rest mass of ψ and Γ_0 is its zero-temperature decay rate, while the K_i are modified Bessel functions of the second kind.

For two-body scatterings $\psi + a \leftrightarrow i + j$, on the other hand, Eq. (B.8) yields

$$\gamma(\psi + a \leftrightarrow i + j) = \frac{T}{64\pi^4} \int\limits_{(m_\psi + m_a)^2}^{\infty} \mathrm{d}s \sqrt{s}\, K_1\left(\frac{\sqrt{s}}{T}\right) \hat{\sigma}(s)\,, \tag{B.10}$$

with the reduced cross-section $\hat{\sigma}$, which is related to the regular total cross section σ by [91]

$$\hat{\sigma}(s) = \frac{8}{s} \left[(p_\psi \cdot p_a)^2 - m_\psi^2 m_a^2\right] \sigma(s)\,. \tag{B.11}$$

Appendix C

Leptogenesis Reaction Rates

For the numerical solutions of the Boltzmann equations in chapters 4 and 7, we used the following reaction rates, as they can mostly be found in Ref. [95].

The decay rate of a single heavy neutrino of mass M and decoupling parameter K is given by [2]

$$D \equiv \frac{\Gamma_D}{Hz} = K\, z\, \frac{K_1(z)}{K_2(z)}\,, \tag{C.1}$$

with $z \equiv M/T$ (T being the temperature) and the modified Bessel functions of the second kind $K_i(z)$.

Further, the $\Delta L = 1$ scattering rates for the s- and t-channel processes of the same particles are given by [91]

$$S_s \equiv \frac{\Gamma_{\Delta L=1,s}}{Hz} = 2 \cdot \frac{K_S}{12} f_s(z)\,, \tag{C.2}$$

$$S_t \equiv \frac{\Gamma_{\Delta L=1,t}}{Hz} = 2 \cdot 2 \cdot \frac{K_S}{12} f_t(z)\,, \tag{C.3}$$

with

$$K_S \equiv \frac{\tilde{m}_1}{m_*^S}\,, \quad m_*^S \equiv \frac{8\pi^2}{9}\frac{m_t^2}{v^2} m_* \approx 10 m_* \tag{C.4}$$

and

$$f_{s/t}(z) \equiv \frac{\int_{z^2}^{\infty} d\psi\, g_{s/t}(\psi/z^2)\sqrt{\psi} K_1(\sqrt{\psi})}{z^2 K_2(z)} \tag{C.5}$$

as well as

$$g_s(x) \equiv \left(\frac{x-1}{x}\right)^2 \tag{C.6}$$

$$g_t(x) \equiv \frac{x-1}{x}\left[\frac{x-2+2a_h}{x-1+a_h} + \frac{1-2a_h}{x-1}\log\left(\frac{x-1+a_h}{a_h}\right)\right]. \tag{C.7}$$

Here, a Higgs mass ($a_h \equiv (m_h/M_1)^2$) had to be introduced to regularize the infrared divergences of the t-channel diagrams. In fact, the quantitative results

are not very dependent of the exact value of the Higgs mass, and in all other equations the Higgs boson and all other particles (except for the right-handed neutrinos) were, therefore, assumed to be massless.

To cut down the time needed for the numerical calculations we only calculated $f_{s/t}(z)$ at a fixed number of points (20-30) and then linearly extrapolated the functions.

Furthermore, the used wash-out rate due to the right-handed neutrinos is given by

$$W = \frac{\Gamma_W}{Hz} = W_{ID} + W_{\Delta L=1} \tag{C.8}$$

with

$$W_{ID} \equiv \frac{1}{2} D \frac{N_{N_1}^{\rm eq}}{N_\ell^{\rm eq}} = \frac{1}{4} K z^3 K_1(z) \tag{C.9}$$

and

$$W_{\Delta L=1} = S_t \frac{N_{N_1}^{\rm eq}}{N_\ell^{\rm eq}} + S_s \frac{N_{N_1}}{N_\ell^{\rm eq}}\,, \tag{C.10}$$

where N_{N_1} is the actual abundance of the right-handed neutrinos in a comoving volume containing one photon, $N_{N_1}^{\rm eq} = 3z^2 K_2(z)/8$ is the corresponding value for an equilibrium distribution, and $N_\ell^{\rm eq} = 3/4$ is the corresponding value for massless leptons.

The generalization to the case of many decaying the neutrinos is, now, simple, since all one has to do is to do the interchange $M_1 \to M_n$ and $K \to K_n$ for each singlet state. However, since we do not consider the reaction rates Γ_i in Eqs. (7.4) and (7.5), but the ratio $\Gamma_i/(Hz)$, we have to remember that the factor Hz in the denominator is, obviously, the same for all different states. To find the correct rates we, therefore, make the transformations

$$D \to D_n : D(z) \to D\left(z\frac{M_n}{M_1}\right)\frac{M_1}{M_n}\,, \tag{C.11}$$

in the respective equations of this appendix. This can, now, be generalized in a straight-forward manner to find the S and W terms (this also includes the substitution $a_h \to a_h(M_1/M_n)^2$).

With these considerations it is, further, also simple to find the rates for the system described by Eqs. (7.19) to (7.25), where we simply use

$$\frac{\Gamma_{D,n}(M_n,T)}{H_0} = D_n(M_n,T)\,\frac{T}{M_1}\,, \tag{C.12}$$

combined with similar adjustments for S and W.

Appendix D

The Davidson-Ibarra Bound With Many Singlets

In this part of the appendix we generalize the treatment from Ref. [99] to find an upper bound for the CP-asymmetry for a setup with n_N heavy singlets and three light neutrinos as it is used in section 7.5.1.

In the case of many singletse, one needs to generalize the Casas-Ibarra parametrization [135] of the Yukawa couplings to

$$g = \frac{1}{\langle\phi\rangle^2} D_{\sqrt{M}} R D_{\sqrt{m}} U^\dagger \,, \tag{D.1}$$

where $D_{\sqrt{M}}$ and $D_{\sqrt{m}}$ are diagonal matrices that contain the masses of the heavy and light neutrinos, respectively. Further, we work in the basis where the heavy mass matrix is diagonal and U is the mixing matrix of the light neutrinos. Additionally, R is a complex $n_N \times 3$ matrix that fulfills the condition

$$R^T R = \mathbb{1}_{3\times 3}. \tag{D.2}$$

Let us use a mathematical trick and introduce $n_N - 3$ additional light neutrinos with zero couplings. We can easily do this, since these particles do not show up in any particle physics experiment. Now, the Yukawa couplings can be parametrized by

$$g = \frac{1}{\langle\phi\rangle^2} D_{\sqrt{M}} R' D'_{\sqrt{m}} U'^\dagger \,, \tag{D.3}$$

with $D'_{\sqrt{m}} = \mathrm{diag}(m_1, m_2, m_3, 0, \ldots, 0)$ and

$$U' \equiv \begin{pmatrix} U & 0 \\ 0 & \mathbb{1}_{(n_N-3)\times(n_N-3)} \end{pmatrix}. \tag{D.4}$$

Most importantly, R' is now an arbitrary complex orthogonal $n_N \times n_N$ matrix with

$$R'^T R' = \mathbb{1}_{n_N \times n_N}. \tag{D.5}$$

Due to this orthogonality Eq. (7.3) can now be transformed in the same way as in the 3×3 case [99], and we, therefore, find

$$\varepsilon_i \approx \frac{3}{16\pi} \frac{M_i}{\langle\phi\rangle^2} \frac{\sum_j m_j^2 \, \mathrm{Im}(R'^2_{1_j})}{\sum_j m_j |R'_{1_j}|^2} \,, \tag{D.6}$$

with $m_k = 0$ for $k > 3$, as they correspond to the particles with zero couplings.

Using $\sum_j R'^2_{1j} = 1$ from Eq. (D.5) we, then, find

$$|\varepsilon_i| \lesssim \frac{3}{16\pi} \frac{M_i}{\langle\phi\rangle^2} \frac{\mathrm{Max}(\{m_j^2\}) - \mathrm{Min}(\{m_j^2\})}{\mathrm{Max}(\{m_j\}) + \mathrm{Min}(\{m_j\})} = \frac{3}{16\pi} \frac{M_i}{\langle\phi\rangle^2} \, m_3 \,, \tag{D.7}$$

where m_3 is essentially a free parameter and which we used in Eq. (7.36).

Bibliography

[1] E. W. Kolb and M. S. Turner, *The early universe*, Front. Phys. **69** (1990), 1–547.

[2] E. W. Kolb and S. Wolfram, *Baryon number generation in the early universe*, Nucl. Phys. **B172** (1980), 224, Erratum-ibid.B195:542,1982.

[3] S. Weinberg, *Gravitation and cosmology: Principles and applications of the general theory of relativity.*, Wiley, 1972.

[4] A. A. Penzias and R. W. Wilson, *A measurement of excess antenna temperature at 4080-mc/s*, Astrophys. J. **142** (1965), 419–421.

[5] WMAP, D. N. Spergel et al., *Wilkinson microwave anisotropy probe (WMAP) three year results: Implications for cosmology*, Astrophys. J. Suppl. **170** (2007), 377, astro-ph/0603449.

[6] K. A. Olive, *Big bang nucleosynthesis: in review of particle physics (rpp 2000)*, Eur. Phys. J. **C15** (2000), 133–135.

[7] D. J. Fixsen et al., *The cosmic microwave background spectrum from the full cobe/firas data set*, Astrophys. J. **473** (1996), 576, astro-ph/9605054.

[8] WMAP, G. Hinshaw et al., *Three-year wilkinson microwave anisotropy probe (WMAP) observations: Temperature analysis*, (0300), astro-ph/0603451.

[9] M. Tegmark, *Doppler peaks and all that: CMB anisotropies and what they can tell us*, (1100), astro-ph/9511148.

[10] V. Sahni and A. A. Starobinsky, *The case for a positive cosmological Λ-term*, Int. J. Mod. Phys. **D9** (2000), 373–444, astro-ph/9904398.

[11] T. Padmanabhan, *Cosmological constant: The weight of the vacuum*, Phys. Rept. **380** (2003), 235–320, hep-th/0212290.

[12] R. K. Sachs and A. M. Wolfe, *Perturbations of a cosmological model and angular variations of the microwave background*, Astrophys. J. **147** (1967), 73–90.

[13] A. R. Liddle and D. H. Lyth, *Cosmological inflation and large-scale structure*, Cambridge Univ. Press, 2000.

[14] A. H. Guth, *The inflationary universe: A possible solution to the horizon and flatness problems*, Phys. Rev. **D23** (1981), 347–356.

[15] A. Albrecht and P. J. Steinhardt, *Cosmology for grand unified theories with radiatively induced symmetry breaking*, Phys. Rev. Lett. **48** (1982), 1220–1223.

[16] A. D. Linde, *A new inflationary universe scenario: A possible solution of the horizon, flatness, homogeneity, isotropy and primordial monopole problems*, Phys. Lett. **B108** (1982), 389–393.

[17] A. D. Linde, *Chaotic inflation*, Phys. Lett. **B129** (1983), 177–181.

[18] L. F. Abbott, E. Farhi, and M. B. Wise, *Particle production in the new inflationary cosmology*, Phys. Lett. **B117** (1982), 29.

[19] A. D. Linde, *Particle physics and inflationary cosmology*, (2005), `hep-th/0503203`.

[20] Supernova Cosmology Project, R. A. Knop et al., *New constraints on ω_m, ω_λ, and w from an independent set of eleven high-redshift supernovae observed with hst*, Astrophys. J. **598** (2003), 102, `astro-ph/0309368`.

[21] E. J. Copeland, M. Sami, and S. Tsujikawa, *Dynamics of dark energy*, Int. J. Mod. Phys. **D15** (2006), 1753–1936, `hep-th/0603057`.

[22] C. Wetterich, *Cosmology and the fate of dilatation symmetry*, Nucl. Phys. **B302** (1988), 668.

[23] B. Ratra and P. J. E. Peebles, *Cosmological consequences of a rolling homogeneous scalar field*, Phys. Rev. **D37** (1988), 3406.

[24] P. G. Ferreira and M. Joyce, *Structure formation with a self-tuning scalar field*, Phys. Rev. Lett. **79** (1997), 4740–4743, `astro-ph/9707286`.

[25] E. J. Copeland, A. R. Liddle, and D. Wands, *Exponential potentials and cosmological scaling solutions*, Phys. Rev. **D57** (1998), 4686–4690, `gr-qc/9711068`.

[26] T. Barreiro, E. J. Copeland, and N. J. Nunes, *Quintessence arising from exponential potentials*, Phys. Rev. **D61** (2000), 127301, `astro-ph/9910214`.

[27] I. Zlatev, L.-M. Wang, and P. J. Steinhardt, *Quintessence, cosmic coincidence, and the cosmological constant*, Phys. Rev. Lett. **82** (1999), 896–899, `astro-ph/9807002`.

[28] U. Seljak, A. Slosar, and P. McDonald, *Cosmological parameters from combining the lyman-alpha forest with cmb, galaxy clustering and sn constraints*, JCAP **0610** (2006), 014, `astro-ph/0604335`.

[29] F. Halzen and A. D. Martin, *Quarks and leptons: An introductory course in modern particle physics*, Wiley, 1984.

[30] O. Nachtmann, *Phänomene und Konzepte der Elementarteilchenphysik*, Vieweg, 1992.

[31] W.-M. Yao et al., *Review of Particle Physics*, Journal of Physics G **33** (2006).

[32] E. K. Akhmedov, *Neutrino physics*, (1999), `hep-ph/0001264`.

[33] N. Cabibbo, *Unitary symmetry and leptonic decays*, Phys. Rev. Lett. **10** (1963), 531–532.

[34] M. Kobayashi and T. Maskawa, *CP violation in the renormalizable theory of weak interaction*, Prog. Theor. Phys. **49** (1973), 652–657.

[35] Z. Maki, M. Nakagawa, and S. Sakata, *Remarks on the unified model of elementary particles*, Prog. Theor. Phys. **28** (1962), 870.

[36] B. Pontecorvo, *Mesonium and antimesonium*, Sov. Phys. JETP **6** (1957), 429.

[37] S. F. King, *Large mixing angle MSW and atmospheric neutrinos from single right-handed neutrino dominance and u(1) family symmetry*, Nucl. Phys. **B576** (2000), 85–105, `hep-ph/9912492`.

[38] V. M. Lobashev et al., *Direct search for mass of neutrino and anomaly in the tritium beta-spectrum*, Phys. Lett. **B460** (1999), 227–235.

[39] C. Kraus et al., *Final results from phase ii of the mainz neutrino mass search in tritium beta decay*, Eur. Phys. J. **C40** (2005), 447–468, `hep-ex/0412056`.

[40] M. Maltoni, T. Schwetz, M. A. Tortola, and J. W. F. Valle, *Status of global fits to neutrino oscillations*, New J. Phys. **6** (2004), 122, `hep-ph/0405172`.

[41] C. D. Froggatt and H. B. Nielsen, *Hierarchy of quark masses, cabibbo angles and cp violation*, Nucl. Phys. **B147** (1979), 277.

[42] F. Wilczek, *Axions and family symmetry breaking*, Phys. Rev. Lett. **49** (1982), 1549–1552.

[43] D. B. Reiss, *Can the family group be a global symmetry?*, Phys. Lett. **B115** (1982), 217.

[44] G. B. Gelmini, S. Nussinov, and T. Yanagida, *Does nature like Nambu-Goldstone bosons?*, Nucl. Phys. **B219** (1983), 31.

[45] J. L. Feng, T. Moroi, H. Murayama, and E. Schnapka, *Third generation familons, b factories, and neutrino cosmology*, Phys. Rev. **D57** (1998), 5875–5892.

[46] CLEO, R. Ammar et al., *Search for the familon via B+- –> π+- X0, B+- –> K+- X0, and B0 –> K0(s) X0 decays*, Phys. Rev. Lett. **87** (2001), 271801, `hep-ex/0106038`.

[47] J. L. Diaz-Cruz and C. E. Pagliarone, *A new family dependent interaction in tevatron top dilepton candidate events?*, (2004), `hep-ph/0412329`.

[48] P. Minkowski, $\mu \to e\,\gamma$ *at a rate of one out of 1-billion muon decays?*, Phys. Lett. **B67** (1977), 421.

[49] T. Yanagida, *Horizontal gauge symmetry and masses of neutrinos*, in Proceedings of the Workshop on the Baryon Number of the Universe and Unified Theories, Tsukuba, Japan, 13-14 Feb 1979, edited by O.Sawada and A. Sugamoto, Report KEK-79-18 (1979).

[50] M. Gell-Mann, P. Ramond, and R. Slansky, *Complex spinors and unified theories*, in *Supergravity*, edited by D. Z. Freedman and P. van Nieuwenhuizen (North-Holland, Amsterdam, 1979).

[51] Y. Nir, *Neutrinos in particle physics*, summer school notes.

[52] S. F. King, *Atmospheric and solar neutrinos with a heavy singlet*, Phys. Lett. **B439** (1998), 350–356, `hep-ph/9806440`.

[53] S. F. King, *Atmospheric and solar neutrinos from single right-handed neutrino dominance and U(1) family symmetry*, Nucl. Phys. **B562** (1999), 57–77, `hep-ph/9904210`.

[54] N. Arkani-Hamed, S. Dimopoulos, G. R. Dvali, and J. March-Russell, *Neutrino masses from large extra dimensions*, Phys. Rev. **D65** (2002), 024032, `hep-ph/9811448`.

[55] K. R. Dienes, E. Dudas, and T. Gherghetta, *Light neutrinos without heavy mass scales: A higher- dimensional seesaw mechanism*, Nucl. Phys. **B557** (1999), 25, `hep-ph/9811428`.

[56] A. Lukas, P. Ramond, A. Romanino, and G. G. Ross, *Solar neutrino oscillation from large extra dimensions*, Phys. Lett. **B495** (2000), 136–146, hep-ph/0008049.

[57] A. Lukas, P. Ramond, A. Romanino, and G. G. Ross, *Neutrino masses and mixing in brane-world theories*, JHEP **04** (2001), 010, hep-ph/0011295.

[58] M.-T. Eisele and N. Haba, *Family symmetry and single right-handed neutrino dominance in five dimensions*, Phys. Rev. **D74** (2006), 073007, hep-ph/0603158.

[59] N. Arkani-Hamed, S. Dimopoulos, and G. R. Dvali, *The hierarchy problem and new dimensions at a millimeter*, Phys. Lett. **B429** (1998), 263–272, hep-ph/9803315.

[60] I. Antoniadis, N. Arkani-Hamed, S. Dimopoulos, and G. R. Dvali, *New dimensions at a millimeter to a fermi and superstrings at a tev*, Phys. Lett. **B436** (1998), 257–263, hep-ph/9804398.

[61] A. D. Dolgov, *NonGUT baryogenesis*, Phys. Rept. **222** (1992), 309–386.

[62] A. Riotto and M. Trodden, *Recent progress in baryogenesis*, Ann. Rev. Nucl. Part. Sci. **49** (1999), 35–75, hep-ph/9901362.

[63] G. Steigman, *Observational tests of antimatter cosmologies*, Ann. Rev. Astron. Astrophys. **14** (1976), 339–372.

[64] WMAP, D. N. Spergel et al., *First year wilkinson microwave anisotropy probe (WMAP) observations: Determination of cosmological parameters*, Astrophys. J. Suppl. **148** (2003), 175, astro-ph/0302209.

[65] K. A. Olive, G. Steigman, and T. P. Walker, *Primordial nucleosynthesis: Theory and observations*, Phys. Rept. **333** (2000), 389–407, astro-ph/9905320.

[66] A. D. Sakharov, *Violation of CP invariance, C asymmetry, and baryon asymmetry of the universe*, Pisma Zh. Eksp. Teor. Fiz. **5** (1967), 32–35.

[67] S. Dodelson and L. M. Widrow, *Baryon symmetric baryogenesis*, Phys. Rev. Lett. **64** (1990), 340–343.

[68] A. G. Cohen and D. B. Kaplan, *Thermodynamic generation of the baryon asymmetry*, Phys. Lett. **B199** (1987), 251.

[69] S. Y. Khlebnikov and M. E. Shaposhnikov, *The statistical theory of anomalous fermion number nonconservation*, Nucl. Phys. **B308** (1988), 885–912.

[70] J. A. Harvey and M. S. Turner, *Cosmological baryon and lepton number in the presence of electroweak fermion number violation*, Phys. Rev. **D42** (1990), 3344–3349.

[71] W. Bernreuther, *CP violation and baryogenesis*, Lect. Notes Phys. **591** (2002), 237–293, hep-ph/0205279.

[72] S. L. Adler, *Axial vector vertex in spinor electrodynamics*, Phys. Rev. **177** (1969), 2426–2438.

[73] J. S. Bell and R. Jackiw, *A pcac puzzle: $\pi_0 \to \gamma\gamma$ in the σ model*, Nuovo Cim. **A60** (1969), 47–61.

[74] D. Bodeker, G. D. Moore, and K. Rummukainen, *Chern-Simons number diffusion and hard thermal loops on the lattice*, Phys. Rev. **D61** (2000), 056003, hep-ph/9907545.

[75] B. A. Campbell, S. Davidson, J. R. Ellis, and K. A. Olive, *On the baryon, lepton flavor and right-handed electron asymmetries of the universe*, Phys. Lett. **B297** (1992), 118–124, hep-ph/9302221.

[76] J. M. Cline, K. Kainulainen, and K. A. Olive, *Protecting the primordial baryon asymmetry from erasure by sphalerons*, Phys. Rev. **D49** (1994), 6394–6409, hep-ph/9401208.

[77] K. Dick, M. Lindner, M. Ratz, and D. Wright, *Leptogenesis with Dirac neutrinos*, Phys. Rev. Lett. **84** (2000), 4039–4042, hep-ph/9907562.

[78] M. Yoshimura, *Unified gauge theories and the baryon number of the universe*, Phys. Rev. Lett. **41** (1978), 281–284.

[79] D. Toussaint, S. B. Treiman, F. Wilczek, and A. Zee, *Matter - antimatter accounting, thermodynamics, and black hole radiation*, Phys. Rev. **D19** (1979), 1036–1045.

[80] S. Weinberg, *Cosmological production of baryons*, Phys. Rev. Lett. **42** (1979), 850–853.

[81] E. W. Kolb and M. S. Turner, *Grand unified theories and the origin of the baryon asymmetry*, Ann. Rev. Nucl. Part. Sci. **33** (1983), 645–696.

[82] D. J. H. Chung, E. W. Kolb, and A. Riotto, *Production of massive particles during reheating*, Phys. Rev. **D60** (1999), 063504, hep-ph/9809453.

[83] M. Y. Khlopov and A. D. Linde, *Is it easy to save the gravitino?*, Phys. Lett. **B138** (1984), 265–268.

[84] J. R. Ellis, J. E. Kim, and D. V. Nanopoulos, *Cosmological gravitino regeneration and decay*, Phys. Lett. **B145** (1984), 181.

[85] L. Kofman, A. D. Linde, and A. A. Starobinsky, *Reheating after inflation*, Phys. Rev. Lett. **73** (1994), 3195–3198, hep-th/9405187.

[86] L. Kofman, A. D. Linde, and A. A. Starobinsky, *Towards the theory of reheating after inflation*, Phys. Rev. **D56** (1997), 3258–3295, hep-ph/9704452.

[87] E. W. Kolb, A. D. Linde, and A. Riotto, *GUT baryogenesis after preheating*, Phys. Rev. Lett. **77** (1996), 4290–4293, hep-ph/9606260.

[88] M. Fukugita and T. Yanagida, *Baryogenesis without grand unification*, Phys. Lett. **B174** (1986), 45.

[89] M. A. Luty, *Baryogenesis via leptogenesis*, Phys. Rev. **D45** (1992), 455–465.

[90] M. Plumacher, *Baryogenesis and lepton number violation*, Z. Phys. **C74** (1997), 549–559, hep-ph/9604229.

[91] M. Plumacher, *Baryon asymmetry, neutrino mixing and supersymmetric so(10) unification*, Nucl. Phys. **B530** (1998), 207–246, hep-ph/9704231.

[92] R. Barbieri, P. Creminelli, A. Strumia, and N. Tetradis, *Baryogenesis through leptogenesis*, Nucl. Phys. **B575** (2000), 61–77, hep-ph/9911315.

[93] W. Buchmuller, P. Di Bari, and M. Plumacher, *Cosmic microwave background, matter-antimatter asymmetry and neutrino masses*, Nucl. Phys. **B643** (2002), 367–390, hep-ph/0205349.

[94] G. F. Giudice, A. Notari, M. Raidal, A. Riotto, and A. Strumia, *Towards a complete theory of thermal leptogenesis in the sm and mssm*, Nucl. Phys. **B685** (2004), 89–149, hep-ph/0310123.

[95] W. Buchmuller, P. Di Bari, and M. Plumacher, *Leptogenesis for pedestrians*, Ann. Phys. **315** (2005), 305–351, hep-ph/0401240.

[96] A. Abada et al., *Flavour matters in leptogenesis*, JHEP **09** (2006), 010, hep-ph/0605281.

[97] L. Covi, E. Roulet, and F. Vissani, *CP violating decays in leptogenesis scenarios*, Phys. Lett. **B384** (1996), 169–174, hep-ph/9605319.

[98] K. Hamaguchi, H. Murayama, and T. Yanagida, *Leptogenesis from sneutrino-dominated early universe*, Phys. Rev. **D65** (2002), 043512, hep-ph/0109030.

[99] S. Davidson and A. Ibarra, *A lower bound on the right-handed neutrino mass from leptogenesis*, Phys. Lett. **B535** (2002), 25–32, hep-ph/0202239.

[100] A. Pilaftsis and T. E. J. Underwood, *Resonant leptogenesis*, Nucl. Phys. **B692** (2004), 303–345, hep-ph/0309342.

[101] T. Hambye, Y. Lin, A. Notari, M. Papucci, and A. Strumia, *Constraints on neutrino masses from leptogenesis models*, Nucl. Phys. **B695** (2004), 169–191, hep-ph/0312203.

[102] G. Lazarides and Q. Shafi, *Origin of matter in the inflationary cosmology*, Phys. Lett. **B258** (1991), 305–309.

[103] T. Asaka, K. Hamaguchi, M. Kawasaki, and T. Yanagida, *Leptogenesis in inflationary universe*, Phys. Rev. **D61** (2000), 083512, hep-ph/9907559.

[104] M. Fukugita and T. Yanagida, *Sphaleron induced baryon number nonconservation and a constraint on majorana neutrino masses*, Phys. Rev. **D42** (1990), 1285–1286.

[105] A. E. Nelson and S. M. Barr, *Upper bound on baryogenesis scale from neutrino masses*, Phys. Lett. **B246** (1990), 141–143.

[106] W. Buchmuller and T. Yanagida, *Baryogenesis and the scale of B-L breaking*, Phys. Lett. **B302** (1993), 240–244.

[107] A. Abada, S. Davidson, F.-X. Josse-Michaux, M. Losada, and A. Riotto, *Flavour issues in leptogenesis*, JCAP **0604** (2006), 004, hep-ph/0601083.

[108] M. Fujii, K. Hamaguchi, and T. Yanagida, *Leptogenesis with almost degenerate majorana neutrinos*, Phys. Rev. **D65** (2002), 115012, hep-ph/0202210.

[109] W. Buchmuller, P. Di Bari, and M. Plumacher, *The neutrino mass window for baryogenesis*, Nucl. Phys. **B665** (2003), 445–468, hep-ph/0302092.

[110] W. Buchmuller and M. Plumacher, *Spectator processes and baryogenesis*, Phys. Lett. **B511** (2001), 74–76, hep-ph/0104189.

[111] E. Nardi, Y. Nir, E. Roulet, and J. Racker, *The importance of flavor in leptogenesis*, JHEP **01** (2006), 164, hep-ph/0601084.

[112] S. Blanchet and P. Di Bari, *Flavor effects on leptogenesis predictions*, JCAP **0703** (2007), 018, hep-ph/0607330.

[113] S. Antusch, J. Kersten, M. Lindner, and M. Ratz, *Running neutrino masses, mixings and CP phases: Analytical results and phenomenological consequences*, Nucl. Phys. **B674** (2003), 401–433, hep-ph/0305273.

[114] M. Lindner and M. M. Muller, *Comparison of Boltzmann equations with quantum dynamics for scalar fields*, Phys. Rev. **D73** (2006), 125002, hep-ph/0512147.

[115] W. Buchmuller and S. Fredenhagen, *Quantum mechanics of baryogenesis*, Phys. Lett. **B483** (2000), 217–224, hep-ph/0004145.

[116] I. Affleck and M. Dine, *A new mechanism for baryogenesis*, Nucl. Phys. **B249** (1985), 361.

[117] M. Dine, L. Randall, and S. D. Thomas, *Baryogenesis from flat directions of the supersymmetric standard model*, Nucl. Phys. **B458** (1996), 291–326, hep-ph/9507453.

[118] M. Dine, L. Randall, and S. D. Thomas, *Supersymmetry breaking in the early universe*, Phys. Rev. Lett. **75** (1995), 398–401, hep-ph/9503303.

[119] F. Bauer, M.-T. Eisele, and M. Garny, *Leptonic dark energy and baryogenesis*, Phys. Rev. **D74** (2006), 023509, hep-ph/0510340.

[120] L. A. Boyle, R. R. Caldwell, and M. Kamionkowski, *Spintessence! new models for dark matter and dark energy*, Phys. Lett. **B545** (2002), 17–22, astro-ph/0105318.

[121] S. R. Coleman, *Q balls*, Nucl. Phys. **B262** (1985), 263.

[122] N. Haba, *5d seesaw, flavor structure, and mass textures*, JHEP **05** (2006), 030, hep-ph/0603119.

[123] J. P. Conlon and D. Cremades, *The neutrino suppression scale from large volumes*, (2006), hep-ph/0611144.

[124] M.-T. Eisele, *Leptogenesis with many neutrinos*, (2007), arXiv:0706.0200 [hep-ph].

[125] W. Buchmuller, K. Hamaguchi, O. Lebedev, and M. Ratz, *Supersymmetric standard model from the heterotic string. ii*, (2006), hep-th/0606187.

[126] W. Buchmuller, K. Hamaguchi, O. Lebedev, S. Ramos-Sanchez, and M. Ratz, *Seesaw neutrinos from the heterotic string*, (2007), hep-ph/0703078.

[127] G. Engelhard, Y. Grossman, E. Nardi, and Y. Nir, *The importance of N_2 leptogenesis*, (2006), hep-ph/0612187.

[128] Y. Nir, *private correspondence*.

[129] A. Pilaftsis, *Leptogenesis in theories with large extra dimensions*, Phys. Rev. **D60** (1999), 105023, hep-ph/9906265.

[130] A. D. Medina and C. E. M. Wagner, *Soft leptogenesis in warped extra dimensions*, JHEP **12** (2006), 037, hep-ph/0609052.

[131] T. Gherghetta, K. Kadota, and M. Yamaguchi, *Warped leptogenesis with dirac neutrino masses*, (2007), arXiv:0705.1749 [hep-ph].

[132] A. Abada, P. Dey, and G. Moreau, *Neutrinos in flat extra dimension: Towards a realistic scenario*, (2006), hep-ph/0611200.

[133] N. Haba, *private notes*.

[134] R. Sundrum, *To the fifth dimension and back. (tasi 2004)*, (2005), hep-th/0508134.

[135] J. A. Casas and A. Ibarra, *Oscillating neutrinos and μ –> e, γ*, Nucl. Phys. **B618** (2001), 171–204, hep-ph/0103065.